

Theoretical Astroparticle Physics

Contents

1. Topics	143
2. Participants	145
2.1. ICRA-Net participants	145
2.2. Past collaborators	145
2.3. Ongoing collaborations	146
2.4. Students	146
3. Brief description	147
3.1. Electron-positron plasma	147
3.1.1. Thermalization of the electron-positron-photon plasma	147
3.1.2. Thermalization of mildly relativistic plasma with proton loading	148
3.1.3. Fireball vs fireshell and equations of motion	148
3.2. Collisionless shockless relativistic electron-ion plasma	149
3.3. Neutrino in cosmology	150
3.3.1. Massive neutrino and structure formation	151
3.3.2. Cellular structure of the Universe	152
3.3.3. Lepton asymmetry of the Universe	152
4. Publications	155
4.1. Publications before 2005	155
4.2. Publications (2005 - 2007)	158
4.3. Publications (2008)	163
4.4. PHD Thesis	164
4.5. Invited talks at international conferences	165
5. APPENDICES	167
A. Kinetic instabilities in collisionless ultra-relativistically streaming cold electron-ion plasma	169
A.1. Introduction	169
A.2. The method	170
A.3. Numerical results	172
A.4. Discussion	176
B. Thermalization of the mildly relativistic plasma	179

B.1.	Introduction	179
B.2.	Qualitative description of the pair plasma	181
B.3.	Pure pair plasma	182
B.4.	Proton loading	188
B.5.	Conservation laws	189
B.6.	Determination of temperature and chemical potentials in kinetic equilibrium	190
B.7.	Binary interactions	193
B.7.1.	Compton scattering $\gamma e^\pm \rightarrow \gamma' e^{\pm'}$	193
B.7.2.	Pair creation and annihilation $\gamma_1 \gamma_2 \rightleftharpoons e^- e^+$	195
B.7.3.	Møller scattering of electrons and positrons $e_1^\pm e_2^\pm \rightarrow e_1^{\pm'} e_2^{\pm'}$	197
B.7.4.	Bhaba scattering of electrons on positrons $e^- e^+ \rightarrow e^- e^+$	199
B.8.	Binary reactions with protons	200
B.8.1.	Compton scattering on protons $\gamma p \rightarrow \gamma' p'$	200
B.8.2.	Electron-proton and positron-proton scattering $e_\pm p \rightarrow e'_\pm p'$	200
B.8.3.	Proton-proton scattering $p_1 p_2 \rightarrow p'_1 p'_2$	201
B.9.	Three-body processes	202
B.10.	Cutoff in the Coulomb scattering	203
B.11.	Mass scaling for the proton-electron/positron reaction	205
B.12.	The definition of matrix elements	206
B.13.	The discretization procedure and the computational scheme	208
B.14.	Numerical results	209
B.14.1.	Case I	209
B.14.2.	Case II	211
B.14.3.	Case III	213
B.15.	Discussion and conclusions	214
C.	Hydrodynamics of the pair plasma	225
C.1.	Local, global and average conservation laws	225
C.1.1.	Particle number	225
C.1.2.	Energy-momentum conservation	229
C.1.3.	Entropy conservation	232
C.1.4.	Analogy with a Friedmann Universe	233
C.2.	Self acceleration of the fireshell	235
D.	Cosmological structure formation	237
D.1.	The Cosmological Principle	237
D.2.	Two-point Correlation Function	238
D.2.1.	Observed Galaxy Distribution	239
D.2.2.	Power Law Clustering and Fractals	240
D.3.	Gravitational instability	242
D.3.1.	Horizon scale and mass evolution	243

D.3.2. Selfgravitating ideal fluid: linear theory	243
D.3.3. Applications	247
D.3.4. Initial spectrum of perturbations	248
D.3.5. Damping of Perturbations	249
D.3.6. Structure formation on late times	250
E. Massive degenerate neutrinos in Cosmology	253
E.1. Neutrino decoupling	253
E.2. The redshifted statistics	254
E.3. Energy density of neutrinos	255
E.3.1. Neutrino mass	256
E.3.2. Chemical potential	257
E.3.3. Neutrino oscillations	258
E.4. The Jeans mass of neutrinos	258
Bibliography	263

Contents

1. Topics

- Electron-positron plasma
 - Thermalization of the electron-positron-photon plasma
 - Thermalization of mildly relativistic plasma with proton loading
 - Fireball vs fireshell and equations of motion
- Collisionless shockless relativistic electron-ion plasma
 - Generation of electromagnetic fields
 - Stochasticization of particles motion
 - Generation of radiation
- Neutrino in cosmology
 - Massive neutrino and structure formation
 - Cellular structure of the Universe
 - Lepton asymmetry of the Universe

1. Topics

2. Participants

2.1. ICRANet participants

- Carlo Luciano Bianco
- Remo Ruffini
- Gregory Vereshchagin
- She-Sheng Xue

2.2. Past collaborators

- Marco Valerio Arbolino (DUNE s.r.l., Italy)
- Andrea Bianconi (INFN Pavia, Italy)
- Neta A. Bahcall (Princeton University, USA)
- Daniella Calzetti (University of Massachusetts, USA)
- Jaan Einasto (Tartu Observatory, Estonia)
- Roberto Fabbri (University of Firenze, Italy)
- Long-Long Feng (University of Science and Technology of China, China)
- Jiang Gong Gao (Xinjiang Institute of Technology, China)
- Mauro Giavalisco (University of Massachusetts, USA)
- Gabriele Ingrosso (INFN, University of Lecce, Italy)
- Yi-peng Jing (Shanghai Astronomical Observatory, China)
- Hyung-Won Lee (Inje University, South Korea)
- Marco Merafina (University of Rome “Sapienza”, Italy)
- Houjun Mo (University of Massachusetts, USA)
- Enn Saar (Tartu Observatory, Estonia)

2. Participants

- Jay D. Salmonson (Livermore Lab, USA)
- Luis Alberto Sanchez (National University Medellin, Colombia)
- Costantino Sigismundi (ICRA and University of Rome "La Sapienza", Italy)
- Doo Jong Song (Korea Astronomy Observatory, South Korea)
- Luigi Stella (Astronomical Observatory of Rome, Italy)
- William Stoeger (Vatican Observatory, University of Arizona USA)
- Sergio Taraglio (ENEA, Italy)
- Gerda Wiedenmann (MPE Garching, Germany)
- Jim Wilson (Livermore Lab, USA)

2.3. Ongoing collaborations

- Alexey Aksenov (ITEP, Russia)
- Valeri Chechetkin (Keldysh Institute, Russia)
- Nikolay Fimin (Keldysh Institute, Russia)
- Massimiliano Lattanzi (Oxford, UK)
- Roustam Zalaletdinov (Tashkent University, Uzbekistan)

2.4. Students

- Gustavo de Barros (IRAP PhD, Brazil)
- Luis Juracy Rangel Lemos (IRAP PhD, Brazil)
- Ivan Siutsou (IRAP PhD, Belarus)

3. Brief description

Astroparticle physics is a new field of research emerging at the intersection of particle physics, astrophysics and cosmology. Theoretical development in these fields is mainly triggered by the growing amount of experimental data of unprecedented accuracy, coming both from the ground based laboratories and from the dedicated space missions.

3.1. Electron-positron plasma

Electron-positron plasma is of interest in many fields of astrophysics, e.g. in the early universe, gamma-ray bursts, active galactic nuclei, the center of our Galaxy, hypothetical quark stars. It is also relevant for the physics of ultraintense lasers and thermonuclear reactions. We study some properties of dense and hot electron-positron plasmas. In particular, we are interested in the issues of its creation and relaxation, its kinetic properties and hydrodynamic description, baryon loading, transition to transparency and radiation from such plasmas.

Two completely different states exist for electron-positron plasma: optically thin and optically thick. Optically thin pair plasma may exist in active galactic nuclei and in X-ray binaries. The theory of relativistic optically thin nonmagnetic plasma and especially its equilibrium configurations was established in the 80s by Svensson, Lightman, Gould and others. It was shown that relaxation of the plasma to some equilibrium state is determined by a dominant reaction, e.g. Compton scattering or bremsstrahlung.

Developments in the theory of gamma ray bursts from one side, and observational data from the other side, unambiguously point out on existence of optically thick pair dominated non-steady phase in the beginning of formation of GRBs. The spectrum of radiation from optically thick plasma is assumed to be thermal. However, in such a transient phenomena as gamma-ray bursts there could be not enough time for the plasma to relax into equilibrium.

3.1.1. Thermalization of the electron-positron-photon plasma

One of crucial assumptions adopted in the literature on gamma-ray bursts (Ruffini et al. (1999), Ruffini et al. (2000)) is that initial state of the pair plasma, formed in the source of the gamma-ray burst is supposed to be thermal, with

3. Brief description

equal temperature of pairs and photons. This assumption was analyzed by Aksenov et al. (2007), Aksenov et al. (2008). The electron-positron-photon plasma was assumed to be homogeneous and isotropic, in the absence of magnetic fields, with average energy per particle bracketing electron rest mass, in the range $0.1\text{MeV} \lesssim \epsilon \lesssim 10\text{MeV}$. Relativistic Boltzmann equations were solved numerically for pairs and photons, starting from arbitrary initial configurations described by the corresponding distribution functions. All binary and triple collisions were accounted for, by the corresponding collisional integrals.

The evolution of the plasma was followed up to reaching thermal equilibrium with the same temperature of photons and pairs, and vanishing chemical potentials of both pairs and photons, for details see Appendix B. It was shown that thermal equilibrium is reached on a short timescale $t < 10^{-12}$ sec, much shorter than the dynamical timescale. The conclusion was reached that initial state of the plasma in GRB sources is indeed thermal.

3.1.2. Thermalization of mildly relativistic plasma with proton loading

Proton loading of electron-positron plasma was considered by Aksenov et al. (2008). This paper systematically presents details of the computational scheme used by Aksenov et al. (2007), as well as generalizes the treatment, considering proton loading of the pair plasma. When proton loading is large, protons thermalize first by proton-proton scattering, and then with the electron-positron-photon plasma by proton-electron scattering. In the opposite case of small proton loading proton-electron scattering dominates over proton-proton one. Thus in all cases the plasma, even with proton admixture, reaches thermal equilibrium configuration on a timescale $t < 10^{-11}$ sec. We show that it is crucial to account for not only binary but also triple direct and inverse interactions between electrons, positrons, photons and protons. Several explicit examples are given and the corresponding timescales for reaching kinetic and thermal equilibria are determined.

3.1.3. Fireball vs fireshell and equations of motion

Gamma-ray bursts are very different from the fireball phenomenon (e.g. atomic bomb explosion) with high temperature inside, blast wave propagating into the surrounding dense atmosphere and a characteristic self-similar motion described by Sedov solution, which can be obtained easily by dimensionality considerations.

In a gamma-ray burst explosion, after appearance of dense and hot optically thick plasma composed of electron-positron pairs and photons it starts to expand adiabatically, governed by equations of relativistic hydrodynam-

ics. The surrounding medium is either rarefied or even absent and the motion is purely relativistic expansion into the vacuum.

The work of Ruffini et al. (1999), Ruffini et al. (2000) on the pair electromagnetic pulse created by a black hole have shown that electron-positron pairs can self-accelerate outwards from the source, and form a relativistic shell expanding with unprecedented large Lorentz factors, of the order of several hundreds. It was shown, that non-equilibrium effects should be taken into account, in particular dynamical approach of the plasma to transparency was described by the usual hydrodynamic equations together with the rate equation for electron-positron pairs

During acceleration phase, occurring because of large radiative pressure, the plasma engulfs certain amount of baryonic matter, and continue to accelerate until the plasma becomes transparent, electron-positron pairs disappear and all photons escape.

Although initially uniform plasma remains uniform during expansion in the comoving frame, it appears as a narrow shell, which we refer to as a fireshell, in the laboratory frame. From hydrodynamic equations it is possible to show (Vereshchagin (2008)) that the thickness of the fireshell indeed remains constant under the condition $\gamma \gg 1$, which is approached soon after beginning of expansion since the scaling law $\gamma \propto r$, characterizes expansion of the radiation-dominated pair plasma. This conclusion was obtained by Ruffini et al. (1999) by the analysis of different geometries of the plasma.

In the work of Bianco et al. (2006) we have compared and contrasted existing models of hydrodynamic evolution of gamma-ray bursts in the literature. It was pointed out, that in spite of many qualitative similarities, several crucial quantitative differences exist, namely a) the appropriate model for geometry of expanding fireshell (PEM-pulse) is given by the constant width approximation; there is no broadening of the fireshell; b) there is a bound on parameter B which comes from violation of constant width approximation, $B \leq 10^{-2}$; c) the rate equation for electron-positron pairs plays crucial role in description of the approach to transparency. Details are given in the Appendix C. All these differences are crucial when the theory is confronted with observations, as shown by Ruffini et al. (2007).

3.2. Collisionless shockless relativistic electron-ion plasma

After transparency is reached photons leave the ultrarelativistic shell, where only electrons and protons remain. Collisions are no longer efficient to maintain common temperature of particles. However, protons and electrons have very different kinetic energy since their mass is different. Hydrodynamic treatment, adopted for description of the fireshell in its optically thick phase

3. Brief description

becomes oversimplified in the optically thin phase. Description of collisionless plasma calls for kinetic treatment. This time, however, since collisions can be neglected, Vlasov-Maxwell equations should be solved.

Chechetkin et al. (2008) consider cold collisionless electron-proton plasma, moving in the vacuum with bulk Lorentz factor $\Gamma = 200$. In order to describe such a system numerical integration of Vlasov-Maxwell equations is performed by a 3-dimensional Lagrange code, see Appendix A. The plasma is shown to experience kinetic instabilities, leading to generation of stochastic electro-magnetic fields on the length scales, smaller than the plasma skin depth L . The motion of electrons and proton randomizes in these stochastic fields, leading to a thermal-like spread in the distribution function of electrons and protons. Both electrons and protons, and the electromagnetic field reach equipartition on a timescale L/c . Large fraction of the momentum, stored initially in protons is converted into Poynting flux.

As the result, expanding shell has complex structure. Particle's distribution functions are anisotropic, but transverse momentum of particles is comparable to the total momentum. Electric and magnetic fields are highly fluctuating. Such inhomogeneous plasma is expected to produce jitter-like radiation. This radiation could explain prompt radiation from GRBs.

3.3. Neutrino in cosmology

Many observational facts make it clear that luminous matter alone cannot account for the whole matter content of the Universe. Among them there is the cosmic background radiation anisotropy spectrum, that is well fitted by a cosmological model in which just a small fraction of the total density is supported by baryons.

In particular, the best fit to the observed spectrum is given by a flat Λ CDM model, namely a model in which the main contribution to the energy density of the Universe comes from vacuum energy and cold dark matter. This result is confirmed by other observational data, like the power spectrum of large scale structures.

Another strong evidence for the presence of dark matter is given by the rotation curves of galaxies. In fact, if we assume a spherical or ellipsoidal mass distribution inside the galaxy, the orbital velocity at a radius r is given by Newton's equation of motion. The peculiar velocity of stars beyond the visible edge of the galaxy should then decrease as $1/r$. What is instead observed is that the velocity stays nearly constant with r . This requires a halo of invisible, dark, matter to be present outside the edge. Galactic size should then be extended beyond the visible edge. From observations it follows that the halo radius is at least 10 times larger than the radius of visible part of the galaxy. Then it follows that a halo is at least 10 times more massive than all stars in a galaxy.

Neutrinos were considered as the best candidate for dark matter about twenty years ago. Indeed, it was shown that if these particles have a small mass $m_\nu \sim 30$ eV, they provide a large energy density contribution up to critical density. Tremaine and Gunn (1979) have claimed, however, that massive neutrinos cannot be considered as dark matter. Their paper was very influential and turned most of cosmologists away from neutrinos as cosmologically important particles.

Tremaine and Gunn paper was based on estimation of lower and upper bounds for neutrino mass; when contradiction with these bounds was found, the conclusion was made that neutrinos cannot supply dark matter. The upper bound was given by cosmological considerations, but compared with the energy density of clustered matter. It is possible, however, that a fraction of neutrinos lays outside galaxies.

Moreover, their lower bound was found on the basis of considerations of galactic halos and derived on the ground of the classical Maxwell-Boltzmann statistics. Gao and Ruffini (1980) established a lower limit on the neutrino mass by the assumption that galactic halos are composed by degenerate neutrinos. Subsequent development of their approach Arbolino and Ruffini (1988) has shown that contradiction with two limits can be avoided.

At the same time, in 1977 the paper by Lee and Weinberg (1977) appeared, in which authors turned their attention to massive neutrinos with $m_\nu > 2$ GeV. Such particles could also provide a large contribution into the energy density of the Universe, in spite of much smaller value of number density.

Recent experimental results from laboratory (see Dolgov (2002) for a review) rule out massive neutrinos with $m_\nu > 2$ GeV. However, the paper by Lee and Weinberg was among the first where very massive particles were considered as candidates for dark matter. This can be considered as the first of cold dark matter models.

Today the interest toward neutrinos as a candidate for dark matter came down, since from one side, the laboratory limit on its mass do not allow for significant contribution to the density of the Universe, and from other side, conventional neutrino dominated models have problems with formation of structure on small scales. However, in these scenarios the role of the chemical potential of neutrinos was overlooked, while it could help solving both problems.

3.3.1. Massive neutrino and structure formation

Lattanzi et al. (2003) have studied the possible role of massive neutrinos in the large scale structure formation. Although now it is clear, that massive light neutrinos cannot be the dominant part of the dark matter, their influence on the large scale structure formation should not be underestimated. In particular, large lepton asymmetry, still allowed by observations, can affect

cosmological constraints on neutrino mass.

3.3.2. Cellular structure of the Universe

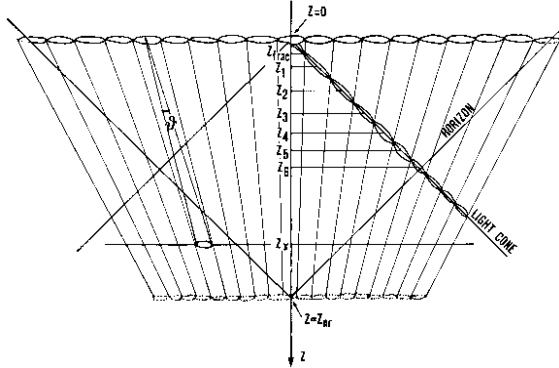


Figure 3.1.: Cellular structure of the Universe.

One of the interesting possibilities, from a conceptual point of view, is the change from the description of the physical properties by a continuous function, to a new picture by introducing a self-similar fractal structure. This approach has been relevant, since the concept of homogeneity and isotropy formerly apply to any geometrical point in space and leads to the concept of a Universe observer-homogeneous Ruffini (1989). Calzetti et al. (1987), Giavalisco (1992), Calzetti et al. (1988) have defined the correlation length of a fractal

$$r_0 = \left(1 - \frac{\gamma}{3}\right)^{1/\gamma} R_S, \quad (3.3.1)$$

where R_S is the sample size, $\gamma = 3 - D$, and D is the Hausdorff dimension of the fractal. Most challenging was the merging of the concepts of fractal, Jeans mass of dark matter and the cellular structure in the Universe, advanced by Ruffini et al. (1988). The cellular structure emerging from this study is represented in Figure 3.1. There the upper cutoff in the fractal structure $R_{\text{cutoff}} \approx 100$ Mpc, was associated to the Jeans mass of the "ino" $M_{\text{cell}} = \left(\frac{m_{pl}}{m_{ino}}\right)^2 m_{pl}$. Details see in Appendix D.

3.3.3. Lepton asymmetry of the Universe

Lattanzi et al. (2005), Lattanzi et al. (2006) studied how the cosmological constraints on neutrino mass are affected by the presence of a lepton asymmetry. The main conclusion is that while constraints on neutrino mass do not change

by the inclusion into the cosmological model the dimensional chemical potential of neutrino, as an additional parameter, the value of lepton asymmetry allowed by the present cosmological data is surprisingly large, being

$$L = \sum_{\nu} \frac{n_{\nu} - n_{\bar{\nu}}}{n_{\gamma}} \lesssim 0.9, \quad (3.3.2)$$

Therefore, large lepton asymmetry is not ruled out by the current cosmological data. Details see in Appendix E.

3. Brief description

4. Publications

4.1. Publications before 2005

1. R. Ruffini, D. J. Song, and L. Stella, "On the statistical distribution off massive fermions and bosons in a Friedmann universe" *Astronomy and Astrophysics*, Vol. 125, (1983) pp. 265-270.

The distribution function of massive Fermi and Bose particles in an expanding universe is considered as well as some associated thermodynamic quantities, pressure and energy density. These considerations are then applied to cosmological neutrinos. A new limit is derived for the degeneracy of a cosmological gas of massive neutrinos.

2. R. Ruffini and D. J. Song, "On the Jeans mass of weakly interacting neutral massive leptons", in *Gamow cosmology*, eds. F. Melchiorri and R. Ruffini, (1986) pp. 370-385.

The cosmological limits on the abundances and masses of weakly interacting neutral particles are strongly affected by the nonzero chemical potentials of these leptons. For heavy leptons ($m_x > \text{GeV}$), the value of the chemical potential must be much smaller than unity in order not to give very high values of the cosmological density parameter and the mass of heavy leptons, or they will be unstable. The Jeans' mass of weakly interacting neutral particles could give the scale of cosmological structure and the masses of astrophysical objects. For a mass of the order 10 eV, the Jeans' mass could give the scenario of galaxy formation, the supercluster forming first and then the smaller scales, such as clusters and galaxies, could form inside the large supercluster.

3. D. Calzetti, M. Giavalisco, R. Ruffini, J. Einasto, and E. Saar, "The correlation function of galaxies in the direction of the Coma cluster", *Astrophysics and Space Science*, Vol. 137 (1987) pp. 101-106.

Data obtained by Einasto et al. (1986) on the amplitude of the correlation function of galaxies in the direction of the Coma cluster are compared with theoretical predictions of a model derived for a self-similar observer-homogeneous structure. The observational samples can be approximated by cones of angular width alpha of about 77 deg. Eliminating sources of large observational error, and by making a specified correction, the observational data are found to agree very well with the theoretical predictions of Calzetti et al. (1987).

4. Publications

4. R. Ruffini, D. J. Song, and S. Taraglio, "The 'ino' mass and the cellular large-scale structure of the universe", *Astronomy and Astrophysics*, Vol. 190, (1988) pp. 1-9.

Within the theoretical framework of a Gamow cosmology with massive "inos", the authors show how the observed correlation functions between galaxies and between clusters of galaxies naturally lead to a "cellular" structure for the Universe. From the size of the "elementary cells" they derive constraints on the value of the masses and chemical potentials of the cosmological "inos". They outline a procedure to estimate the "effective" average mass density of the Universe. They also predict the angular size of the inhomogeneities to be expected in the cosmological black body radiation as remnants of this cellular structure. A possible relationship between the model and a fractal structure is indicated.

5. D. Calzetti, M. Giavalisco, and R. Ruffini, "The normalization of the correlation functions for extragalactic structures", *Astronomy and Astrophysics*, Vol. 198 (1988), pp. 1-15.

It is shown that the spatial two-point correlation functions for galaxies, clusters and superclusters depend explicitly on the spatial volume of the statistical sample considered. Rules for the normalization of the correlation functions are given and the traditional classification of galaxies into field galaxies, clusters and superclusters is replaced by the introduction of a single fractal structure, with a lower cut-off at galactic scales. The roles played by random and stochastic fractal components in the galaxy distribution are discussed in detail.

6. M. V. Arbolino and R. Ruffini, "The ratio between the mass of the halo and visible matter in spiral galaxies and limits on the neutrino mass", *Astronomy and Astrophysics*, Vol. 192, (1988) pp. 107-116.

Observed rotation curves for galaxies with values of the visible mass ranging over three orders of magnitude together with considerations involving equilibrium configurations of massive neutrinos, impose constraints on the ratio between the masses of visible and dark halo components in spiral galaxies. Upper and lower limits are derived for the mass of the particles making up the dark matter.

7. A. Bianconi, H. W. Lee, and R. Ruffini, "Limits from cosmological nucleosynthesis on the leptonic numbers of the universe", *Astronomy and Astrophysics*, Vol. 241 (1991) pp. 343-357.

Constraints on chemical potentials and masses of 'inos' are calculated using cosmological standard nucleosynthesis processes. It is shown that the electron neutrino chemical potential (ENCP) should not be greater than a value of the order of 1, and that the possible effective chemical potential of the other neutrino species should be about 10 times the ENCP in order not to conflict

with observational data. The allowed region (consistent with the He-4 abundance observations) is insensitive to the baryon to proton ratio η , while those imposed by other light elements strongly depend on η .

8. R. Ruffini, J. D. Salmonson, J. R. Wilson, and S.-S. Xue, "On the pair electromagnetic pulse of a black hole with electromagnetic structure", *Astronomy and Astrophysics*, Vol. 350 (1999) pp. 334-343.

We study the relativistically expanding electron-positron pair plasma formed by the process of vacuum polarization around an electromagnetic black hole (EMBH). Such processes can occur for EMBH's with mass all the way up to $6 \cdot 10^5 M_\odot$. Beginning with a idealized model of a Reissner-Nordstrom EMBH with charge to mass ratio $\xi = 0.1$, numerical hydrodynamic calculations are made to model the expansion of the pair-electromagnetic pulse (PEM pulse) to the point that the system is transparent to photons. Three idealized special relativistic models have been compared and contrasted with the results of the numerically integrated general relativistic hydrodynamic equations. One of the three models has been validated: a PEM pulse of constant thickness in the laboratory frame is shown to be in excellent agreement with results of the general relativistic hydrodynamic code. It is remarkable that this precise model, starting from the fundamental parameters of the EMBH, leads uniquely to the explicit evaluation of the parameters of the PEM pulse, including the energy spectrum and the astrophysically unprecedented large Lorentz factors (up to $6 \cdot 10^3$ for a $10^3 M_\odot$ EMBH). The observed photon energy at the peak of the photon spectrum at the moment of photon decoupling is shown to range from 0.1 MeV to 4 MeV as a function of the EMBH mass. Correspondingly the total energy in photons is in the range of 10^{52} to 10^{54} ergs, consistent with observed gamma-ray bursts. In these computations we neglect the presence of baryonic matter which will be the subject of forthcoming publications.

9. R. Ruffini, J. D. Salmonson, J. R. Wilson, and S.-S. Xue, "On the pair-electromagnetic pulse from an electromagnetic black hole surrounded by a baryonic remnant", *Astronomy and Astrophysics*, Vol. 359 (2000) pp. 855-864.

The interaction of an expanding Pair-Electromagnetic pulse (PEM pulse) with a shell of baryonic matter surrounding a Black Hole with electromagnetic structure (EMBH) is analyzed for selected values of the baryonic mass at selected distances well outside the dyadosphere of an EMBH. The dyadosphere, the region in which a super critical field exists for the creation of e^+e^- pairs, is here considered in the special case of a Reissner-Nordstrom geometry. The interaction of the PEM pulse with the baryonic matter is described using a simplified model of a slab of constant thickness in the laboratory frame (constant-thickness approximation) as well as performing the integration of the general relativistic hydrodynamical equations. Te validation of the constant-thickness approximation, already presented in a previous paper Ruffini et al. (1999) for a

PEM pulse in vacuum, is here generalized to the presence of baryonic matter. It is found that for a baryonic shell of mass-energy less than 1% of the total energy of the dyadosphere, the constant-thickness approximation is in excellent agreement with full general relativistic computations. The approximation breaks down for larger values of the baryonic shell mass, however such cases are of less interest for observed Gamma Ray Bursts (GRBs). On the basis of numerical computations of the slab model for PEM pulses, we describe (i) the properties of relativistic evolution of a PEM pulse colliding with a baryonic shell; (ii) the details of the expected emission energy and observed temperature of the associated GRBs for a given value of the EMBH mass; $10^3 M_\odot$, and for baryonic mass-energies in the range 10^{-8} to 10^{-2} the total energy of the dyadosphere.

10. M. Lattanzi, R. Ruffini, and G. Vereshchagin, "On the possible role of massive neutrinos in cosmological structure formation", in Cosmology and Gravitation, eds. M. Novello and S. E. Perez Bergliaffa, Vol. 668 of AIP Conference Series, (2003) pp. 263–287.

In addition to the problem of galaxy formation, one of the greatest open questions of cosmology is represented by the existence of an asymmetry between matter and antimatter in the baryonic component of the Universe. We believe that a net lepton number for the three neutrino species can be used to understand this asymmetry. This also implies an asymmetry in the matter-antimatter component of the leptons. The existence of a nonnull lepton number for the neutrinos can easily explain a cosmological abundance of neutrinos consistent with the one needed to explain both the rotation curves of galaxies and the flatness of the Universe. Some propedeutic results are presented in order to attack this problem.

4.2. Publications (2005 - 2007)

1. A.G. Aksenov, R. Ruffini and G.V. Vereshchagin, "Thermalization of nonequilibrium electron-positron-photon plasmas", Physical Review Letters, Vol. 99 (2007) No 12, 125003.

Starting from a nonequilibrium configuration we analyze the role of the direct and the inverse binary and triple interactions in reaching thermal equilibrium in a homogeneous isotropic pair plasma. We focus on energies in the range $0.1 - 10$ MeV. We numerically integrate the relativistic Boltzmann equation with the exact QED collisional integrals taking into account all binary and triple interactions. We show that first, when a detailed balance is reached for all binary interactions on a time scale $t_k < 10^{-14}$ sec, photons and electron-positron pairs establish kinetic equilibrium. Subsequently, when triple interactions satisfy the detailed balance on a time scale $t_{eq} < 10^{-12}$ sec, the plasma

reaches thermal equilibrium. It is shown that neglecting the inverse triple interactions prevents reaching thermal equilibrium. Our results obtained in the theoretical physics domain also find application in astrophysics and cosmology.

2. C.L. Bianco, R. Ruffini, G.V. Vereshchagin and S.-S. Xue, "Equations of Motion and Initial and Boundary Conditions for Gamma-ray Burst", Journal of the Korean Physical Society, Vol. 49 (2006) No. 2, pp. 722-731.

We compare and contrast the different approaches to the optically thick adiabatic phase of GRB all the way to the transparency. Special attention is given to the role of the rate equation to be self consistently solved with the relativistic hydrodynamic equations. The works of Shemi and Piran (1990), Piran, Shemi and Narayan (1993), Meszaros, Laguna and Rees (1993) and Ruffini, Salmonson, Wilson and Xue (1999,2000) are compared and contrasted. The role of the baryonic loading in these three treatments is pointed out. Constraints on initial conditions for the fireball produced by electro-magnetic black hole are obtained.

3. P. Singh, K. Vandersloot and G.V. Vereshchagin, "Nonsingular bouncing universes in loop quantum cosmology", Physical Review D, Vol. 74 (2006) 043510.

Nonperturbative quantum geometric effects in loop quantum cosmology (LQC) predict a ρ^2 modification to the Friedmann equation at high energies. The quadratic term is negative definite and can lead to generic bounces when the matter energy density becomes equal to a critical value of the order of the Planck density. The nonsingular bounce is achieved for arbitrary matter without violation of positive energy conditions. By performing a qualitative analysis we explore the nature of the bounce for inflationary and cyclic model potentials. For the former we show that inflationary trajectories are attractors of the dynamics after the bounce implying that inflation can be harmoniously embedded in LQC. For the latter difficulties associated with singularities in cyclic models can be overcome. We show that nonsingular cyclic models can be constructed with a small variation in the original cyclic model potential by making it slightly positive in the regime where scalar field is negative.

4. M. Lattanzi, R. Ruffini and G.V. Vereshchagin, "Joint constraints on the lepton asymmetry of the Universe and neutrino mass from the Wilkinson Microwave Anisotropy Probe", Physical Review D, Vol. 72 (2005) 063003.

We use the Wilkinson Microwave Anisotropy Probe (WMAP) data on the spectrum of cosmic microwave background anisotropies to put constraints on the present amount of lepton asymmetry L , parametrized by the dimensionless chemical potential (also called degeneracy parameter) ξ and on the effective

number of relativistic particle species. We assume a flat cosmological model with three thermally distributed neutrino species having all the same mass and chemical potential, plus an additional amount of effectively massless exotic particle species. The extra energy density associated to these species is parametrized through an effective number of additional species ΔN_{others}^{eff} . We find that $0 < |\xi| < 1.1$ and correspondingly $0 < |L| < 0.9$ at 2σ , so that WMAP data alone cannot firmly rule out scenarios with a large lepton number; moreover, a small preference for this kind of scenarios is actually found. We also discuss the effect of the asymmetry on the estimation of other parameters and, in particular, of the neutrino mass. In the case of perfect lepton symmetry, we obtain the standard results. When the amount of asymmetry is left free, we find at 2sigma. Finally we study how the determination of $|L|$ is affected by the assumptions on ΔN_{others}^{eff} . We find that lower values of the extra energy density allow for larger values of the lepton asymmetry, effectively ruling out, at 2sigma level, lepton symmetric models with $\Delta N_{others}^{eff} \simeq 0$.

5. G.V. Vereshchagin, "Gauge Theories of Gravity with the Scalar Field in Cosmology", in "Frontiers in Field Theory", edited by O. Kovras, Nova Science Publishers, New York, (2005), pp. 213-255 (ISBN: 1-59454-127-2).

Brief introduction into gauge theories of gravity is presented. The most general gravitational lagrangian including quadratic on curvature, torsion and non-metricity invariants for metric-affine gravity is given. Cosmological implications of gauge gravity are considered. The problem of cosmological singularity is discussed within the framework of general relativity as well as gauge theories of gravity. We consider the role of scalar field in connection to this problem. Initial conditions for nonsingular homogeneous isotropic Universe filled by single scalar field are discussed within the framework of gauge theories of gravity. Homogeneous isotropic cosmological models including ultrarelativistic matter and scalar field with gravitational coupling are investigated. We consider different symmetry states of effective potential of the scalar field, in particular restored symmetry at high temperatures and broken symmetry. Obtained bouncing solutions can be divided in two groups, namely nonsingular inflationary and

oscillating solutions. It is shown that inflationary solutions exist for quite general initial conditions like in the case of general relativity. However, the phase space of the dynamical system, corresponding to the cosmological equations is bounded. Violation of the uniqueness of solutions on the boundaries of the phase space takes place. As a result, it is impossible to define either the past or the future for a given solution. However, definitely there are singular solutions and therefore the problem of cosmological singularity cannot be solved in models with the scalar field within gauge theories of gravity.

6. R. Ruffini, M. G. Bernardini, C. L. Bianco, L. Caito, P. Chardonnet, M.

G. Dainotti, F. Fraschetti, R. Guida, M. Rotondo, G. Vereshchagin, L. Vitagliano, S.-S. Xue,

"The Blackholic energy and the canonical Gamma-Ray Burst" in Cosmology and Gravitation: XIIth Brazilian School of Cosmology and Gravitation, edited by M. Novello and S.E. Perez Bergliaffa, AIP Conference Proceedings, Vol. 910, Melville, New York, 2007, pp. 55-217.

Gamma-Ray Bursts (GRBs) represent very likely "the" most extensive computational, theoretical and observational effort ever carried out successfully in physics and astrophysics. The extensive campaign of observation from space based X-ray and γ -ray observatory, such as the Vela, CGRO, BeppoSAX, HETE-II, INTEGRAL, Swift, R-XTE, Chandra, XMM satellites, have been matched by complementary observations in the radio wavelength (e.g. by the VLA) and in the optical band (e.g. by VLT, Keck, ROSAT). The net result is unprecedented accuracy in the received data allowing the determination of the energetics, the time variability and the spectral properties of these GRB sources. The very fortunate situation occurs that these data can be confronted with a mature theoretical development. Theoretical interpretation of the above data allows progress in three different frontiers of knowledge: a) the ultrarelativistic regimes of a macroscopic source moving at Lorentz gamma factors up to ~ 400 ; b) the occurrence of vacuum polarization process verifying some of the yet untested regimes of ultrarelativistic quantum field theories; and c) the first evidence for extracting, during the process of gravitational collapse leading to the formation of a black hole, amounts of energies up to 10^{55} ergs of blackholic energy — a new form of energy in physics and astrophysics. We outline how this progress leads to the confirmation of three interpretation paradigms for GRBs proposed in July 2001. Thanks mainly to the observations by Swift and the optical observations by VLT, the outcome of this analysis points to the existence of a "canonical" GRB, originating from a variety of different initial astrophysical scenarios. The commonality of these GRBs appears to be that they all are emitted in the process of formation of a black hole with a negligible value of its angular momentum. The following sequence of events appears to be canonical: the vacuum polarization process in the dyadosphere with the creation of the optically thick self accelerating electron-positron plasma; the engulfment of baryonic mass during the plasma expansion; adiabatic expansion of the optically thick "fireshell" of electron-positron-baryon plasma up to the transparency; the interaction of the accelerated baryonic matter with the interstellar medium (ISM). This leads to the canonical GRB composed of a proper GRB (P-GRB), emitted at the moment of transparency, followed by an extended afterglow. The sole parameters in this scenario are the total energy of the dyadosphere E_{dyu} , the fireshell baryon loading M_B defined by the dimensionless parameter $B = M_B c^2 / E_{dyu}$, and the ISM filamentary distribution around the source. In the limit $B \rightarrow 0$ the total energy is radiated in the P-GRB with a vanishing contribution in the afterglow. In this limit, the canonical

4. Publications

GRBs explain as well the short GRBs. In these lecture notes we systematically outline the main results of our model comparing and contrasting them with the ones in the current literature. In both cases, we have limited ourselves to review already published results in refereed publications. We emphasize as well the role of GRBs in testing yet unexplored grounds in the foundations of general relativity and relativistic field theories.

7. M. Lattanzi, R. Ruffini and G.V. Vereshchagin, "Do WMAP data constraint the lepton asymmetry of the Universe to be zero?" in Albert Einstein Century International Conference, edited by J.-M. Alimi, and A. Füzfa, AIP Conference Proceedings, Vol. 861, Melville, New York, 2006, pp.912-919.

It is shown that extended flat Λ CDM models with massive neutrinos, a sizeable lepton asymmetry and an additional contribution to the radiation content of the Universe, are not excluded by the Wilkinson Microwave Anisotropy Probe (WMAP) first year data. We assume a flat cosmological model with three thermally distributed neutrino species having all the same mass and chemical potential, plus an additional amount of effectively massless exotic particle species X. After maximizing over seven other cosmological parameters, we derive from WMAP first year data the following constraints for the lepton asymmetry L of the Universe (95% CL): $0 < |L| < 0.9$, so that WMAP data alone cannot firmly rule out scenarios with a large lepton number; moreover, a small preference for this kind of scenarios is actually found. We also find for the neutrino mass $m_\nu < 1.2\text{eV}$ and for the effective number of relativistic particle species $-0.45 < \Delta N^{eff} < 2.10$, both at 95% CL. The limit on ΔN^{eff} is more restrictive than others found in the literature, but we argue that this is due to our choice of priors.

8. R. Ruffini, C.L. Bianco, G.V. Vereshchagin, S.-S. Xue "Baryonic loading and e^+e^- rate equation in GRB sources" to appear in the proceedings of "Relativistic Astrophysics and Cosmology - Einstein's Legacy" Meeting, November 7-11, 2005, Munich, Germany.

The expansion of the electron-positron plasma in the GRB phenomenon is compared and contrasted in the treatments of Meszaros, Laguna and Rees, of Shemi, Piran and Narayan, and of Ruffini et al. The role of the correct numerical integration of the hydrodynamical equations, as well as of the rate equation for the electron-positron plasma loaded with a baryonic mass, are outlined and confronted for crucial differences.

9. G.V. Vereshchagin, M. Lattanzi, H.W. Lee, R. Ruffini, "Cosmological massive neutrinos with nonzero chemical potential: I. Perturbations in cosmological models with neutrino in ideal fluid approximation", in proceedings of the Xth Marcel Grossmann Meeting on Recent Develop-

ments in Theoretical and Experimental General Relativity, World Scientific: Singapore, 2005, vol. 2, pp. 1246-1248.

Recent constraints on neutrino mass and chemical potential are discussed with application to large scale structure formation. Power spectra in cosmological model with hot and cold dark matter, baryons and cosmological term are calculated in newtonian approximation using linear perturbation theory. All components are considered to be ideal fluids. Dissipative processes are taken into account by initial spectrum of perturbations so the problem is reduced to a simple system of equations. Our results are in good agreement with those obtained before using more complicated treatments.

10. M. Lattanzi, H.W. Lee, R. Ruffini, G.V. Vereshchagin, "Cosmological massive neutrinos with nonzero chemical potential: II. Effect on the estimation of cosmological parameters", in proceedings of the Xth Marcel Grossmann Meeting on Recent Developments in Theoretical and Experimental General Relativity, World Scientific: Singapore, 2005, vol. 2, pp. 1255-1257.

The recent analysis of the cosmic microwave background data carried out by the WMAP team seems to show that the sum of the neutrino mass is <0.7 eV. However, this result is not model-independent, depending on precise assumptions on the cosmological model. We study how this result is modified when the assumption of perfect lepton symmetry is dropped out.

11. R. Ruffini, M. Lattanzi and G. Vereshchagin, "On the possible role of massive neutrinos in cosmological structure formation" in Cosmology and Gravitation: Xth Brazilian School of Cosmology and Gravitation, edited by M. Novello and S.E. Perez Bergliaffa, AIP Conference Proceedings, Vol. 668, Melville, New York, 2003, pp.263-287.

In addition to the problem of galaxy formation, one of the greatest open questions of cosmology is represented by the existence of an asymmetry between matter and antimatter in the baryonic component of the Universe. We believe that a net lepton number for the three neutrino species can be used to understand this asymmetry. This also implies an asymmetry in the matter-antimatter component of the leptons. The existence of a nonnull lepton number for the neutrinos can easily explain a cosmological abundance of neutrinos consistent with the one needed to explain both the rotation curves of galaxies and the flatness of the Universe. Some propedeutic results are presented in order to attack this problem.

4.3. Publications (2008)

1. A.G. Aksenov, C.L. Bianco, R. Ruffini and G.V. Vereshchagin, "GRBs and the thermalization process of electron-positron plasmas" in the Pro-

ceedings of the "Gamma Ray Bursts 2007" meeting, AIP Conf.Proc. 1000 (2008) 309-312.

We discuss temporal evolution of the pair plasma, created in Gamma-Ray Bursts sources. A particular attention is paid to the relaxation of plasma into thermal equilibrium. We also discuss the connection between the dynamics of expansion and spatial geometry of plasma. The role of the baryonic loading parameter is emphasized.

2. A. G. Aksenov, R. Ruffini, and G. V. Vereshchagin, "Thermalization of Electron-Positron-Photon Plasmas with an Application to GRB" in RELATIVISTIC ASTROPHYSICS: 4th Italian-Sino Workshop, AIP Conference Proceedings, Vol. 966, Melville, New York, 2008, pp. 191-196.

The pair plasma with photon energies in the range $0.1 - 10\text{MeV}$ is believed to play crucial role in cosmic Gamma-Ray Bursts. Starting from a nonequilibrium configuration we analyze the role of the direct and the inverse binary and triple interactions in reaching thermal equilibrium in a homogeneous isotropic pair plasma. We numerically integrate the relativistic Boltzmann equation with the exact QED collisional integrals taking into account all binary and triple interactions. We show that first, when a detailed balance is reached for all binary interactions on a time scale $t_k = 10^{-14}\text{sec}$, photons and electronpositron pairs establish kinetic equilibrium. Subsequently, when triple interactions satisfy the detailed balance on a time scale $t_{eq} = 10^{-12}\text{sec}$, the plasma reaches thermal equilibrium. It is shown that neglecting the inverse triple interactions prevents reaching thermal equilibrium. Our results obtained in the theoretical physics domain also find application in astrophysics and cosmology.

3. R. Ruffini, and G. V. Vereshchagin, S.-S. Xue, "Vacuum Polarization and Electron-Positron Plasma Oscillations" in RELATIVISTIC ASTROPHYSICS: 4th Italian-Sino Workshop, AIP Conference Proceedings, Vol. 966, Melville, New York, 2008, pp. 207-212.

We study plasma oscillations of electrons-positron pairs created by the vacuum polarization in an uniform electric field. Our treatment, encompassing the case of $E > E_c$, shows also in the case $E < E_c$ the existence of a maximum Lorentz factor acquired by electrons and positrons and allows determination of the a maximal length of oscillation. We quantitatively estimate how plasma oscillations reduce the rate of pair creation and increase the time scale of the pair production.

4.4. PHD Thesis

Title of the thesis: "Pair plasma and Gamma-Ray Bursts". Supervisor: prof. R. Ruffini. Thesis presented on the 20th of May 2008, at the Department of Physics, University of Rome "Sapienza".

4.5. Invited talks at international conferences

1. "Thermalization of the pair plasma with proton loading"
(with R. Ruffini, and A.G. Aksenov)
Probing Stellar Populations out to the Distant Universe, Cefalu', Italy,
September 7-19, 2008.
2. "Thermalization of the pair plasma with proton loading"
(with R. Ruffini, and A.G. Aksenov)
3rd Stueckelberg Workshop, Pescara, Italy, 8-18 July, 2008.
3. "Thermalization of the pair plasma"
(G.V. Vereshchagin, R. Ruffini, and A.G. Aksenov)
4. "Non-singular solutions in Loop Quantum Cosmology"
(G.V. Vereshchagin)
2nd Stueckelberg Workshop, Pescara, Italy, 3-7 September, 2007.
5. "(From) massive neutrinos and inos and the upper cutoff to the fractal
structure of the Universe (to recent progress in theoretical cosmology)"
(G.V. Vereshchagin, M. Lattanzi and R. Ruffini)
A Century of Cosmology, San Servolo, Venice, Italy, 27-31 August, 2007.
6. "Pair creation and plasma oscillations"
(G.V. Vereshchagin, R. Ruffini, and S.-S. Xue)
4th Italian-Sino Workshop on Relativistic Astrophysics, Pescara, Italy,
20-29 July, 2007.
7. "Thermalization of electron-positron plasma in GRB sources"
(with R. Ruffini, and A.G. Aksenov)
Xth Italian-Korean Symposium on Relativistic Astrophysics, Pescara,
Italy, 25-30 June, 2007.
8. "Kinetics and hydrodynamics of the pair plasma"
(G.V. Vereshchagin, R. Ruffini, C.L. Bianco, A.G. Aksenov)
9. "Pair creation and plasma oscillations"
(G.V. Vereshchagin, R. Ruffini and S.-S. Xue)
Cesare Lattes Meeting on GRBs, Black Holes and Supernovae, Mangaratiba-
Portobello, Brazil, 26 February - 3 March 2007.

4. Publications

10. "Cavallo-Rees classification revisited"
(G.V. Vereshchagin, R.Ruffini and S.-S. Xue)
On recent developments in theoretical and experimental general relativity, gravitation and relativistic field theories: XIth Marcel Grossmann Meeting, Berlin, Germany, 23-29 July, 2006.
11. "Kinetic and thermal equilibria in the pair plasma"
(G.V. Vereshchagin)
The 1st Bego scientific rencontro, Nice, 5-16 February 2006.
12. "From semi-classical LQC to Friedmann Universe"
(G.V. Vereshchagin)
Loops '05, Potsdam, Golm, Max-Plank Institut für Gravitationsphysik (Albert-Einstein-Institut), 10-14 October 2005.
13. "Equations of motion, initial and boundary conditions for GRBs"
(G.V. Vereshchagin, R. Ruffini and S.-S. Xue)
IXth Italian-Korean Symposium on Relativistic Astrophysics, Seoul, Mt. Kumgang, Korea, 19-24 July 2005.
14. "On the Cavallo-Rees classification and GRBs"
(G.V. Vereshchagin, R. Ruffini and S.-S. Xue)
II Italian-Sino Workshop on Relativistic Astrophysics, Pescara, Italy, 10-20 June, 2005.

5. APPENDICES

5. APPENDICES

A. Kinetic instabilities in collisionless ultra-relativistically streaming cold electron-ion plasma

A.1. Introduction

Current interest in collisionless electron-ion plasmas is threefold. First of all, collisionless plasma is thought to exist in astrophysical environments such as jets in active galactic nuclei (see e.g. Begelman et al. (1994); Maraschi (2003)), microquasars, pulsar winds and supernova remnants (see e.g. Blandford and Eichler (1987)), as well as in gamma-ray bursts (GRBs), see e.g. Piran (2005). Secondly, experimental observation and study of such plasma under the same conditions as in astrophysics, is becoming possible also in the laboratory, see e.g. Medvedev and Spitkovsky (2008). Thirdly, collisionless plasma, with its numerous instabilities, is extremely complex object and its theoretical understanding has been boosted only recently, thanks to development and application of fully three-dimensional computer simulations, using extensively parallel computing see e.g. Hededal (2005); Silva (2006).

One of the most interesting phenomena in collisionless plasma is occurrence of collisionless shocks. Such shocks, which unlike usual hydrodynamic shocks are mediated by electromagnetic fields Silva (2006); Waxman (2006), are believed to be places of particle acceleration from the one hand, and intense photon emission from the other hand. Nonrelativistic collisionless shocks are believed to be the sources of photon emission in supernovae remnants Blandford and Eichler (1987), while relativistic shocks are considered as giving origin to the gamma and X-ray radiation coming from GRBs Medvedev and Loeb (1999); Gruzinov and Waxman (1999). Occurrence of such shocks in the case of GRBs is expected due to interaction and subsequent deceleration of ultrarelativistic blast waves propagating from the source of a GRB into a rarefied interstellar medium (ISM). Since, from the one hand, magnetic fields in the ISM can be amplified after the passage of the shock, and, from the other hand, electrons can be accelerated by the shock, conditions for synchrotron emission by electrons, are expected to be reached Medvedev (2000). In fact, it was expected, and partially supported by earlier simula-

A. Kinetic instabilities in collisionless ultra-relativistically streaming cold electron-ion plasma

tions, that electrons are efficiently accelerated by the shock, and their distribution functions acquire a power law form Silva et al. (2003); Frederiksen et al. (2004); Hededal et al. (2004); Nishikawa et al. (2006). Recent simulations, reaching greater spatial and temporal resolution, show that the distribution of particles is thermal-like, with no evidence for power law tails Spitkovsky (2005); Ramirez-Ruiz et al. (2007); Spitkovsky (2008a), see however Spitkovsky (2008b). Even more severe constraints on synchrotron models of GRBs come from the fact that all simulations show quickly decaying electromagnetic field in the downstream. Such a field is too weak to power radiation, which is observed from GRBs Waxman (2006); Chang et al. (2008).

In this Letter we discuss dynamical and microphysical properties of ultra-relativistically expanding into the vacuum plasma shell, being composed of electrons and protons, totally neutral. Such a shell is collisionless and shockless. Development of plasma instabilities in the shell is studied, and, as a consequence, occurrence of inhomogeneous electromagnetic fields, which presence change in turn the dynamics of particles. We argue that many processes, occurring in the shell, remind those, taking place in collisionless shock, among them reaching energy equipartition between electrons, protons and electromagnetic field Chang et al. (2008). Basic difference, however is that electromagnetic fields are generated in all the volume occupied by the shell which is much larger than the volume where magnetic field is sustained in the case of the shock.

The paper is organized as follows. In Section 2 we introduce basic equations and discuss the method. In Section 3 results of numerical simulations are presented. In Section 4 discussion of the main results is given. Conclusions follow in Section 5.

A.2. The method

Consider collisionless ultrarelativistically streaming plasma shell consisting of equal amount N of electrons with mass m_e and protons with mass m_p . Such a plasma is described self-consistently by the system of Vlasov–Maxwell equations which represent plasma as a continuous medium and takes into account only collective interactions of particles via electromagnetic field.

The problem does not contain intrinsic scale and therefore the length is measured in arbitrary units L . Following Diachenko (1985); Ginzburg et al. (2004) we introduce dimensionless units summarized in Tab. A.1.

Table A.1.: Dimensionless units.

Quantity	Units
Charge \tilde{e}_i	$e_i = \tilde{e}_i/e$
Mass \tilde{m}_i	$m_i = \tilde{m}_i/m_e$
Energy \tilde{w}	$w = \tilde{w}/(m_e c^2)$
Momentum $\tilde{\mathbf{p}}$	$\mathbf{p} = \tilde{\mathbf{p}}/(m_e c)$
Electric field strength $\tilde{\mathbf{E}}$	$\mathbf{E} = \tilde{\mathbf{E}} e L / (m_e c^2)$
Magnetic field strength $\tilde{\mathbf{H}}$	$\mathbf{H} = \tilde{\mathbf{H}} e L / (m_e c^2)$
Number density \tilde{n}_i	$n_i = 4\pi e^2 L^2 \tilde{n}_i / (m_e c^2)$
Distribution function \tilde{f}_i	$f_i = 2e^2 \tilde{f}_i / L.$

In these units Vlasov–Maxwell equations read

$$\frac{\partial f_i}{\partial t} + \mathbf{v}_i \frac{\partial f_i}{\partial \mathbf{r}} + e_i (\mathbf{E} + \mathbf{v}_i \times \mathbf{H}) \frac{\partial f_i}{\partial \pm \mathbf{p}} = 0, \quad (\text{A.2.1})$$

$$\frac{\partial \mathbf{E}}{\partial t} - \nabla \times \mathbf{H} + \mathbf{j} = 0, \quad \frac{\partial \mathbf{H}}{\partial t} + \nabla \times \mathbf{E} = 0, \quad (\text{A.2.2})$$

$$\nabla \cdot \mathbf{R} = \rho, \quad \nabla \cdot \mathbf{H} = 0. \quad (\text{A.2.3})$$

where $\mathbf{v}_i = \partial w / \partial \mathbf{p}_i$ is particle velocity, $w = (\mathbf{p}_i^2 + m_i^2)^{1/2}$ is particle energy, and index "i" denotes type of particles. Charge density ρ and current \mathbf{j} are

$$\rho = \sum_i e_i \int f_i(\mathbf{r}, \mathbf{p}, t) d\mathbf{p}, \quad \mathbf{j} = \sum_i e_i \int \mathbf{v}_i f_i(\mathbf{r}, \mathbf{p}, t) d\mathbf{p}. \quad (\text{A.2.4})$$

The difficulty with direct numerical solution of equations (A.2.1-A.2.3) is reflected by the fact that the distribution function depends on seven variables. The problem is intrinsically spatially three-dimensional and time-dependent. Moreover, the number of particles in realistic physical problems is very large.

We adopt a "macroparticle method" Birdsall and Langdon (1985); Sigov (2001) which introduces a grid in the phase space and assigns to each grid a "macroparticle" with the mass m_M and charge e_M given by the sum of masses and charges of particles occupying a given cell. Due to mass and charge conservation it follows that

$$m_M n_M = m_i n_i, \quad e_M n_M = e_i n_i,$$

and then charge to mass ratio e_i/m_i , plasma frequency $\omega_{0i} = (4\pi e^2 n_i/m_i)^{1/2}$ and Debye length $d_i = \omega^{-1}(kT_i/m_i)^{1/2}$ are the same for real particles and macroparticles. Consequently, all dynamical properties of a plasma, consisting of macroparticle are identical to those of a plasma, consisting of real particles.

In our dimensionless units the plasma skin depth is $c/\omega_p = L$. Notice, that

for relativistic systems the plasma frequency depends on the Lorentz gamma factor $\omega_i = \omega_{0i}\Gamma^{-1/2}$, where Γ is bulk Lorentz factor of the plasma.

Vlasov equation (A.2.1) is usually obtained in the plasma theory from the Liouville theorem closing the BBGKY hierarchy by neglecting two-particle correlation functions. Another way to obtain this equation, which shows close relation between the macroparticle method and the Vlasov equation, is due to Klimontovich Klimontovich (1997).

Introducing Klimontovich distribution functions for the microspopic phase density

$$f_i(\mathbf{r}, \mathbf{p}, t) = \int \delta[\mathbf{r} - \mathbf{R}(t, \omega)] \delta[\mathbf{p} - \mathbf{P}(t, \omega)] d\omega, \quad (\text{A.2.5})$$

where ω is Lagrange coordinate along trajectory of the particle, into (A.2.1) we obtain for functions $\mathbf{R}(t, \omega)$, $\mathbf{P}(t, \omega)$ the Hamiltonian system

$$\frac{\partial \mathbf{R}}{\partial t} = \mathbf{v}(\mathbf{P}), \quad \frac{\partial \mathbf{P}}{\partial t} = \sum_i e_i \left[\mathbf{E}(\mathbf{R}, t) + \frac{1}{c} \mathbf{v}(\mathbf{P}) \times \mathbf{H}(\mathbf{R}, t) \right]. \quad (\text{A.2.6})$$

Consequently for the charge density and current we have

$$\begin{aligned} \tilde{\rho}(t, \mathbf{r}) &= \sum_i e_i \int \delta[\mathbf{r} - \mathbf{R}(t, \omega)] d\omega, \\ \tilde{\mathbf{j}}(t, \mathbf{r}) &= \sum_i e_i \int \delta[\mathbf{r} - \mathbf{R}(t, \omega)] \mathbf{v}[\mathbf{P}(t, \omega)] d\omega. \end{aligned}$$

Distribution function in energy is defined as

$$F_i(w) = \frac{dE_i}{dw}, \quad E_i = \int f_i(\mathbf{r}, \mathbf{p}, t) w d\mathbf{p} d\mathbf{r}, \quad (\text{A.2.7})$$

where E_i is the total energy of particles of a given sort.

While Vlasov equation, unlike macroparticle method, deals with ensamble averaged one-particle distribution function, equations (A.2.6) and (A.2.1) and identical for the Klimontovich function (A.2.5). Besides, solution of equations (A.2.2),(A.2.3) and (A.2.6) is an approximate solution to the Vlasov-Maxwell system with the accuracy $\mathcal{O}(\mu)$, where $\mu = (nd)^{-1}$ is the plasma parameter Birdsall and Langdon (1985); Sigov (2001).

A.3. Numerical results

We follow the time evolution of plasma within the spatial region chosen as a three-dimensional rectangular box with the longer side coinciding with the z -direction, having square perpendicular section. This simulation region represents a part of the shell. All particles are located initially at the bottom of

the simulation region, being homogeneously distributed on the plane (x, y) and occupying part of the volume in the range of z coordinate. Velocities of all particles are equal and point in positive z -direction, so particles stream along the longer side of the rectangular box until reach the top.

Soon after simulation starts generation of small-scale inhomogeneous non-stationary electromagnetic field occurs due to plasma instability. Particles moving in such a field deviate from their original trajectories since inhomogeneous electromagnetic field induce randomization of motion of particles. In order to avoid loss of particles periodic boundary conditions are imposed on the walls of the simulation volume.

The simulation region dimensions are $X_0 = Y_0 = 0.3$, $Z_0 = 10.0$. Periodicity conditions guarantee number of particles conservation as well as conservation of projection of their momenta on orthogonal to z -axis plane. Electrons and protons initially have equal number densities $n_e = n_p$. At the moment $t = 0$ the distribution functions of electrons and protons are represented by Dirac δ -functions, which means particles have negligible thermal velocities, compared to their kinetic energy. Initial value of the Lorentz factor $\Gamma_0 = 223.6$. Electromagnetic field is absent. Total number of macroparticles is 1.44×10^6 . One macroparticle represents 25 real particles.

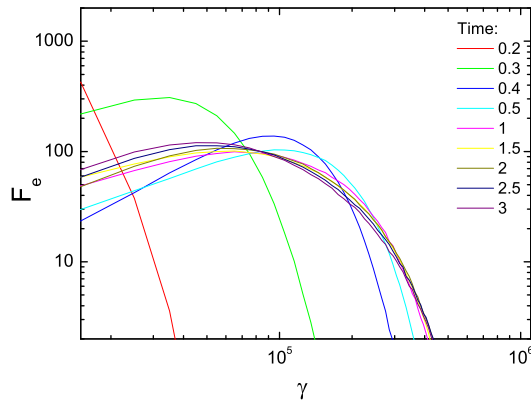


Figure A.1: Energy distribution function of electrons for different time moments. At the moment $t = 0$ the energy distribution is the Dirac δ -function (not shown). In course of time the distribution function spreads and its maximum is shifted to higher energies.

We define the average Lorentz factor of particles $\gamma_i = \sum_a w_a / (Nm_i c^2)$, where a counts particles of a given type and N is total number of particles of a given type. Distribution functions of electrons and protons as functions of their average Lorentz factors are shown in Figs. A.1 and A.2. Initially the distribution functions are represented by the Dirac δ -functions peaked in initial

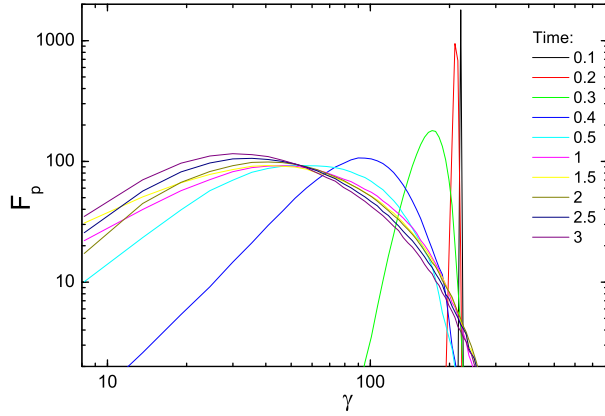


Figure A.2.: Energy distribution function of protons for different time moments. At the moment $t = 0$ the energy distribution is the Dirac δ -function, but protons contain much more energy than electrons due to difference of their masses. In course of time the distribution function spreads and its maximum is shifted to lower energies. This is an indication that the bulk Lorentz factor of the plasma decreases.

value of the Lorentz factor Γ_0 . On a timescale $t \simeq 0.2$ both distribution functions of electrons (protons) spread significantly, also shifting towards higher (lower) energies. It means that average energies of particles start to change, together with the balance of total energy in electrons and protons. This rapid spread of distribution functions proceed until $t \simeq 0.5$, when distributions already remind thermal ones with power law in lower energy part, and exponential decline in the higher energy part. The form of distribution functions does not change substantially after this moment, however the maximum still moves.

The energy of particles, computed as the integral (A.2.7), is shown in Fig. A.3 by the red line for protons and black line for electrons, along with the energy in electromagnetic field (green line). Since the plasma is collisionless, particles can interact only via electromagnetic field. Therefore by the time when distribution functions of electrons and protons start to change we expect generation of electromagnetic fields. This is indeed the case as shown in Fig. A.3. In this way the energy is redistributed not only between the particles, but also between particles and fields. The redistribution process is rather efficient so that at the moment $t \simeq 0.5$ the energy in all components nearly reach equipartition. The energy in particles components experience damped oscillations after $t \simeq 0.5$, while the energy in electromagnetic field grows monotonically reaching super-equipartition values after $t \simeq 2$. The energy conservation is verified by the blue line, shown in Fig A.3.

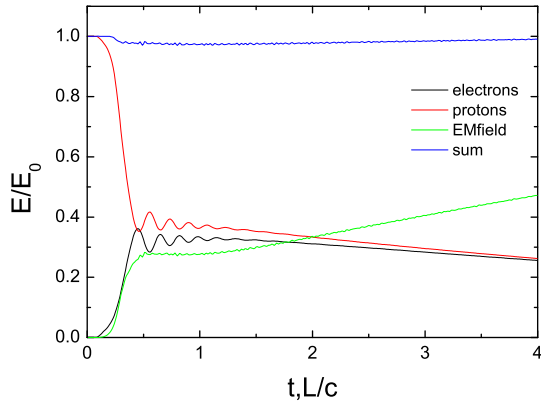


Figure A.3.: Energy of electrons, protons and electromagnetic field in the simulation region. At the moment $t = 0$ almost all energy is stored in kinetic energy of protons. Propagation of particles with different masses (electrons and protons) generate stochastic electromagnetic fields which in turn change trajectories of particles. Thus kinetic energy of protons is transferred into the electromagnetic field. Electrons are accelerated by the structures in this stochastic field, so the energy of protons is transferred into electrons as well. In a short time L/c equipartition of energy is reached for protons, electrons and electromagnetic field. As one can see, later the energy in electromagnetic field is even greater than the energy in protons.

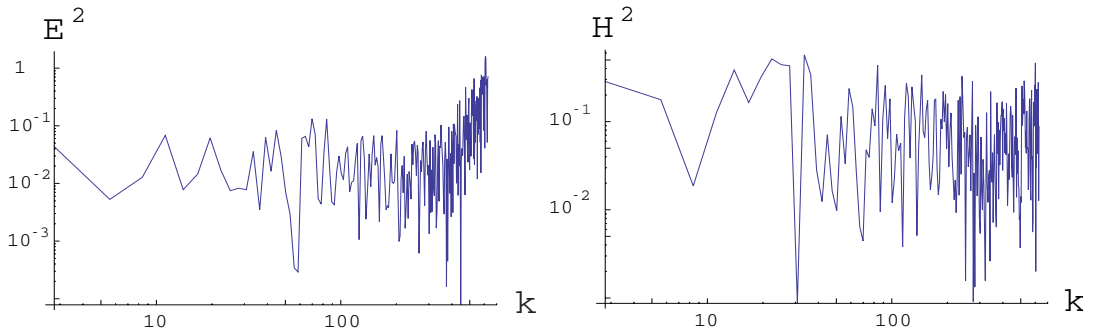


Figure A.4.: Energy density in electric and magnetic fields as function of the wavenumber k , for the moment $t = 1.9$. While most energy is in small-scale fluctuations in electric field, magnetic field fluctuations do not possess characteristic scale.

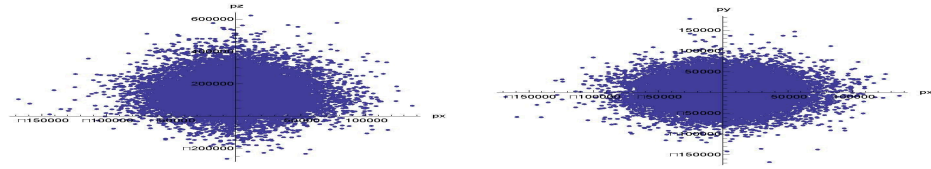


Figure A.5.: Projections of momenta of electrons in p_y, p_x and p_z, p_x planes for $t = 1$. Momentum distribution of particles is anisotropic.

Energy density of electric and magnetic fields as function of the wavenumber k is shown in Fig. A.4 for a section at $X = Y = 0.1, Z$. The corresponding wavelength can be obtained as usual by $l = 2\pi/k$. Most energy in electric field is concentrated as short wavelengths $l \simeq 0.01$.

Momentum distribution of electrons is shown in Fig. A.5, for $t = 1$. At this moment electrons trajectories do not remind initial trajectores and there is considerable amount of particles moving backwards. The momentum distribution is anisotropic in p_z, p_x plane, since majority of particle is moving in the positive z -direction. However, it is isotropic in p_y, p_x plane.

In Fig. A.6 electric and magnetic field strengths are shown in the section of the simulation region with $Z = 7.5$.

A.4. Discussion

In this paper we presented results of numerical simulations of collisionless ultrarelativistically streaming neutral electron-ion plasma. This problem, although showing some similarities with the currently popular collisionless shocks simulation problem, e.g. Spitkovsky (2008a), is at the same time very different. Firstly, in these works collisionless shocks in the electron-positron or electron-ion relativistic plasmas formed due to interaction of counter-streaming relativistic jets are considered, while in our case the medium is *shockless* and streams in only one direction as a whole. Secondly, for the electron-ion case unrealistic values of ion to electron mass ratio are taken, while we consider



Figure A.6.: Electric (left) and magnetic (right) field strengths in sections $Z = 7.5$.

real value of the mass ratio $\tilde{m}_p/\tilde{m}_e = 1836$. Thirdly, most simulations are performed in two-dimensions, while we solve Vlasov-Maxwell equations in fully three-dimensional setup.

Similarities, found between our results and the results of simulations of collisionless shock include: a) generation of stochastic inhomogeneous electromagnetic fields, rapidly changing in space and time; b) equipartition of energies between protons, electrons and electromagnetic fields; c) acceleration of electrons due to stochastization of their motion and energy transfer from protons via scattering on inhomogeneities of electromagnetic fields; d) thermal-like energy distributions of electrons and protons; e) absence of high-energy power-law tails in energy distributions of electrons or protons; f) filament-like spatial structure of magnetic fields.

The major difference, however, with all previous works is that kinetic instability observed in the simulations occurs on spatial scales, much smaller than the skin depth scale c/ω_p .

B. Thermalization of the mildly relativistic plasma

B.1. Introduction

An electron-positron plasma is of interest in many fields of physics and astrophysics. One of the crucial quantities in this analysis is the timescale of the thermalization process. In the early universe Weinberg (1972), Kolb and Turner (1990), Hu (1995), Weinberg (2008) during the lepton era, ultrarelativistic electron-positron pairs contribute to the matter contents of the Universe. In gamma-ray bursts (GRBs) electron-positron pairs play essential role in the dynamics of expansion Goodman (1986), Piran (1999), Ruffini et al. (1999). Indications exist on the presence of the pair plasma also in active galactic nuclei Wardle et al. (1998), in the center of our Galaxy Churazov et al. (2005), around hypothetical quark stars Usov (1998). In the laboratory pair plasma is expected to appear in the fields of ultra intense lasers Blaschke et al. (2006), where particle production may serve as a diagnostic tool for high-energy plasma Kuznetsova et al. (2008).

In many stationary astrophysical sources the pair plasma is thought to be in thermodynamic equilibrium. A detailed study of the relevant processes Bisnovatyi-Kogan et al. (1971), Weaver (1976), Lightman (1982), Gould (1982), Stepney and Guilbert (1983), Coppi and Blandford (1990), radiatiation mechanisms Lightman and Band (1981), possible equilibrium configurations Lightman (1982), Svensson (1982a), Guilbert and Stepney (1985) and spectra Zdziarski (1984) in an optically thin pair plasma has been carried out. Particular attention has been given to collisional relaxation process Gould (1981), Stepney (1983), pair production and annihilation Svensson (1982b), relativistic bremsstrahlung Gould (1980), Haug (1985), double Compton scattering Lightman (1981), Gould (1984).

An equilibrium occurs if the sum of all reaction rates vanishes. For instance, electron-positron pairs are in equilibrium when the net pair production (annihilation) rate is zero. This can be achieved by variety of ways and the corresponding condition can be represented as a system of algebraic equations Svensson (1984). However, the main assumption made in all the above mentioned works is that the plasma is assumed to obey relativistic quantum statistics. The latter is shown to be possible, in principle, in the range of temperatures up to 10 MeV Bisnovatyi-Kogan et al. (1971), Stepney (1983). Our

B. Thermalization of the mildly relativistic plasma

main task is to prove that independently of a wide set of initial conditions, thermal equilibrium forms for the phase space distribution functions are recovered during the process of thermalization by two body and three body direct and inverse particle-particle collisions.

At the same time, in some cases mentioned above the pair plasma can be optically thick. Although moderately thick plasmas have been considered in the literature Guilbert and Stepney (1985), only qualitative description Bisnovatyi-Kogan et al. (1971), Svensson (1982a) is available for large optical depths. Assumption of thermal equilibrium is often adopted for rapidly evolving systems such as GRBs without explicit proof Goodman (1986), Piran (1999), Ruffini et al. (1999), Iwamoto and Takahara (2004). Then hydrodynamic approximation is usually applied both for leptons and photons. However, particles may not be in equilibrium initially. Moreover, they may not reach an equilibrium in rapidly evolving systems such as the early Universe or transient events, when the energy is released on a very short timescale.

Ultrarelativistic expansion of GRBs sources is unprecedented in astrophysics. There are indications that relativistic jets in X-ray binaries have Lorentz factors $\gamma \sim 2 - 10$ while in active galactic nuclei $\gamma \sim 10 - 20$ Miller-Jones et al. (2006). Some GRBs sources have $\gamma \sim 400$ and possibly more Vergani (2007), see however even in the absence of jets []. There is a consensus in the literature that the acceleration required to reach ultrarelativistic velocities in GRBs comes from the pressure of an ultrarelativistic electron-positron pairs and photons. Therefore, the source does not move as a whole, but expands as a finite size shell (in laboratory frame) from a compact region, almost reaching the speed of light. The bulk of radiation is emitted far from the region of formation of the plasma, when it becomes optically thin for photons, trapped initially inside by the huge optical depth. Thus plasma is optically thick at the moment of its formation and intense interactions between electrons, positrons and photons take place in it. Even if initially the energy is released in the form of only photons, or only pairs, the process of creation and annihilation of pairs soon redistribute the energy between particles in such a way that the final state will be a mixture of pairs and photons. The main question arises: *what is the initial state, prior to expansion, of the pair plasma?* Is it in a kind of equilibrium and, if so, is it thermal equilibrium, as expected from the optically thick plasma? Stationary sources in astrophysics have enough time for such an equilibrium to be achieved. On the contrary, for GRBs with the timescale of expansion of the order of milliseconds it is not clear *a priori* that an equilibrium can be reached.

In the literature there is no consensus on this point. Some authors considered thermal equilibrium as the initial state prior to expansion Goodman (1986), Ruffini et al. (1999), while others did not Cavallo and Rees (1978). In fact, the detailed study of the pair plasma equilibrium configurations, performed in Svensson (1982a), cannot answer this question, because essentially nonequilibrium processes have to be considered.

Thus, observations provide motivation for theoretical analysis of physical conditions taking place in the sources of GRBs and, more generally, in nonequilibrium optically thick pair plasma. Notice that there is substantial difference between the ion-electron plasma on the one hand and electron-positron plasma on the other hand. Firstly, the former is collisionless in the wide range of parameters Landau and Lifshitz (1981), while collisions are always essential in the latter. Secondly, when collisions are important relevant interactions in the former case are Coulomb scattering of particles which are usually described by the classical Rutherford cross-section. In contrast, interactions in the pair plasma are described by quantum cross-sections even if the plasma itself can be still treated as classical one.

Our study reported in Aksenov et al. (2007), Aksenov et al. (2008) in the case of pure pair plasma clarified the issue of initial state of the pair plasma in GRBs sources. Our numerical calculations show that the pair plasma on a timescale $t \lesssim 10^{-12}$ sec reach thermal equilibrium prior to expansion, due to intense binary and triple collisions. In this paper we present details about the computational scheme adopted in Aksenov et al. (2007) and turn to a more general case, the pair plasma loaded with baryons. Occurrence of the thermalization process and the corresponding timescales are necessary for determining the dynamics of GRBs. Thermalization timescales $t \lesssim 10^{-12}$ sec are indeed necessary in order to relate the observed properties of GRBs to the nature of the source, see e.g. Ruffini et al. (2007).

B.2. Qualitative description of the pair plasma

First of all we specify the domain of parameters characterizing the pair plasma considered in this paper. It is convenient to use dimensionless parameters usually adopted for this purpose.

We consider mildly relativistic pair plasma, thus the average energy per particle ϵ brackets the electron rest mass energy

$$0.1 \lesssim \frac{\epsilon}{mc^2} \lesssim 10. \quad (\text{B.2.1})$$

The lower boundary is required for significant concentrations of pairs, while the upper boundary is set to avoid substantial production of other particles such as muons and neutrinos.

We define the plasma parameter $g = (n_- d^3)^{-1}$, where $d = \sqrt{\frac{k_B T_-}{4\pi e^2 n_-}} = \frac{c}{\omega} \sqrt{\theta_-}$ is the Debye length, k_B is Boltzmann's constant, e , n_- and T_- are the electron charge, number density and temperature respectively, c the speed of light, $\theta_- = k_B T_- / (mc^2)$ is dimensionless temperature, $\omega = \sqrt{4\pi e^2 n_- / m}$ is the plasma frequency and m is the electron mass. To ensure applicability of kinetic approach it is necessary that the plasma parameter is small, $g \ll 1$.

This condition means that kinetic energy of particles dominates their potential energy due to mutual interaction. For the pair plasma considered in this paper this condition is satisfied.

Further, the classicality parameter, defined as $\varkappa = e^2/(\hbar v_r) = \alpha/\beta_r$, where \hbar is Planck's constant, $\alpha = e^2/(\hbar c)$ is the fine structure constant, $v_r = \beta_r c$ is mean relative velocity of particles, see (B.10.12). The condition $\varkappa \gg 1$ means that particles collisions can be considered classically, while for $\varkappa \ll 1$ quantum description is required. In our case both for pairs and protons quantum cross-sections are used since $\varkappa < 1$.

The strength of screening of the Coulomb interactions is characterized by the Coulomb logarithm $\Lambda = \mathcal{M}dv_r/\hbar$, where \mathcal{M} is the reduced mass. For electron-electron or electron-positron scattering the reduced mass is just $m/2$, while for electron-proton or positron-proton scattering the reduced mass is just the proton mass $\mathcal{M} \simeq M$; for proton-proton scattering $\mathcal{M} \simeq M/2$. Coulomb logarithm varies with mean particle velocity and Debye length, and it cannot be set a constant as is usually done in most of studies of the pair plasma.

Finally, we consider pair plasma with linear dimensions R exceeding the mean free path of photons $l = (n_- \sigma)^{-1}$, where σ is the corresponding total cross-section. Thus the optical depth $\tau = n\sigma R \gg 1$ is large, and interactions between photons and other particles have to be taken in due account. We discuss these interaction in the next Section.

Note that natural parameters for perturbative expansion in the problem under consideration are the fine structure constant α and the electron-proton mass ratio m/M .

B.3. Pure pair plasma

For simplicity we first consider pure pair plasma composed of electrons e^- , positrons e^+ , and photons γ . We will turn to a more general case, including protons p in the next Section. We assume that pairs or photons appear by some physical process in the region with a size R and on a timescale $t < R/c$. We further assume that distribution functions of particles depend neither on spatial coordinates nor on the direction of momenta. We then have $f_i = f_i(\epsilon, t)$, namely we consider isotropic distributions functions in momentum space for a spatially uniform plasma.

To make sure that classical kinetic description is adequate we estimate the dimensionless degeneracy temperature

$$\theta_F = \left[\left(\frac{\hbar}{mc} \right)^2 \left(3\pi^2 n_- \right)^{\frac{2}{3}} + 1 \right]^{1/2} - 1, \quad (\text{B.3.1})$$

and compare it with the estimated temperature in thermal equilibrium. With

our initial conditions (B.2.1) the degeneracy temperature is always smaller than the temperature in thermal equilibrium and therefore we can safely apply the classical kinetic approach. Besides, since we deal with ideal plasma with the plasma parameter $g \sim 10^{-3}$ it is enough to consider only one-particle distribution functions. These considerations justify our computational approach based on classical relativistic Boltzmann equation. At the same time the right hand side of Boltzmann equations contains collisional integrals as functions of quantum matrix elements, as discussed below and in Appendices C-E.

Relativistic Boltzmann equations Belyaev and Budker (1956), Mihalas and Mihalas (1984) in spherically symmetric case for which the original code is designed Aksenov et al. (2004) are

$$\begin{aligned} \frac{1}{c} \frac{\partial f_i}{\partial t} + \beta_i \left(\mu \frac{\partial f_i}{\partial r} + \frac{1 - \mu^2}{r} \frac{\partial f_i}{\partial \mu} \right) - \nabla U \frac{\partial f_i}{\partial \mathbf{p}} = \\ = \sum_q (\eta_i^q - \chi_i^q f_i), \end{aligned} \quad (\text{B.3.2})$$

where $\mu = \cos \vartheta$, ϑ is the angle between the radius vector \mathbf{r} from the origin and the particle momentum \mathbf{p} , U is a potential due to an external force, $\beta_i = v_i/c$ are particles velocities, $f_i(\epsilon, t)$ are their distribution functions, the index i denotes the type of particle, ϵ is its energy, and η_i^q and χ_i^q are the emission and the absorption coefficients for the production of a particle of type “ i ” via the physical process labeled by q . This is a coupled system of partial-integro-differential equations. For homogeneous and isotropic distribution functions of electrons, positrons and photons (B.3.2) reduces to

$$\frac{1}{c} \frac{\partial f_i}{\partial t} = \sum_q (\eta_i^q - \chi_i^q f_i), \quad (\text{B.3.3})$$

which is a coupled system of integro-differential equations. In (B.3.3) we also explicitly neglected the Vlasov term, describing collisionless interaction of particles in the mean field, since energy density of fluctuations of the electromagnetic field are many orders of magnitude smaller than the energy density of particles Lemoine (1995).

Therefore, the left-hand side of the Boltzmann equation is reduced to partial derivative of the distribution function with respect to time. The right-hand side contains collisional integrals, representing interactions between electrons, positrons and photons.

As example of collisional integral consider absorption coefficient for Compton scattering which is given by

$$\chi^{\text{cs}} f_\gamma = \int d\mathbf{k}' d\mathbf{p} d\mathbf{p}' W_{\mathbf{k}', \mathbf{p}'; \mathbf{k}, \mathbf{p}} f_\gamma(\mathbf{k}, t) f_\pm(\mathbf{p}, t), \quad (\text{B.3.4})$$

where \mathbf{p} and \mathbf{k} are momenta of electron (positron) and photon respectively, $d\mathbf{p} = d\epsilon_{\pm} do_{\pm} \beta_{\pm}^2 / c^3$, $d\mathbf{k}' = d\epsilon'_{\gamma} \epsilon'^2_{\gamma} do'_{\gamma} / c^3$ and the transition function $W_{\mathbf{k}', \mathbf{p}'; \mathbf{k}, \mathbf{p}}$ is related to the transition probability differential $dw_{\mathbf{k}', \mathbf{p}'; \mathbf{k}, \mathbf{p}}$ per unit time as

$$W_{\mathbf{k}', \mathbf{p}'; \mathbf{k}, \mathbf{p}} d\mathbf{k}' d\mathbf{p}' \equiv V dw_{\mathbf{k}', \mathbf{p}'; \mathbf{k}, \mathbf{p}}. \quad (\text{B.3.5})$$

The differential probability $dw_{\mathbf{k}', \mathbf{p}'; \mathbf{k}, \mathbf{p}} = w_{\mathbf{k}', \mathbf{p}'; \mathbf{k}, \mathbf{p}} d\mathbf{k}' d\mathbf{p}'$ is given by (B.7.3).

Given the momentum conservation one can perform one integration over $d\mathbf{p}'$ in (B.3.4) as

$$\int d\mathbf{p}' \delta(\mathbf{k} + \mathbf{p} - \mathbf{k}' - \mathbf{p}') \rightarrow 1, \quad (\text{B.3.6})$$

but it is necessary to take into account the momentum conservation in the next integration over $d\mathbf{k}'$, so we have

$$\begin{aligned} & \int d\epsilon'_{\gamma} \delta(\epsilon_{\gamma} + \epsilon_{\pm} - \epsilon'_{\gamma} - \epsilon'_{\pm}) = \\ &= \int d(\epsilon'_{\gamma} + \epsilon'_{\pm}) \frac{1}{|\partial(\epsilon'_{\gamma} + \epsilon'_{\pm})/\partial\epsilon'_{\gamma}|} \delta(\epsilon_{\gamma} + \epsilon_{\pm} - \epsilon'_{\gamma} - \epsilon'_{\pm}) \rightarrow \\ & \rightarrow \frac{1}{|\partial(\epsilon'_{\gamma} + \epsilon'_{\pm})/\partial\epsilon'_{\gamma}|} \equiv J_{\text{cs}}, \end{aligned} \quad (\text{B.3.7})$$

where the Jacobian of the transformation is

$$J_{\text{cs}} = \frac{1}{1 - \beta'_{\pm} \mathbf{b}'_{\pm} \cdot \mathbf{b}'_{\pm}}, \quad (\text{B.3.8})$$

and $\mathbf{b}_i = \mathbf{p}_i / p$, $\mathbf{b}'_i = \mathbf{p}'_i / p'$, $\mathbf{b}'_{\pm} = (\beta_{\pm} \epsilon_{\pm} \mathbf{b}_{\pm} + \epsilon_{\gamma} \mathbf{b}_{\gamma} - \epsilon'_{\gamma} \mathbf{b}'_{\gamma}) / (\beta'_{\pm} \epsilon'_{\pm})$.

Finally, for the absorption coefficient we have

$$\chi^{\text{cs}} f_{\gamma} = - \int do'_{\gamma} d\mathbf{p} \frac{\epsilon'_{\gamma} |M_{fi}|^2 \hbar^2 c^2}{16 \epsilon_{\pm} \epsilon'_{\gamma} \epsilon'_{\pm}} J_{\text{cs}} f_{\gamma}(\mathbf{k}, t) f_{\pm}(\mathbf{p}, t), \quad (\text{B.3.9})$$

where the matrix element here is dimensionless. This integral is evaluated numerically.

For all binary interactions we use exact QED matrix elements which can be found in the standard textbooks, e.g. in Berestetskii et al. (1982), Greiner and Reinhardt (2003), Akhiezer and Berestetskii (1981), and are given in B.7.

In order to account for charge screening in Coulomb scattering we introduced the minimal scattering angles following Haug (1988), see Section B.10. This allows to apply the same scheme for the computation of emission and absorption coefficients even for Coulomb scattering, while many treatments in the literature use the Fokker-Planck approximation, e.g. Pilla and Shaham (1997).

For such a dense plasma collisional integrals in (B.3.3) should include not

only binary interactions, having order α^2 in Feynmann diagrams, but also triple ones, having order α^3 Berestetskii et al. (1982). As example for triple interactions consider relativistic bremsstrahlung

$$e_1 + e_2 \leftrightarrow e'_1 + e'_2 + \gamma'. \quad (\text{B.3.10})$$

For the time derivative, for instance, of the distribution function f_2 in the direct and in the inverse reactions (B.3.10) one has

$$\begin{aligned} \dot{f}_2 = & \int d\mathbf{p}_1 d\mathbf{p}'_1 d\mathbf{p}'_2 d\mathbf{k}' \left[W_{\mathbf{p}'_1, \mathbf{p}'_2, \mathbf{k}'; \mathbf{p}_1, \mathbf{p}_2} f'_1 f'_2 f'_k - \right. \\ & \left. - W_{\mathbf{p}_1, \mathbf{p}_2; \mathbf{p}'_1, \mathbf{p}'_2, \mathbf{k}'} f_1 f_2 \right] = \int d\mathbf{p}_1 d\mathbf{p}'_1 d\mathbf{p}'_2 d\mathbf{k}' \frac{c^6 \hbar^3}{(2\pi)^2} \times \\ & \times \frac{\delta^{(4)}(P_f - P_i) |M_{fi}|^2}{2^5 \epsilon_1 \epsilon_2 \epsilon'_1 \epsilon'_2 \epsilon'_\gamma} \left[f'_1 f'_2 f'_k - \frac{1}{(2\pi\hbar)^3} f_1 f_2 \right], \end{aligned} \quad (\text{B.3.11})$$

where

$$\begin{aligned} d\mathbf{p}_1 d\mathbf{p}_2 W_{\mathbf{p}'_1, \mathbf{p}'_2, \mathbf{k}'; \mathbf{p}_1, \mathbf{p}_2} &\equiv V^2 dw_1, \\ d\mathbf{p}'_1 d\mathbf{p}'_2 d\mathbf{k}' W_{\mathbf{p}_1, \mathbf{p}_2; \mathbf{p}'_1, \mathbf{p}'_2, \mathbf{k}'} &\equiv V dw_2, \end{aligned}$$

and dw_1 and dw_2 are given by (B.12.3) for the inverse and direct process (B.3.10) respectively. The matrix element here has dimensions of the length squared, see Section B.12.

In the case of the distribution functions (B.3.16), see below, we have multipliers proportional to $\exp \frac{v}{k_B T}$ in front of the integrals. The calculation of emission and absorption coefficients is then reduced to the well known thermal equilibrium case Svensson (1984). In fact, since reaction rates of triple interactions are α times smaller than binary reaction rates, we expect that binary reactions come to detailed balance first. Only when binary reactions are all balanced, triple interactions become important. In addition, when binary reactions come into balance, distribution functions already acquire the form (B.3.16). Although there is no principle difficulty in computations using exact matrix elements for triple reactions as well, our simplified scheme allows for much faster numerical computation. The corresponding reaction rates for triple interactions are given in Section B.9.

We consider all possible binary and triple interactions between electrons, positrons and photons as summarized in table B.1.

Each of the above mentioned reactions is characterized by the corresponding timescale and optical depth. For Compton scattering of an electron, for instance, we have

$$t_{\text{cs}} = \frac{1}{\sigma_T n_\pm c}, \quad \tau_{\text{cs}} = \sigma_T n_\pm R, \quad (\text{B.3.12})$$

Binary interactions	Radiative and pair producing variants
Møller and Bhabha $e_1^\pm e_2^\pm \rightarrow e_1^{\pm'} e_2^{\pm'}$ $e^\pm e^\mp \rightarrow e^{\pm'} e^{\mp'}$	Bremsstrahlung $e_1^\pm e_2^\pm \leftrightarrow e_1^{\pm'} e_2^{\pm'} \gamma$ $e^\pm e^\mp \leftrightarrow e^{\pm'} e^{\mp'} \gamma$
Single Compton $e^\pm \gamma \rightarrow e^\pm \gamma'$	Double Compton $e^\pm \gamma \leftrightarrow e^{\pm'} \gamma' \gamma''$
Pair production and annihilation $\gamma \gamma' \leftrightarrow e^\pm e^\mp$	Radiative pair production and 3-photon annihilation $\gamma \gamma' \leftrightarrow e^\pm e^\mp \gamma''$ $e^\pm e^\mp \leftrightarrow \gamma \gamma' \gamma''$ $e^\pm \gamma \leftrightarrow e^{\pm'} e^{\mp} e^{\pm''}$

Table B.1.: Microphysical processes in the pair plasma.

where $\sigma_T = \frac{8\pi}{3}\alpha^2(\frac{\hbar}{mc})^2$ is the Thomson cross-section. There are two timescales in our problem that characterize the condition of detailed balance between direct and inverse reactions, t_{cs} for binary and $\alpha^{-1}t_{\text{cs}}$ for triple interactions respectively.

Notice, that electron-positron pair can annihilate into neutrino channel with the main contribution from the reaction $e^\pm e^\mp \rightarrow \nu \bar{\nu}$. By this process the energy could leak out from the plasma if it is transparent for neutrinos. The optical depth and energy loss for this process has been estimated following Beaudet et al. (1967) by using Fermi theory, see also Dicus (1972), Misiaszek et al. (2006) for calculations within electro-weak theory.

The optical depth is given by (B.3.12) with the cross-section

$$\sigma_{\nu \bar{\nu}} \sim \frac{g^2}{\pi} \left(\frac{\hbar}{mc} \right)^2, \quad (\text{B.3.13})$$

where $g \simeq 10^{-12}$ is the weak interaction coupling constant and we assumed typical energies of electron and positron to be $\sim mc^2$ and their relative velocities $v \sim c$. Numerically $\sigma_{\nu \bar{\nu}}/\sigma_T = \frac{3}{8\pi^2}(g/\alpha)^2 \simeq 7 \times 10^{-22}$. For GRBs sources the plasma may be both transparent and opaque to neutrino production. The energy loss when pairs are relativistic and nondegenerate is

$$\frac{d\rho}{dt} = \frac{128g^2}{\pi^5} \eta(5)\eta(4)\theta^9 mc^2 \left(\frac{mc}{\hbar} \right)^3 \left(\frac{mc^2}{\hbar} \right). \quad (\text{B.3.14})$$

The ratio between the energy lost due to neutrinos and the energy of ph-

tons in thermal equilibrium is then

$$\begin{aligned} \frac{1}{\rho_\gamma} \frac{d\rho}{dt} \Delta t &= \frac{64g^2}{3\pi^3} \eta(5)\eta(4)\theta^5 \left(\frac{mc^2}{\hbar} \right) \Delta t \simeq \\ &\simeq 1.2 \times 10^{-3} \theta^5 \frac{\Delta t}{1 \text{ sec}}. \end{aligned} \quad (\text{B.3.15})$$

For instance, for GRBs sources with the dynamical time $\Delta t \sim 10^{-3}$ sec, the energy loss due to neutrinos becomes relevant Koers and Wijers (2005) for high temperatures $\theta > 15$. However, on the timescale of relaxation to thermal equilibrium $\Delta t \sim 10^{-12}$ sec the energy loss is negligible.

We choose arbitrary initial distribution functions and find a common development. At a certain time t_k the distribution functions always have evolved in a functional form on the entire energy range, and depend only on two parameters. We find in fact for the distribution functions the expressions

$$f_i(\varepsilon) = \frac{2}{(2\pi\hbar)^3} \exp\left(-\frac{\varepsilon - \nu_i}{\theta_i}\right), \quad (\text{B.3.16})$$

with chemical potential $\nu_i \equiv \frac{\varphi_i}{mc^2}$ and temperature $\theta_i \equiv \frac{k_B T_i}{m_e c^2}$, where $\varepsilon \equiv \frac{\epsilon}{m_e c^2}$ is the energy of the particle. Such a configuration corresponds to a kinetic equilibrium Kolb and Turner (1990), Pilla and Shaham (1997), Ehlers (1973) in which particles acquire a common temperature and nonzero chemical potentials. At the same time we found that triple interactions become essential for $t > t_k$, after the establishment of kinetic equilibrium. In strict mathematical sense the sufficient condition for reaching thermal equilibrium is when all direct reactions are exactly balanced with their inverse. Therefore, in principle, not only triple, but also four-particle, five-particle and so on reaction have to be accounted for in equation (B.3.3). The timescale for reaching thermal equilibrium will be then determined by the slowest reaction which is not balanced with its inverse. We stress, however, that the necessary condition is the detailed balance at least in triple interactions, since binary reactions do not change chemical potentials.

Notice that similar method to ours was applied in Pilla and Shaham (1997) in order to compute spectra of particles in kinetic equilibrium. However, although the approach was similar, the computation was never carried out in order to actually observe the reaching of thermal equilibrium.

Finally, it is worth mentioning the physical meaning of the chemical potential ν_k in kinetic equilibrium entering the formula (B.3.16). In the case of pure pair plasma a non-zero chemical potential represents deviation from the thermal equilibrium through the relation

$$\nu_k = \theta \ln(n_k/n_{\text{th}}), \quad (\text{B.3.17})$$

where n_{th} are concentrations of particles in thermal equilibrium.

B.4. Proton loading

So far we dealt with leptons, having the same mass but opposite charges. In that case the condition of electric neutrality is identically fulfilled. We described electrons and positrons with the same distribution function. Situation becomes more complicated when admixture of protons is allowed. Since charge neutrality

$$n_- = n_+ + n_p. \quad (\text{B.4.1})$$

is required, the number of electrons is not equal to the number of protons. In such a case a new dimensionless parameter, the baryonic loading \mathbf{B} , can be introduced as

$$\mathbf{B} = \frac{NMc^2}{\mathcal{E}} = \frac{n_p Mc^2}{\rho_r}, \quad (\text{B.4.2})$$

where N and n_p are the number and the concentration of protons, \mathcal{E} and $\rho_r = \rho_\gamma + \rho_+ + \rho_-$ are radiative energy and energy density respectively. Since in relativistic plasma electrons and positrons move with almost the speed of light, both photons and pairs in thermal equilibrium behave as relativistic fluid with equation of state $p_r \simeq \rho_r/3$. At the same time, protons are relatively cold particles, with negligible pressure and dust-like equation of state $p \simeq 0$. In this way by introducing parameter \mathbf{B} we distinguish a radiation-dominated ($\mathbf{B} < 1$) from a matter-dominated ($\mathbf{B} > 1$) plasma. For electrically neutral plasmas there exists an upper limit on the parameter \mathbf{B} defined by (B.4.2), which is $\mathbf{B} \leq M/m$.

In the range of energies (B.2.1) the radiative energy density can be approximated as $\rho_r \sim n_- mc^2$, and then we have for concentrations $n_p \sim n_- \mathbf{B} \frac{m}{M}$. If protons and electrons are at the same temperature then from the equality of the kinetic energy of a proton $\epsilon_{k,p} = \frac{Mv_p^2}{2}$ and the one of an electron $\epsilon_{k,-} \sim mc^2$ we have $\frac{v_p}{c} \sim \sqrt{\frac{m}{M}}$, therefore protons are indeed nonrelativistic.

In presence of protons additional binary reactions consist of Coulomb collisions between electrons (positrons) and protons, scattering of protons on protons and Compton scattering of protons. Additional triple reactions are radiative variants of these reactions, see Table B.2.

Protons can be thermalized in two ways: either in a two-step process first between themselves and then by electron/positron-proton collisions, or just by the latter mechanism. The rate of proton-proton collisions is a factor $\sqrt{\frac{m}{M} \frac{n_p}{n_-}} \sim \mathbf{B} \left(\frac{m}{M}\right)^{3/2}$ smaller than the rate of electron-electron collisions, see (B.8.15). The rate of proton-electron/positron collisions is a factor $\frac{\epsilon}{Mc^2} \sim \frac{m}{M}$ smaller than the one of electron-electron collisions, see (B.8.11). Therefore,

Binary interactions	Radiative and pair producing variants
Coulomb scattering $p_1 p_2 \rightarrow p'_1 p'_2$ $p e^\pm \rightarrow p' e^{\pm\prime}$	Bremsstrahlung $p_1 p_2 \leftrightarrow p'_1 p'_2 \gamma$ $p e^\pm \leftrightarrow p' e^{\pm\prime} \gamma$ $p e_1^\pm \leftrightarrow p' e_1^{\pm\prime} e^\pm e^\mp$
Single Compton $p \gamma \rightarrow p' \gamma'$	Double Compton $p \gamma \leftrightarrow p' \gamma' \gamma''$ $p \gamma \leftrightarrow p' e^\pm e^\mp$

Table B.2.: Microphysical processes in the pair plasma involving protons.

for $\mathbf{B} > \sqrt{\frac{m}{M}}$ proton-proton collisions are faster, while for $\mathbf{B} < \sqrt{\frac{m}{M}}$ proton-electron/positron ones predominate.

B.5. Conservation laws

Conservation laws consist of baryon number, charge and energy conservations. In addition, in binary reactions particle number is conserved.

Energy conservation law can be rewritten for the spectral density

$$\frac{d}{dt} \sum_i \rho_i = 0, \quad \text{or} \quad \frac{d}{dt} \sum_{i,\omega} Y_{i,\omega} = 0, \quad (\text{B.5.1})$$

where

$$Y_{i,\omega} = \int_{\epsilon_{i,\omega} - \Delta\epsilon_{i,\omega}/2}^{\epsilon_{i,\omega} + \Delta\epsilon_{i,\omega}/2} E_i d\epsilon. \quad (\text{B.5.2})$$

Particle's conservation law in binary reactions gives

$$\frac{d}{dt} \sum_i n_i = 0, \quad \text{or} \quad \frac{d}{dt} \sum_{i,\omega} \frac{Y_{i,\omega}}{\epsilon_{i,\omega}} = 0. \quad (\text{B.5.3})$$

Since baryonic number is conserved, therefore the number density of protons is a constant

$$\frac{dn_p}{dt} = 0. \quad (\text{B.5.4a})$$

For electrically neutral plasma considered in this paper charge conservation implies (B.4.1).

B.6. Determination of temperature and chemical potentials in kinetic equilibrium

Consider distribution functions for photons and pairs in the most general form (B.3.16). If one supposes that reaction rate for the Bhabha scattering vanishes, i.e. there is equilibrium with respect to reaction

$$e^+ + e^- \leftrightarrow +e^{+'} + e^{-'}, \quad (\text{B.6.5})$$

then the corresponding condition can be written in the following way

$$f_+(1 - f_+')f_-(1 - f_-') = f_+'(1 - f_+)f_-'(1 + f_-), \quad (\text{B.6.6})$$

where Bose-Einstein enhancement along with Pauli blocking factors are taken into account for generality, it can be shown that electrons and positrons have the same temperature

$$\theta_+ = \theta_- \equiv \theta_\pm, \quad (\text{B.6.7})$$

and they have arbitrary chemical potentials.

With (B.6.7) analogous consideration for the Compton scattering

$$e^\pm + \gamma \leftrightarrow +e^{\pm'} + \gamma', \quad (\text{B.6.8})$$

gives

$$f_\pm(1 - f_\pm')f_\gamma(1 + f_\gamma') = f_\pm'(1 - f_\pm)f_\gamma'(1 + f_\gamma), \quad (\text{B.6.9})$$

and leads to equality of temperatures of pairs and photons

$$\theta_\pm = \theta_\gamma \equiv \theta_k, \quad (\text{B.6.10})$$

with arbitrary chemical potentials. If, in addition, reaction rate in the pair-creation and annihilation process

$$e^\pm + e^\mp \leftrightarrow \gamma + \gamma' \quad (\text{B.6.11})$$

vanishes too, i.e. there is equilibrium with respect to pair production and annihilation, with the corresponding condition,

$$f_+f_-(1 + f_\gamma)(1 + f_\gamma') = f_\gamma f_\gamma'(1 - f_+)(1 - f_-), \quad (\text{B.6.12})$$

it turns out that also chemical potentials of pairs and photons satisfy the following condition

$$\nu_+ + \nu_- = 2\nu_\gamma. \quad (\text{B.6.13})$$

However, since, generally speaking, $\nu_\gamma \neq 0$ the condition (B.6.13) does not imply $\nu_+ = \nu_-$. These considerations were for the first time applied by Ehlers in Ehlers (1973) and we will call (B.6.6),(B.6.9) and (B.6.12) the *Ehlers balance*

	Interaction	Parameters of DFs
I	e^+e^- scattering	$\theta_+ = \theta_-, \forall \nu_+, \nu_-$
II	$e^\pm p$ scattering	$\theta_p = \theta_\pm, \forall \nu_\pm, \nu_p$
III	$e^\pm \gamma$ scattering	$\theta_\gamma = \theta_\pm, \forall \nu_\gamma, \nu_\pm$
IV	pair production	$\nu_+ + \nu_- = 2\nu_\gamma, \text{ if } \theta_\gamma = \theta_\pm$
V	Tripe interactions	$\nu_\gamma, \nu_\pm = 0, \text{ if } \theta_\gamma = \theta_\pm$

Table B.3.: Relations between parameters of equilibrium DFs fulfilling detailed balance conditions for the reactions shown in Tab. B.1.

conditions.

Analogous consideration for the detailed balance conditions in different reactions lead to relations between temperatures and chemical potentials summarized in table B.3.

The timescales of pair production and annihilation processes as well as Compton scattering are nearly equal in the range of energies of interest and are given by (B.3.12). Therefore, kinetic equilibrium is first established simultaneously for electrons, positrons and photons. They reach the same temperature, but with chemical potentials different from zero. Later on, the temperatures of this electron-positron-photon plasma and the one of protons reach a common value.

In order to find temperatures and chemical potentials we have to implement the following constraints: energy conservation (B.5.1), particle number conservation (B.5.3), charge conservation (B.4.1), condition for the chemical potentials (B.6.13).

Given (B.3.16) we have for photons

$$\frac{\rho_\gamma}{n_\gamma mc^2} = 3\theta_\gamma, \quad n_\gamma = \frac{1}{V_0} \exp\left(\frac{\nu_\gamma}{\theta_\gamma}\right) 2\theta_\gamma^3, \quad (\text{B.6.14})$$

for pairs

$$\frac{\rho_\pm}{n_\pm mc^2} = j_2(\theta_\pm), \quad n_\pm = \frac{1}{V_0} \exp\left(\frac{\nu_\pm}{\theta_\pm}\right) j_1(\theta_\pm), \quad (\text{B.6.15})$$

and for protons

$$\frac{\rho_p}{Mn_p c^2} = 1 + \frac{3}{2} \frac{m}{M} \theta_p, \quad (\text{B.6.16})$$

$$n_p = \frac{1}{V_0} \sqrt{\frac{\pi}{2}} \left(\frac{M}{m}\right)^{3/2} \exp\left(\frac{\nu_p - \frac{M}{m}}{\theta_p}\right) \theta_p^{\frac{3}{2}}, \quad (\text{B.6.17})$$

where we assumed that protons are nonrelativistic, and we denoted the Comp-

ton volume

$$V_0 = \frac{1}{8\pi} \left(\frac{2\pi\hbar}{mc} \right)^3, \quad (\text{B.6.18})$$

and functions j_1 and j_2 are defined as

$$j_1(\theta) = \theta K_2(\theta^{-1}) \rightarrow \begin{cases} \sqrt{\frac{\pi}{2}} e^{-\frac{1}{\theta}} \theta^{3/2}, & \theta \rightarrow 0 \\ 2\theta^3, & \theta \rightarrow \infty \end{cases}, \quad (\text{B.6.19})$$

$$j_2(\theta) = \frac{3K_3(\theta^{-1}) + K_1(\theta^{-1})}{4K_2(\theta^{-1})} \rightarrow \begin{cases} 1 + \frac{3\theta}{2}, & \theta \rightarrow 0 \\ 3\theta, & \theta \rightarrow \infty \end{cases}. \quad (\text{B.6.20})$$

For pure electron-positron-photon plasma in kinetic equilibrium, summing up energy densities in (B.6.14),(B.6.15) and using (B.6.7),(B.6.10) and (B.6.13) we obtain

$$\sum_{e^+, e^-, \gamma} \rho_i = \frac{2mc^2}{V_0} \exp\left(\frac{\nu_k}{\theta_k}\right) \left[3\theta^4 + j_1(\theta_k)j_2(\theta_k) \right], \quad (\text{B.6.21})$$

and analogously for number densities we get

$$\sum_{e^+, e^-, \gamma} n_i = \frac{2}{V_0} \exp\left(\frac{\nu_k}{\theta_k}\right) \left[\theta_k^3 + j_1(\theta_k) \right]. \quad (\text{B.6.22})$$

From (B.6.21) and (B.6.22) two unknowns, ν_k and θ_k can be found.

When protons are present, in most cases the electron-positron-photon plasma reaches kinetic equilibrium first, while protons join the plasma later. In that case, the temperature of protons θ_p is different from the rest of particles, so while $\theta_+ = \theta_- = \theta_\gamma = \theta_k$, $\theta_p \neq \theta_k$.

Then summing up energy densities in (B.6.14),(B.6.15) we obtain

$$\begin{aligned} \sum_{e^+, e^-, \gamma} \rho_i &= \frac{mc^2}{V_0} \left\{ \left[1 - \frac{n_p V_0}{j_1(\theta_k)} \exp\left(-\frac{\nu_+}{\theta_k}\right) \right]^{\frac{1}{2}} \times \right. \\ &\quad \left. \times 6\theta_k^4 \exp\left(\frac{\nu_+}{\theta_k}\right) + \left[2j_1(\theta_k) \exp\left(\frac{\nu_+}{\theta_k}\right) - n_p V_0 \right] j_2(\theta_k) \right\}, \end{aligned} \quad (\text{B.6.23})$$

and analogously for number densities we get

$$\begin{aligned} \sum_{e^+, e^-, \gamma} n_i &= \frac{1}{V_0} \left\{ \left[1 - \frac{n_p V_0}{j_1(\theta_k)} \exp\left(-\frac{\nu_+}{\theta_k}\right) \right]^{\frac{1}{2}} \times \right. \\ &\quad \left. \times 6\theta_k^4 \exp\left(\frac{\nu_+}{\theta_k}\right) + 2j_1(\theta_k) \exp\left(\frac{\nu_+}{\theta_k}\right) \right\}. \end{aligned} \quad (\text{B.6.24})$$

From (B.6.23) and (B.6.24) two unknowns, ν_+ and θ_k can be found. Then

the rest of the chemical potentials are obtained from

$$\exp\left(\frac{\nu_-}{\theta_k}\right) = \exp\left(\frac{\nu_+}{\theta_k}\right) + \frac{n_p V_0}{j_1(\theta_k)}, \quad (\text{B.6.25})$$

$$\exp\left(\frac{\nu_\gamma}{\theta_k}\right) = \exp\left(\frac{\nu_+}{\theta_k}\right) \left[1 + \frac{n_p V_0}{j_1(\theta_k)} \exp\left(-\frac{\nu_+}{\theta_k}\right)\right]^{\frac{1}{2}}, \quad (\text{B.6.26})$$

The temperature and chemical potential of protons can be found separately from (B.6.16),(B.6.17).

In thermal equilibrium ν_γ vanishes and one has

$$\nu_- = \theta_k \operatorname{arcsinh} \left[\frac{n_p V_0}{2j_1(\theta_k)} \right], \quad \nu_+ = -\nu_-, \quad (\text{B.6.27})$$

which both reduce to $\nu_- = \nu_+ = 0$ for $n_p = 0$. At the same time, for $n_p > 0$ one always has $\nu_- > 0$ and $\nu_+ < 0$ in thermal equilibrium. The chemical potential of protons in thermal equilibrium is determined from (B.6.17) for $\theta_k = \theta_{\text{th}}$, where θ_{th} is the temperature in thermal equilibrium.

B.7. Binary interactions

B.7.1. Compton scattering $\gamma e^\pm \rightarrow \gamma' e^{\pm'}$

The time evolution of the distribution functions of photons and pair particles due to Compton scattering may be described by Landau and Lifshitz (1981),Ochelkov et al. (1979)

$$\begin{aligned} \left(\frac{\partial f_\gamma(\mathbf{k}, t)}{\partial t} \right)_{\gamma e^\pm \rightarrow \gamma' e^{\pm'}} &= \int d\mathbf{k}' d\mathbf{p} d\mathbf{p}' V w_{\mathbf{k}', \mathbf{p}'; \mathbf{k}, \mathbf{p}} \times \\ &\times [f_\gamma(\mathbf{k}', t) f_{\pm'}(\mathbf{p}', t) - f_\gamma(\mathbf{k}, t) f_{\pm}(\mathbf{p}, t)], \end{aligned} \quad (\text{B.7.1})$$

$$\begin{aligned} \left(\frac{\partial f_{\pm}(\mathbf{p}, t)}{\partial t} \right)_{\gamma e^\pm \rightarrow \gamma' e^{\pm'}} &= \int d\mathbf{k} d\mathbf{k}' d\mathbf{p}' V w_{\mathbf{k}', \mathbf{p}'; \mathbf{k}, \mathbf{p}} \times \\ &\times [f_\gamma(\mathbf{k}', t) f_{\pm'}(\mathbf{p}', t) - f_\gamma(\mathbf{k}, t) f_{\pm}(\mathbf{p}, t)], \end{aligned} \quad (\text{B.7.2})$$

where

$$w_{\mathbf{k}', \mathbf{p}'; \mathbf{k}, \mathbf{p}} = \frac{\hbar^2 c^6}{(2\pi)^2 V} \delta(\epsilon_\gamma - \epsilon_{\pm} - \epsilon'_\gamma - \epsilon'_{\pm}) \delta(\mathbf{k} + \mathbf{p} - \mathbf{k}' - \mathbf{p}') \frac{|M_{fi}|^2}{16\epsilon_\gamma \epsilon_{\pm} \epsilon'_\gamma \epsilon'_{\pm}}, \quad (\text{B.7.3})$$

is the probability of the process,

$$|M_{fi}|^2 = 2^6 \pi^2 \alpha^2 \left[\frac{m^2 c^2}{s - m^2 c^2} + \frac{m^2 c^2}{u - m^2 c^2} + \left(\frac{m^2 c^2}{s - m^2 c^2} + \frac{m^2 c^2}{u - m^2 c^2} \right)^2 - \frac{1}{4} \left(\frac{s - m^2 c^2}{u - m^2 c^2} + \frac{u - m^2 c^2}{s - m^2 c^2} \right) \right], \quad (\text{B.7.4})$$

is the square of the matrix element, $s = (\mathbf{p} + \mathbf{k})^2$ and $u = (\mathbf{p} - \mathbf{k}')^2$ are invariants, $\mathbf{k} = (\epsilon_\gamma/c)(1, \mathbf{e}_\gamma)$ and $\mathbf{p} = (\epsilon_\pm/c)(1, \beta_\pm \mathbf{e}_\pm)$ are energy-momentum four vectors of photons and electrons, respectively, $d\mathbf{p} = d\epsilon_\pm do \epsilon_\pm^2 \beta_\pm / c^3$, $d\mathbf{k}' = d\epsilon'_\gamma \epsilon'_\gamma^2 do'_\gamma / c^3$ and $do = d\mu d\phi$.

The energies of photon and positron (electron) after the scattering are

$$\epsilon'_\gamma = \frac{\epsilon_\pm \epsilon_\gamma (1 - \beta_\pm \mathbf{b}_\pm \cdot \mathbf{b}_\gamma)}{\epsilon_\pm (1 - \beta_\pm \mathbf{b}_\pm \cdot \mathbf{b}'_\gamma) + \epsilon_\gamma (1 - \mathbf{b}_\gamma \cdot \mathbf{b}'_\gamma)}, \quad \epsilon'_\pm = \epsilon_\pm + \epsilon_\gamma - \epsilon'_\gamma, \quad (\text{B.7.5})$$

$$\mathbf{b}_i = \mathbf{p}_i/p, \mathbf{b}'_i = \mathbf{p}'_i/p', \mathbf{b}'_\pm = (\beta_\pm \epsilon_\pm \mathbf{b}_\pm + \epsilon_\gamma \mathbf{b}_\gamma - \epsilon'_\gamma \mathbf{b}'_\gamma) / (\beta'_\pm \epsilon'_\pm).$$

For photons, the absorption coefficient (B.3.9) in the Boltzmann equations (B.3.3) is

$$\chi_\gamma^{\gamma e^\pm \rightarrow \gamma' e^{\pm'}} f_\gamma = -\frac{1}{c} \left(\frac{\partial f_\gamma}{\partial t} \right)_{\gamma e^\pm \rightarrow \gamma' e^{\pm'}}^{\text{abs}} = \int dn_\pm do'_\gamma J_{\text{cs}} \frac{\epsilon'_\gamma |M_{fi}|^2 \hbar^2 c^2}{16 \epsilon_\pm \epsilon'_\gamma \epsilon'_\pm} f_\gamma, \quad (\text{B.7.6})$$

where $dn_i = d\epsilon_i do_i \epsilon_i^2 \beta_i f_i / c^3 = d\epsilon_i do_i E_i / (2\pi \epsilon_i)$.

From equations (B.7.1) and (B.7.6), we can write the absorption coefficient for photon energy density E_γ averaged over the ϵ, μ -grid with zone numbers ω and k as

$$\begin{aligned} (\chi E)_{\gamma, \omega}^{\gamma e^\pm \rightarrow \gamma' e^{\pm'}} &\equiv \frac{1}{\Delta \epsilon_{\gamma, \omega}} \int_{\epsilon_\gamma \in \Delta \epsilon_{\gamma, \omega}} d\epsilon_\gamma d\mu_\gamma (\chi E)_\gamma^{\gamma e^\pm \rightarrow \gamma' e^{\pm'}} = \\ &= \frac{1}{\Delta \epsilon_{\gamma, \omega}} \int_{\epsilon_\gamma \in \Delta \epsilon_{\gamma, \omega}} dn_\gamma dn_\pm do'_\gamma J_{\text{cs}} \frac{\epsilon'_\gamma |M_{fi}|^2 \hbar^2 c^2}{16 \epsilon_\pm \epsilon'_\pm}, \end{aligned} \quad (\text{B.7.7})$$

where the Jacobian of the transformation is

$$J_{\text{cs}} = \frac{\epsilon'_\gamma \epsilon'_\pm}{\epsilon_\gamma \epsilon_\pm (1 - \beta_\pm \mathbf{b}_\pm \cdot \mathbf{b}_\pm)}. \quad (\text{B.7.8})$$

Similar integrations can be performed for the other terms of equations (B.7.1),

(B.7.2), and we obtain

$$\eta_{\gamma,\omega}^{\gamma e^\pm \rightarrow \gamma' e^{\pm'}} = \frac{1}{\Delta\epsilon_{\gamma,\omega}} \int_{\epsilon'_\gamma \in \Delta\epsilon_{\gamma,\omega}} dn_\gamma dn_\pm do'_\gamma J_{\text{cs}} \frac{\epsilon'_\gamma |M_{fi}|^2 \hbar^2 c^2}{16\epsilon_\pm \epsilon_\gamma \epsilon'_\pm}, \quad (\text{B.7.9})$$

$$\eta_{\pm,\omega}^{\gamma e^\pm \rightarrow \gamma' e^{\pm'}} = \frac{1}{\Delta\epsilon_{\pm,\omega}} \int_{\epsilon'_\pm \in \Delta\epsilon_{\pm,\omega}} dn_\gamma dn_\pm do'_\gamma J_{\text{cs}} \frac{\epsilon'_\gamma |M_{fi}|^2 \hbar^2 c^2}{16\epsilon_\pm \epsilon_\gamma}, \quad (\text{B.7.10})$$

$$(\chi E)_{\pm,\omega}^{\gamma e^\pm \rightarrow \gamma' e^{\pm'}} = \frac{1}{\Delta\epsilon_{\pm,\omega}} \int_{\epsilon_\pm \in \Delta\epsilon_{\pm,\omega}} dn_\gamma dn_\pm do'_\gamma J_{\text{cs}} \frac{\epsilon'_\gamma |M_{fi}|^2 \hbar^2 c^2}{16\epsilon_\gamma \epsilon'_\pm}. \quad (\text{B.7.11})$$

In order to perform integrals (B.7.7)-(B.7.11) numerically over ϕ ($0 \leq \phi \leq 2\pi$) we introduce a uniform grid $\phi_{l \mp 1/2}$ with $1 \leq l \leq l_{\max}$ and $\Delta\phi_l = (\phi_{l+1/2} - \phi_{l-1/2})/2 = 2\pi/l_{\max}$. We assume that any function of ϕ in equations (B.7.7)-(B.7.9) in the interval $\Delta\phi_j$ is equal to its value at $\phi = \phi_j = (\phi_{l-1/2} + \phi_{l+1/2})/2$. It is necessary to integrate over ϕ only once at the beginning of calculations. The number of intervals of the ϕ -grid depends on the average energy of particles and is typically taken as $l_{\max} = 2k_{\max} = 64$.

B.7.2. Pair creation and annihilation $\gamma_1 \gamma_2 \rightleftarrows e^- e^+$

The rates of change of the distribution function due to pair creation and annihilation are

$$\left(\frac{\partial f_{\gamma_j}(\mathbf{k}_i, t)}{\partial t} \right)_{\gamma_1 \gamma_2 \rightarrow e^- e^+} = - \int d\mathbf{k}_j d\mathbf{p}_- d\mathbf{p}_+ V w_{\mathbf{p}_-, \mathbf{p}_+; \mathbf{k}_1, \mathbf{k}_2} f_{\gamma_1}(\mathbf{k}_1, t) f_{\gamma_2}(\mathbf{k}_2, t), \quad (\text{B.7.12})$$

$$\left(\frac{\partial f_{\gamma_i}(\mathbf{k}_i, t)}{\partial t} \right)_{e^- e^+ \rightarrow \gamma_1 \gamma_2} = \int d\mathbf{k}_j d\mathbf{p}_- d\mathbf{p}_+ V w_{\mathbf{k}_1, \mathbf{k}_2; \mathbf{p}_-, \mathbf{p}_+} f_-(\mathbf{p}_-, t) f_+(\mathbf{p}_+, t), \quad (\text{B.7.13})$$

for $i = 1, j = 2$, and for $j = 1, i = 2$.

$$\left(\frac{\partial f_\pm(\mathbf{p}_\pm, t)}{\partial t} \right)_{\gamma_1 \gamma_2 \rightarrow e^- e^+} = \int d\mathbf{p}_\mp d\mathbf{k}_1 d\mathbf{k}_2 V w_{\mathbf{p}_-, \mathbf{p}_+; \mathbf{k}_1, \mathbf{k}_2} f_\gamma(\mathbf{k}_1, t) f_\gamma(\mathbf{k}_2, t), \quad (\text{B.7.14})$$

$$\left(\frac{\partial f_\pm(\mathbf{p}_\pm, t)}{\partial t} \right)_{e^- e^+ \rightarrow \gamma_1 \gamma_2} = - \int d\mathbf{p}_\mp d\mathbf{k}_1 d\mathbf{k}_2 V w_{\mathbf{k}_1, \mathbf{k}_2; \mathbf{p}_-, \mathbf{p}_+} f_-(\mathbf{p}_-, t) f_+(\mathbf{p}_+, t), \quad (\text{B.7.15})$$

where

$$w_{\mathbf{p}_-, \mathbf{p}_+; \mathbf{k}_1, \mathbf{k}_2} = \frac{\hbar^2 c^6}{(2\pi)^2 V} \delta(\epsilon_- + \epsilon_+ - \epsilon_1 - \epsilon_2) \delta(\mathbf{p}_- + \mathbf{p}_+ - \mathbf{k}_1 - \mathbf{k}_2) \frac{|M_{fi}|^2}{16\epsilon_- \epsilon_+ \epsilon_1 \epsilon_2}. \quad (\text{B.7.16})$$

Here, the matrix element $|M_{fi}|^2$ is given by equation (B.7.4) with the new invariants $s = (\mathfrak{p}_- - \mathfrak{k}_1)^2$ and $u = (\mathfrak{p}_- - \mathfrak{k}_2)^2$, see Berestetskii et al. (1982).

The energies of photons created via annihilation of a e^\pm pair are

$$\epsilon_1(\mathbf{b}_1) = \frac{m^2 c^4 + \epsilon_- \epsilon_+ (1 - \beta_- \beta_+ \mathbf{b}_- \cdot \mathbf{b}_+)}{\epsilon_- (1 - \beta_- \mathbf{b}_- \cdot \mathbf{b}_1) + \epsilon_+ (1 - \beta_+ \mathbf{b}_+ \cdot \mathbf{b}_1)}, \quad \epsilon_2(\mathbf{b}_1) = \epsilon_- + \epsilon_+ - \epsilon_1, \quad (\text{B.7.17})$$

while the energies of pair particles created by two photons are found from

$$\epsilon_-(\mathbf{b}_-) = \frac{B \mp \sqrt{B^2 - AC}}{A}, \quad \epsilon_+(\mathbf{b}_-) = \epsilon_1 + \epsilon_2 - \epsilon_-, \quad (\text{B.7.18})$$

where $A = (\epsilon_1 + \epsilon_2)^2 - [(\epsilon_1 \mathbf{b}_1 + \epsilon_2 \mathbf{b}_2) \cdot \mathbf{b}_-]^2$, $B = (\epsilon_1 + \epsilon_2) \epsilon_1 \epsilon_2 (1 - \mathbf{b}_1 \cdot \mathbf{b}_2)$, $C = m_e^2 c^4 [(\epsilon_1 \mathbf{b}_1 + \epsilon_2 \mathbf{b}_2) \cdot \mathbf{b}_-]^2 + \epsilon_1^2 \epsilon_2^2 (1 - \mathbf{b}_1 \cdot \mathbf{b}_2)^2$. Only one root in equation (B.7.18) has to be chosen. From energy-momentum conservation

$$\mathfrak{k}_1 + \mathfrak{k}_2 - \mathfrak{p}_- = \mathfrak{p}_+, \quad (\text{B.7.19})$$

taking square from the energy part we have

$$\epsilon_1^2 + \epsilon_2^2 + \epsilon_-^2 + 2\epsilon_1\epsilon_2 - 2\epsilon_1\epsilon_- - 2\epsilon_2\epsilon_- = \epsilon_+^2, \quad (\text{B.7.20})$$

and taking square from the momentum part we get

$$\epsilon_1^2 + \epsilon_2^2 + \epsilon_-^2 \beta_-^2 + 2\epsilon_1\epsilon_2 \mathbf{b}_1 \cdot \mathbf{b}_2 - 2\epsilon_1\epsilon_- \beta_- \mathbf{b}_1 \cdot \mathbf{b}_- - 2\epsilon_2\epsilon_- \beta_- \mathbf{b}_2 \cdot \mathbf{b}_- = (\epsilon_+ \beta_+)^2. \quad (\text{B.7.21})$$

There are no additional roots because of the arbitrary \mathbf{e}_+

$$\begin{aligned} \epsilon_1\epsilon_2(1 - \mathbf{b}_1 \cdot \mathbf{b}_2) - \epsilon_1\epsilon_-(1 - \beta_- \mathbf{b}_1 \cdot \mathbf{b}_-) - \epsilon_2\epsilon_-(1 - \beta_- \mathbf{b}_2 \cdot \mathbf{b}_-) &= 0, \\ \epsilon_- \beta_- (\epsilon_1 \mathbf{b}_1 + \epsilon_2 \mathbf{b}_2) \cdot \mathbf{b}_- &= \epsilon_- (\epsilon_1 + \epsilon_2) - \epsilon_1 \epsilon_2 (1 - \mathbf{b}_1 \cdot \mathbf{b}_2). \end{aligned} \quad (\text{B.7.22})$$

Eliminating β we obtain

$$\begin{aligned} \epsilon_1^2 \epsilon_2^2 (1 - \mathbf{b}_1 \cdot \mathbf{b}_2)^2 - 2\epsilon_1\epsilon_2(1 - \mathbf{b}_1 \cdot \mathbf{b}_2)(\epsilon_1 + \epsilon_2)\epsilon_- + \\ + \left\{ (\epsilon_1 + \epsilon_2)^2 - [(\epsilon_1 \mathbf{b}_1 + \epsilon_2 \mathbf{b}_2) \cdot \mathbf{b}_-]^2 \right\} \epsilon_-^2 = \\ = [(\epsilon_1 \mathbf{b}_1 + \epsilon_2 \mathbf{b}_2) \cdot \mathbf{b}_-] (-m^2), \end{aligned} \quad (\text{B.7.23})$$

Therefore, the condition to be checked reads

$$\begin{aligned} \epsilon_- \beta_- [(\epsilon_1 \mathbf{b}_1 + \epsilon_2 \mathbf{b}_2) \cdot \mathbf{b}_-]^2 &= [\epsilon_- (\epsilon_1 + \epsilon_2) - (\epsilon_1 \epsilon_2)(1 - \mathbf{b}_1 \cdot \mathbf{b}_2)] \times \\ &\times [(\epsilon_1 \mathbf{b}_1 + \epsilon_2 \mathbf{b}_2) \cdot \mathbf{b}_-] \geq 0. \end{aligned} \quad (\text{B.7.24})$$

Finally, integration of equations (B.7.12)-(B.7.15) yields

$$\begin{aligned}\eta_{\gamma,\omega}^{e^-e^+\rightarrow\gamma_1\gamma_2} &= \frac{1}{\Delta\epsilon_{\gamma,\omega}} \int_{\epsilon_1 \in \Delta\epsilon_{\gamma,\omega}} d^2n_{\pm} J_{\text{ca}} \frac{\epsilon_1^2 |M_{fi}|^2 \hbar^2 c^2}{16\epsilon_- \epsilon_+ \epsilon_2} + \\ &+ \frac{1}{\Delta\epsilon_{\gamma,\omega}} \int_{\epsilon_2 \in \Delta\epsilon_{\gamma,\omega}} d^2n_{\pm} J_{\text{ca}} \frac{\epsilon_1 |M_{fi}|^2 \hbar^2 c^2}{16\epsilon_- \epsilon_+},\end{aligned}\quad (\text{B.7.25})$$

$$\begin{aligned}(\chi E)_{e,\omega}^{e^-e^+\rightarrow\gamma_1\gamma_2} &= \frac{1}{\Delta\epsilon_{e,\omega}} \int_{\epsilon_- \in \Delta\epsilon_{e,\omega}} d^2n_{\pm} J_{\text{ca}} \frac{\epsilon_1 |M_{fi}|^2 \hbar^2 c^2}{16\epsilon_+ \epsilon_2} + \\ &+ \frac{1}{\Delta\epsilon_{e,\omega}} \int_{\epsilon_+ \in \Delta\epsilon_{e,\omega}} d^2n_{\pm} J_{\text{ca}} \frac{\epsilon_1 |M_{fi}|^2 \hbar^2 c^2}{16\epsilon_- \epsilon_2},\end{aligned}\quad (\text{B.7.26})$$

$$\begin{aligned}(\chi E)_{\gamma,\omega}^{\gamma_1\gamma_2\rightarrow e^-e^+} &= \frac{1}{\Delta\epsilon_{\gamma,\omega}} \int_{\epsilon_1 \in \Delta\epsilon_{\gamma,\omega}} d^2n_{\gamma} J_{\text{ca}} \frac{\epsilon_- \beta_- |M_{fi}|^2 \hbar^2 c^2}{16\epsilon_2 \epsilon_+} + \\ &+ \frac{1}{\Delta\epsilon_{\gamma,\omega}} \int_{\epsilon_2 \in \Delta\epsilon_{\gamma,\omega}} d^2n_{\gamma} J_{\text{ca}} \frac{\epsilon_- \beta_- |M_{fi}|^2 \hbar^2 c^2}{16\epsilon_1 \epsilon_+},\end{aligned}\quad (\text{B.7.27})$$

$$\begin{aligned}\eta_{e,\omega}^{\gamma_1\gamma_2\rightarrow e^-e^+} &= \frac{1}{\Delta\epsilon_{e,\omega}} \int_{\epsilon_- \in \Delta\epsilon_{e,\omega}} d^2n_{\gamma} J_{\text{ca}} \frac{\epsilon_-^2 \beta_- |M_{fi}|^2 \hbar^2 c^2}{16\epsilon_1 \epsilon_2 \epsilon_+} + \\ &+ \frac{1}{\Delta\epsilon_{e,\omega}} \int_{\epsilon_+ \in \Delta\epsilon_{e,\omega}} d^2n_{\gamma} J_{\text{ca}} \frac{\epsilon_- \beta_- |M_{fi}|^2 \hbar^2 c^2}{16\epsilon_1 \epsilon_2},\end{aligned}\quad (\text{B.7.28})$$

where $d^2n_{\pm} = dn_- dn_+ do_1$, $d^2n_{\gamma} = dn_{\gamma_1} dn_{\gamma_2} do_-$, $dn_{\pm} = d\epsilon_{\pm} do_{\pm} \epsilon_{\pm}^2 \beta_{\pm} f_{\pm}$, $dn_{\gamma_{1,2}} = d\epsilon_{1,2} do_{1,2} \epsilon_{1,2}^2 f_{\gamma_{1,2}}$ and the Jacobian is

$$J_{\text{ca}} = \frac{\epsilon_+ \beta_-}{(\epsilon_+ + \epsilon_-) \beta_- - (\epsilon_1 \mathbf{b}_1 + \epsilon_2 \mathbf{b}_2) \cdot \mathbf{b}_-}. \quad (\text{B.7.29})$$

B.7.3. Møller scattering of electrons and positrons

$$e_1^{\pm} e_2^{\pm} \rightarrow e_1^{\pm'} e_2^{\pm'}$$

The time evolution of the distribution functions of electrons (or positrons) is described by

$$\begin{aligned}\left(\frac{\partial f_i(\mathbf{p}_i, t)}{\partial t} \right)_{e_1 e_2 \rightarrow e'_1 e'_2} &= \int d\mathbf{p}_j d\mathbf{p}'_1 d\mathbf{p}'_2 V w_{\mathbf{p}'_1, \mathbf{p}'_2; \mathbf{p}_1, \mathbf{p}_2} \times \\ &\times [f_1(\mathbf{p}'_1, t) f_2(\mathbf{p}'_2, t) - f_1(\mathbf{p}_1, t) f_2(\mathbf{p}_2, t)],\end{aligned}\quad (\text{B.7.30})$$

with $i = 1$, $j = 2$, and with $j = 1$, $i = 2$, and where

$$w_{\mathbf{p}'_1, \mathbf{p}'_2; \mathbf{p}_1, \mathbf{p}_2} = \frac{\hbar^2 c^6}{(2\pi)^2 V} \delta(\epsilon_1 + \epsilon_2 - \epsilon'_1 - \epsilon'_2) \delta(\mathbf{p}_1 + \mathbf{p}_2 - \mathbf{p}'_1 - \mathbf{p}'_2) \frac{|M_{fi}|^2}{16\epsilon_1\epsilon_2\epsilon'_1\epsilon'_2}, \quad (\text{B.7.31})$$

$$|M_{fi}|^2 = 2^6 \pi^2 \alpha^2 \left\{ \frac{1}{t^2} \left[\frac{s^2 + u^2}{2} + 4m^2 c^2(t - m^2 c^2) \right] + \right. \quad (\text{B.7.32})$$

$$\left. + \frac{1}{u^2} \left[\frac{s^2 + t^2}{2} + 4m^2 c^2(u - m^2 c^2) \right] + \frac{4}{tu} \left(\frac{s}{2} - m^2 c^2 \right) \left(\frac{s}{2} - 3m^2 c^2 \right) \right\}, \quad (\text{B.7.33})$$

with $s = (\mathbf{p}_1 + \mathbf{p}_2)^2 = 2(m^2 c^2 + \mathbf{p}_1 \cdot \mathbf{p}_2)$, $t = (\mathbf{p}_1 - \mathbf{p}'_1)^2 = 2(m^2 c^2 - \mathbf{p}_1 \cdot \mathbf{p}'_1)$, and $u = (\mathbf{p}_1 - \mathbf{p}'_2)^2 = 2(m^2 c^2 - \mathbf{p}_1 \cdot \mathbf{p}'_2)$ Berestetskii et al. (1982).

The energies of final-state particles are given by (B.7.18) with new coefficients $\tilde{A} = (\epsilon_1 + \epsilon_2)^2 - (\epsilon_1 \beta_1 \mathbf{b}_1 \cdot \mathbf{b}'_1 + \epsilon_2 \beta_2 \mathbf{b}_2 \cdot \mathbf{b}'_1)^2$, $\tilde{B} = (\epsilon_1 + \epsilon_2)[m^2 c^4 + \epsilon_1 \epsilon_2 (1 - \beta_1 \beta_2 \mathbf{b}_1 \cdot \mathbf{b}_2)]$, and $\tilde{C} = m^2 c^4 (\epsilon_1 \beta_1 \mathbf{b}_1 \cdot \mathbf{b}'_1 + \epsilon_2 \beta_2 \mathbf{b}_2 \cdot \mathbf{b}'_1)^2 + [m^2 c^4 + \epsilon_1 \epsilon_2 (1 - \beta_1 \beta_2 \mathbf{b}_1 \cdot \mathbf{b}_2)]^2$. The condition to be checked is

$$[\epsilon'_1(\epsilon_1 + \epsilon_2) - m^2 c^4 - (\epsilon_1 \epsilon_2)(1 - \beta_1 \beta_2 \mathbf{b}_1 \cdot \mathbf{b}_2)] [(\epsilon_1 \beta_1 \mathbf{b}_1 + \epsilon_2 \beta_2 \mathbf{b}_2) \cdot \mathbf{b}'_1] \geq 0. \quad (\text{B.7.34})$$

Integration of equations (B.7.30), similar to the case of Compton scattering in Section B.7.1 yields

$$\begin{aligned} \eta_{e,\omega}^{e_1 e_2 \rightarrow e'_1 e'_2} &= \frac{1}{\Delta \epsilon_{e,\omega}} \int_{\epsilon'_1 \in \Delta \epsilon_{e,\omega}} d^2 n J_{\text{ms}} \frac{\epsilon'_1 \beta'_1 |M_{fi}|^2 \hbar^2 c^2}{16 \epsilon_1 \epsilon_2 \epsilon'_2} + \\ &+ \frac{1}{\Delta \epsilon_{e,\omega}} \int_{\epsilon'_2 \in \Delta \epsilon_{e,\omega}} d^2 n J_{\text{ms}} \frac{\epsilon'_1 \beta'_1 |M_{fi}|^2 \hbar^2 c^2}{16 \epsilon_1 \epsilon_2}, \end{aligned} \quad (\text{B.7.35})$$

$$\begin{aligned} (\chi E)_{e,\omega}^{e_1 e_2 \rightarrow e'_1 e'_2} &= \frac{1}{\Delta \epsilon_{e,\omega}} \int_{\epsilon_1 \in \Delta \epsilon_{e,\omega}} d^2 n J_{\text{ms}} \frac{\epsilon'_1 \beta'_1 |M_{fi}|^2 \hbar^2 c^2}{16 \epsilon_2 \epsilon'_2} + \\ &+ \frac{1}{\Delta \epsilon_{e,\omega}} \int_{\epsilon_2 \in \Delta \epsilon_{e,\omega}} d^2 n J_{\text{ms}} \frac{\epsilon'_1 \beta'_1 |M_{fi}|^2 \hbar^2 c^2}{16 \epsilon_1 \epsilon'_2}, \end{aligned} \quad (\text{B.7.36})$$

where $d^2 n = dn_1 dn_2 do'_1$, $dn_{1,2} = d\epsilon_{1,2} do_{1,2} \epsilon_{1,2}^2 \beta_{1,2} f_{1,2}$, and the Jacobian is

$$J_{\text{ms}} = \frac{\epsilon'_2 \beta'_2}{(\epsilon'_1 + \epsilon'_2) \beta'_1 - (\epsilon_1 \beta_1 \mathbf{b}_1 + \epsilon_2 \beta_2 \mathbf{b}_2) \cdot \mathbf{b}'_1}. \quad (\text{B.7.37})$$

B.7.4. Bhaba scattering of electrons on positrons

$$e^- e^+ \rightarrow e^-' e^+$$

The time evolution of the distribution functions of electrons and positrons due to Bhaba scattering is described by

$$\left(\frac{\partial f_{\pm}(\mathbf{p}_{\pm}, t)}{\partial t} \right)_{e^- e^+ \rightarrow e^-' e^+} = \int d\mathbf{p}_{\mp} d\mathbf{p}'_{-} d\mathbf{p}'_{+} V w_{\mathbf{p}'_{-}, \mathbf{p}'_{+}; \mathbf{p}_{-}, \mathbf{p}_{+}} \times \quad (\text{B.7.38}) \\ \times [f_{-}(\mathbf{p}'_{-}, t) f_{+}(\mathbf{p}'_{+}, t) - f_{-}(\mathbf{p}_{-}, t) f_{+}(\mathbf{p}_{+}, t)],$$

where

$$w_{\mathbf{p}'_{-}, \mathbf{p}'_{+}; \mathbf{p}_{-}, \mathbf{p}_{+}} = \frac{\hbar^2 c^6}{(2\pi)^2 V} \delta(\epsilon_{-} + \epsilon_{+} - \epsilon'_{-} - \epsilon'_{+}) \delta(\mathbf{p}_{-} + \mathbf{p}_{+} - \mathbf{p}'_{-} - \mathbf{p}'_{+}) \frac{|M_{fi}|^2}{16\epsilon_{-}\epsilon_{+}\epsilon'_{-}\epsilon'_{+}}, \quad (\text{B.7.39})$$

and $|M_{fi}|$ is given by the equation (B.7.33), but the invariants are $s = (\mathbf{p}_{-} - \mathbf{p}'_{+})^2$, $t = (\mathbf{p}_{+} - \mathbf{p}'_{+})^2$ and $u = (\mathbf{p}_{-} + \mathbf{p}_{+})^2$. The final energies ϵ'_{-} , ϵ'_{+} are functions of the outgoing particle directions in a way similar to that in Section B.7.3, see also Berestetskii et al. (1982).

Integration of equations (B.7.38) yields

$$\eta_{\pm, \omega}^{e^- e^+ \rightarrow e^-' e^+} = \frac{1}{\Delta\epsilon_{\pm, \omega}} \int_{\epsilon'_{-} \in \Delta\epsilon_{e, \omega}} d^2 n'_{\pm} J_{\text{bs}} \frac{\epsilon'^2 \beta'_{-} |M_{fi}|^2 \hbar^2 c^2}{16\epsilon_{-}\epsilon_{+}\epsilon'_{+}} + \\ + \frac{1}{\Delta\epsilon_{\pm, \omega}} \int_{\epsilon'_{+} \in \Delta\epsilon_{e, \omega}} d^2 n'_{\pm} J_{\text{bs}} \frac{\epsilon'_{-} \beta'_{-} |M_{fi}|^2 \hbar^2 c^2}{16\epsilon_{-}\epsilon_{+}}, \quad (\text{B.7.40})$$

$$(\chi E)_{\pm, \omega}^{e^- e^+ \rightarrow e^-' e^+} = \frac{1}{\Delta\epsilon_{\pm, \omega}} \int_{\epsilon_{-} \in \Delta\epsilon_{e, \omega}} d^2 n'_{\pm} J_{\text{bs}} \frac{\epsilon'_{-} \beta'_{-} |M_{fi}|^2 \hbar^2 c^2}{16\epsilon_{+}\epsilon'_{+}} + \\ + \frac{1}{\Delta\epsilon_{\pm, \omega}} \int_{\epsilon_{+} \in \Delta\epsilon_{e, \omega}} d^2 n'_{\pm} J_{\text{bs}} \frac{\epsilon'_{-} \beta'_{-} |M_{fi}|^2 \hbar^2 c^2}{16\epsilon_{-}\epsilon'_{+}}, \quad (\text{B.7.41})$$

where $d^2 n'_{\pm} = dn_{-} dn_{+} do'_{-}$, $dn_{\pm} = d\epsilon_{\pm} do_{\pm} \epsilon_{\pm}^2 \beta_{\pm} f_{\pm}$, and the Jacobian is

$$J_{\text{bs}} = \frac{\epsilon'_{+} \beta'_{+}}{(\epsilon'_{-} + \epsilon'_{+}) \beta'_{-} - (\epsilon_{-} \beta_{-} \mathbf{b}_{-} \cdot \mathbf{b}'_{-} + \epsilon_{+} \beta_{+} \mathbf{b}_{+} \cdot \mathbf{b}'_{+}) \cdot \mathbf{b}'_{-}}. \quad (\text{B.7.42})$$

Analogously to the case of pair creation and annihilation in Section (B.7.2) the energies of final state particles are given by (B.7.18) with the coefficients $\check{A} = (\epsilon_{-} + \epsilon_{+})^2 - (\epsilon_{-} \beta_{-} \mathbf{b}_{-} \cdot \mathbf{b}'_{-} + \epsilon_{+} \beta_{+} \mathbf{b}_{+} \cdot \mathbf{b}'_{+})^2$, $\check{B} = (\epsilon_{-} + \epsilon_{+}) [m^2 + \epsilon_{-} \epsilon_{+} (1 - \beta_{-} \beta_{+} \mathbf{b}_{-} \cdot \mathbf{b}_{+})]$, $\check{C} = [m^2 + \epsilon_{-} \epsilon_{+} (1 - \beta_{-} \beta_{+} \mathbf{b}_{-} \cdot \mathbf{b}_{+})]^2 + m^2 [\epsilon_{-} \beta_{-} \mathbf{b}_{-} \cdot \mathbf{b}'_{-} + \epsilon_{+} \beta_{+} \mathbf{b}_{+} \cdot \mathbf{b}'_{+}]^2$. In order to select the correct root one has to check the condition (B.7.34) changing the subscripts $1 \rightarrow -, 2 \rightarrow +$.

B.8. Binary reactions with protons

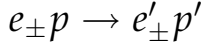
B.8.1. Compton scattering on protons $\gamma p \rightarrow \gamma' p'$

The rate for this process $t_{\gamma p}^{-1}$, compared to the rate of Compton scattering of electrons $t_{\gamma e}^{-1}$ is much longer,

$$t_{\gamma p}^{-1} = \frac{n_p}{n_{\pm}} \left(\frac{\epsilon_{\pm}}{Mc^2} \right)^2 t_{\gamma e}^{-1} \quad \epsilon \geq mc^2. \quad (\text{B.8.1})$$

Moreover, it is longer than any timescale for binary and triple reactions considered in this paper and thus we exclude this reaction from the computations.

B.8.2. Electron-proton and positron-proton scattering



The time evolution of the distribution functions of electrons due to $ep \rightarrow e' p'$ is described by

$$\left(\frac{\partial f_{\pm}(\mathbf{p}, t)}{\partial t} \right)_{ep \rightarrow e' p'} = \int d\mathbf{q} d\mathbf{p}' d\mathbf{q}' V w_{\mathbf{p}', \mathbf{q}'; \mathbf{p}, \mathbf{q}} \times \\ \times [f_{\pm}(\mathbf{p}', t) f_p(\mathbf{q}', t) - f_{\pm}(\mathbf{p}, t) f_p(\mathbf{q}, t)], \quad (\text{B.8.2})$$

$$\left(\frac{\partial f_p(\mathbf{q}, t)}{\partial t} \right)_{ep \rightarrow e' p'} = \int d\mathbf{p} d\mathbf{p}' d\mathbf{q}' V w_{\mathbf{p}', \mathbf{q}'; \mathbf{p}, \mathbf{q}} \\ \times [f_{\pm}(\mathbf{p}', t) f_p(\mathbf{q}', t) - f_{\pm}(\mathbf{p}, t) f_p(\mathbf{q}, t)], \quad (\text{B.8.3})$$

where

$$w_{\mathbf{p}', \mathbf{q}'; \mathbf{p}, \mathbf{q}} = \frac{\hbar^2 c^6}{(2\pi)^2 V} \delta(\epsilon_e + \epsilon_p - \epsilon'_e - \epsilon'_p) \delta(\mathbf{p} + \mathbf{q} - \mathbf{p}' - \mathbf{q}') \frac{|M_{fi}|^2}{16\epsilon_e \epsilon_p \epsilon'_e \epsilon'_p}, \quad (\text{B.8.4})$$

$$|M_{fi}|^2 = 2^6 \pi^2 \alpha^2 \frac{1}{t^2} \left\{ \frac{1}{2} (s^2 + u^2) + (m^2 c^2 + M^2 c^2)(2t - m^2 c^2 - M^2 c^2) \right\}, \quad (\text{B.8.5})$$

the invariants are $s = (\mathbf{p} + \mathbf{q})^2 = m^2 c^2 + M^2 c^2 + 2\mathbf{p} \cdot \mathbf{q}$, $t = (\mathbf{p} - \mathbf{p}')^2 = 2(m^2 c^2 - \mathbf{p} \cdot \mathbf{p}') = 2(M^2 c^2 - \mathbf{q} \cdot \mathbf{q}')$ and $u = (\mathbf{p} - \mathbf{q}')^2 = m^2 c^2 + M^2 c^2 - 2\mathbf{p} \cdot \mathbf{q}'$, $s + t + u = 2(m^2 c^2 + M^2 c^2)$. The energies of particles after interaction are given by (B.7.18) with $\bar{A} = (\epsilon_{\pm} + \epsilon_p)^2 - [(\epsilon_{\pm} \beta_{\pm} \mathbf{b}_{\pm} + \epsilon_p \beta_p \mathbf{b}_p) \cdot \mathbf{b}'_{\pm}]^2$, $\bar{B} = (\epsilon_{\pm} + \epsilon_p)[m^2 c^4 + \epsilon_{\pm} \epsilon_p (1 - \beta_{\pm} \beta_p \mathbf{b}_{\pm} \cdot \mathbf{b}_p)]$, $\bar{C} = m^2 c^4 \{(\epsilon_{\pm} \beta_{\pm} \mathbf{b}_{\pm} \cdot \mathbf{b}'_{\pm} + \epsilon_p \beta_p \mathbf{b}_p \cdot \mathbf{b}'_{\pm})^2 + [m^2 c^4 + \epsilon_{\pm} \epsilon_p]$. The correct root is selected by the condition (B.7.34) with the substitution $1 \rightarrow \pm, 2 \rightarrow p$.

Absorption and emission coefficients for this reaction are

$$(\chi E)_{\pm,\omega}^{ep} = \frac{1}{\Delta\epsilon_{\pm,\omega}} \int_{\epsilon_{\pm} \in \Delta\epsilon_{\pm,\omega}} dn_{\pm} dn_p do'_{\pm} J_{ep} \frac{\epsilon'^2 \beta'_{\pm} \epsilon_{\pm} |M_{fi}|^2 \hbar^2 c^2}{16\epsilon_{\pm} \epsilon_p \epsilon'_{\pm} \epsilon'_p}, \quad (\text{B.8.6})$$

$$(\chi E)_{p,\omega}^{ep} = \frac{1}{\Delta\epsilon_{p,\omega}} \int_{\epsilon_p \in \Delta\epsilon_{p,\omega}} dn_{\pm} dn_p do'_{\pm} J_{ep} \frac{\epsilon'^2 \beta'_{\pm} \epsilon_p |M_{fi}|^2 \hbar^2 c^2}{16\epsilon_{\pm} \epsilon_p \epsilon'_{\pm} \epsilon'_p}, \quad (\text{B.8.7})$$

$$\eta_{\pm,\omega}^{ep} = \frac{1}{\Delta\epsilon_{\pm,\omega}} \int_{\epsilon'_{\pm} \in \Delta\epsilon_{\pm,\omega}} dn_{\pm} dn_p do'_{\pm} J_{ep} \frac{\epsilon'^2 \beta'_{\pm} \epsilon'_{\pm} |M_{fi}|^2 \hbar^2 c^2}{16\epsilon_{\pm} \epsilon_p \epsilon'_{\pm} \epsilon'_p}, \quad (\text{B.8.8})$$

$$\eta_{p,\omega}^{ep} = \frac{1}{\Delta\epsilon_{p,\omega}} \int_{\epsilon'_p \in \Delta\epsilon_{p,\omega}} dn_{\pm} dn_p do'_{\pm} J_{ep} \frac{\epsilon'^2 \beta'_{\pm} \epsilon'_p |M_{fi}|^2 \hbar^2 c^2}{16\epsilon_{\pm} \epsilon_p \epsilon'_{\pm} \epsilon'_p}, \quad (\text{B.8.9})$$

where $dn_i = d\epsilon_i do_i \epsilon_i^2 \beta_i f_i$, $i = \pm, p$, and the Jacobian is

$$J_{ep} = \frac{\epsilon'_p \beta'_p}{(\epsilon'_{\pm} + \epsilon'_p) \beta'_{\pm} - (\epsilon_p \beta_p \mathbf{b}_p + \epsilon_{\pm} \beta_{\pm} \mathbf{b}_{\pm}) \cdot \mathbf{b}'_{\pm}}. \quad (\text{B.8.10})$$

The rate for proton-electron (proton-positron) scattering is

$$t_{ep}^{-1} \approx \frac{\epsilon}{Mc^2} t_{ee}^{-1}, \quad \epsilon_{\pm} \ll \epsilon_p. \quad (\text{B.8.11})$$

B.8.3. Proton-proton scattering $p_1 p_2 \rightarrow p'_1 p'_2$

This reaction is similar to $e_1 e_2 \rightarrow e'_1 e'_2$, described in Section B.7.3. The time evolution of the distribution functions of electrons is described by

$$\left(\frac{\partial f_i(\mathbf{p}_i, t)}{\partial t} \right)_{p_1 p_2 \rightarrow p'_1 p'_2} = \int d\mathbf{q}_j d\mathbf{q}'_1 d\mathbf{q}'_2 V w_{\mathbf{q}'_1, \mathbf{q}'_2; \mathbf{q}_1, \mathbf{q}_2} \times \quad (\text{B.8.12}) \\ \times [f_1(\mathbf{q}'_1, t) f_2(\mathbf{q}'_2, t) - f_1(\mathbf{q}_1, t) f_2(\mathbf{q}_2, t)],$$

with $j = 3 - i$, and where

$$w_{\mathbf{q}'_1, \mathbf{q}'_2; \mathbf{q}_1, \mathbf{q}_2} = \frac{\hbar^2 c^6}{(2\pi)^2 V} \delta(\epsilon_1 + \epsilon_2 - \epsilon'_1 - \epsilon'_2) \delta(\mathbf{q}_1 + \mathbf{q}_2 - \mathbf{q}'_1 - \mathbf{q}'_2) \frac{|M_{fi}|^2}{16\epsilon_1 \epsilon_2 \epsilon'_1 \epsilon'_2}, \quad (\text{B.8.13})$$

$$|M_{fi}|^2 = 2^6 \pi^2 \alpha^2 \left\{ \frac{1}{t^2} \left[\frac{s^2 + u^2}{2} + 4M^2 c^2 (t - M^2 c^2) \right] + \right. \\ \left. \frac{1}{u^2} \left[\frac{s^2 + t^2}{2} + 4M^2 c^2 (u - M^2 c^2) \right] + \frac{4}{tu} \left(\frac{s}{2} - M^2 c^2 \right) \left(\frac{s}{2} - 3M^2 c^2 \right) \right\}, \quad (\text{B.8.14})$$

and the invariants are $s = (\mathbf{q}_1 + \mathbf{q}_2)^2 = 2(M^2c^2 + \mathbf{q}_1 \cdot \mathbf{q}_2)$, $t = (\mathbf{q}_1 - \mathbf{q}'_1)^2 = 2(M^2c^2 - \mathbf{q}_1 \cdot \mathbf{q}'_1)$, and $u = (\mathbf{q}_1 - \mathbf{q}'_2)^2 = 2(M^2c^2 - \mathbf{q}_1 \cdot \mathbf{q}'_2)$.

For the rate we have

$$t_{pp}^{-1} \approx \sqrt{\frac{m}{M}} \frac{n_p}{n_{\pm}} t_{ee}^{-1}, \quad v_p \approx \sqrt{\frac{m}{M}} v_{\pm}, \quad v_{\pm} \approx c. \quad (\text{B.8.15})$$

B.9. Three-body processes

We adopt emission coefficients for triple interactions from Svensson (1984).

Bremsstrahlung

$$\eta_{\gamma}^{e^+ e^- \rightarrow e^+ e^- \gamma} = (n_+^2 + n_-^2) \frac{16}{3} \frac{\alpha c}{\epsilon} \left(\frac{e^2}{mc^2} \right)^2 \ln \left[4\xi(11.2 + 10.4\theta^2) \frac{\theta}{\epsilon} \right] \frac{\frac{3}{5}\sqrt{2}\theta + 2\theta^2}{\exp(1/\theta)K_2(1/\theta)}, \quad (\text{B.9.1})$$

$$\eta_{\gamma}^{e^- e^+ \rightarrow e^- e^+ \gamma} = n_+ n_- \frac{16}{3} \frac{2\alpha c}{\epsilon} \left(\frac{e^2}{mc^2} \right)^2 \ln \left[4\xi(1 + 10.4\theta^2) \frac{\theta}{\epsilon} \right] \frac{\sqrt{2} + 2\theta + 2\theta^2}{\exp(1/\theta)K_2(1/\theta)}, \quad (\text{B.9.2})$$

$$\eta_{\gamma}^{pe^{\pm} \rightarrow p'e^{\pm} \gamma} = (n_+ + n_-) n_p \frac{16}{3} \frac{\alpha c}{\epsilon} \left(\frac{e^2}{mc^2} \right)^2 \ln \left[4\xi(1 + 3.42\theta) \frac{\theta}{\epsilon} \right] \frac{1 + 2\theta + 2\theta^2}{\exp(1/\theta)K_2(1/\theta)}, \quad (\text{B.9.3})$$

where $\xi = e^{-0.5772}$, and $K_2(1/\theta)$ is the modified Bessel function of the second kind of order 2.

Double Compton scattering

$$\eta_{\gamma}^{e^{\pm} \gamma \rightarrow e^{\pm} \gamma' \gamma''} = (n_+ + n_-) n_{\gamma} \frac{128}{3} \frac{\alpha c}{\epsilon} \left(\frac{e^2}{mc^2} \right)^2 \frac{\theta^2}{1 + 13.91\theta + 11.05\theta^2 + 19.92\theta^3}, \quad (\text{B.9.4})$$

Three photon annihilation

$$\eta_{\gamma}^{e^{\pm} e^{\mp} \rightarrow \gamma \gamma' \gamma''} = n_+ n_- \alpha c \left(\frac{e^2}{mc^2} \right)^2 \frac{1}{\epsilon} \frac{\frac{4}{\theta} \left(2 \ln^2 2\xi\theta + \frac{\pi^2}{6} - \frac{1}{2} \right)}{4\theta + \frac{1}{\theta^2} \left(2 \ln^2 2\xi\theta + \frac{\pi^2}{6} - \frac{1}{2} \right)}, \quad (\text{B.9.5})$$

where we have joined two limiting approximations given by Svensson (1984).

Radiative pair production

$$\eta_e^{\gamma \gamma' \rightarrow \gamma'' e^{\pm} e^{\mp}} = \eta_{\gamma}^{e^{\pm} e^{\mp} \rightarrow \gamma \gamma' \gamma''} \frac{n_{\gamma}^2}{n_+ n_-} \left[\frac{K_2(1/\theta)}{2\theta^2} \right]^2. \quad (\text{B.9.6})$$

Electron-photon pair production

$$\eta_{\gamma}^{e_1^{\pm}\gamma \rightarrow e_1^{\pm'}e^{\pm}e^{\mp}} = \begin{cases} (n_+ + n_-)n_{\gamma}\alpha c \left(\frac{e^2}{mc^2}\right)^2 \exp\left(-\frac{2}{\theta}\right) 16.1\theta^{0.541}, & \theta \leq 2, \\ (n_+ + n_-)n_{\gamma}\alpha c \left(\frac{e^2}{mc^2}\right)^2 \left(\frac{56}{9} \ln 2\xi\theta - \frac{8}{27}\right) \frac{1}{1+0.5/\theta}, & \theta > 2. \end{cases} \quad (\text{B.9.7})$$

Proton-photon pair production

$$\eta_{\gamma}^{p\gamma \rightarrow p'e^{\pm}e^{\mp}} = \begin{cases} n_p n_{\gamma}\alpha c \left(\frac{e^2}{mc^2}\right)^2 \exp\left(-\frac{2}{\theta}\right) \frac{1}{1+0.9\theta}, & \theta \leq 1.25277, \\ n_p n_{\gamma}\alpha c \left(\frac{e^2}{mc^2}\right)^2 \left[\frac{28}{9} (\ln 2\xi\theta + 1.7) - \frac{92}{27}\right], & \theta > 1.25277. \end{cases} \quad (\text{B.9.8})$$

We use the absorption coefficient for three-body processes written as

$$\chi_{\gamma}^{3p} = \eta_{\gamma}^{3p} / E_{\gamma}^{eq}, \quad (\text{B.9.9})$$

where η_{γ}^{3p} is the sum of the emission coefficients of photons in the three particle processes, $E_{\gamma}^{eq} = 2\pi e^3 f_{\gamma}^{eq} / c^3$, where f_{γ}^{eq} is given by (B.3.16).

From equation (B.13.4), the law of energy conservation in the three-body processes is

$$\int \sum_i (\eta_i^{3p} - \chi_i^{3p} E_i) d\mu d\epsilon = 0. \quad (\text{B.9.10})$$

For exact conservation of energy in these processes we introduce the following coefficients of emission and absorption for electrons:

$$\chi_e^{3p} = \frac{\int (\eta_{\gamma}^{3p} - \chi_{\gamma}^{3p} E_{\gamma}) d\epsilon d\mu}{\int E_e d\epsilon d\mu}, \quad \eta_e^{3p} = 0, \quad \int (\eta_{\gamma}^{3p} - \chi_{\gamma}^{3p} E_{\gamma}) d\epsilon d\mu > 0, \quad (\text{B.9.11})$$

or

$$\frac{\eta_e^{3p}}{E_e} = -\frac{\int (\eta_{\gamma}^{3p} - \chi_{\gamma}^{3p} E_{\gamma}) d\epsilon d\mu}{\int E_e d\epsilon d\mu}, \quad \chi_e^{3p} = 0, \quad \int (\eta_{\gamma}^{3p} - \chi_{\gamma}^{3p} E_{\gamma}) d\epsilon d\mu < 0. \quad (\text{B.9.12})$$

B.10. Cutoff in the Coulomb scattering

Denote quantities in the center of mass (CM) frame with index 0, and with prime after interaction. Suppose we have two particles with masses m_1 and m_2 . The change of the angle of the first particle in CM system is

$$\theta_{10} = \arccos(\mathbf{b}_{10} \cdot \mathbf{b}'_{10}), \quad (\text{B.10.1})$$

the numerical grid size is $\Delta\theta_g$, the minimal angle at the scattering is θ_{\min} .

By definition in the in CM frame

$$\mathbf{p}_{10} + \mathbf{p}_{20} = 0, \quad (\text{B.10.2})$$

where

$$\mathbf{p}_{i0} = \mathbf{p}_i + \left[(\Gamma - 1)(\mathbf{N}\mathbf{p}_i) - \Gamma \frac{V}{c} \frac{\epsilon_i}{c} \right] \mathbf{N}, \quad i = 1, 2, \quad (\text{B.10.3})$$

and

$$\epsilon_i = \Gamma(\epsilon_{i0} + \mathbf{V}\mathbf{p}_{i0}). \quad (\text{B.10.4})$$

Then for the velocity of the CM frame we have

$$\frac{\mathbf{V}}{c} = c \frac{\mathbf{p}_1 + \mathbf{p}_2}{\epsilon_1 + \epsilon_2}, \quad \mathbf{N} = \frac{\mathbf{V}}{V}, \quad \Gamma = \frac{1}{\sqrt{1 - \left(\frac{V}{c}\right)^2}}. \quad (\text{B.10.5})$$

By definition

$$\mathbf{b}_{10} = \mathbf{b}_{20}, \quad \mathbf{b}'_{10} = \mathbf{b}'_{20}, \quad (\text{B.10.6})$$

and then

$$\begin{aligned} |\mathbf{p}_{10}| &= |\mathbf{p}_{20}| = p_0 \equiv \\ &\equiv \frac{1}{c} \sqrt{\epsilon_{10}^2 - m_1^2 c^4} = \frac{1}{c} \sqrt{\epsilon_{20}^2 - m_2^2 c^4}, \end{aligned} \quad (\text{B.10.7})$$

where

$$\epsilon_{10} = \frac{(\epsilon_1 + \epsilon_2)^2 - \Gamma^2(m_2^2 - m_1^2)c^4}{2(\epsilon_1 + \epsilon_2)\Gamma}, \quad (\text{B.10.8})$$

$$\epsilon_{20} = \frac{(\epsilon_1 + \epsilon_2)^2 + \Gamma^2(m_2^2 - m_1^2)c^4}{2(\epsilon_1 + \epsilon_2)\Gamma}. \quad (\text{B.10.9})$$

Haug (1988) gives the minimal scattering angle in the center of mass system

$$\theta_{\min} = \frac{2\hbar}{\mathcal{M}cD} \frac{\gamma_r}{(\gamma_r + 1)\sqrt{2(\gamma_r - 1)}}, \quad (\text{B.10.10})$$

where \mathcal{M} , as above, is the reduced mass, the maximum impact parameter (neglecting the effect of protons) is

$$D = \frac{c^2}{\omega} \frac{p_0}{\epsilon_{10}}, \quad (\text{B.10.11})$$

and the invariant Lorentz factor of relative motion (e.g. Haug (1988)) is

$$\gamma_r = \frac{1}{\sqrt{1 - \left(\frac{v_r}{c}\right)^2}} = \frac{\epsilon_1 \epsilon_2 - \mathbf{p}_1 \mathbf{p}_2 c^2}{m_1 m_2 c^4}. \quad (\text{B.10.12})$$

In the CM frame we finally obtain

$$t_{\min} = 2 \left[(mc)^2 - \left(\frac{\epsilon_{10}}{c}\right)^2 \left(1 - \beta_{10}^2 \cos \theta_{\min}\right) \right]$$

Since it is invariant, we then replace t in the denominator of $|M_{fi}|^2$ in (B.7.33) by the value $t \sqrt{1 + t_{\min}^2 / t^2}$ to implement the cutoff scheme. Also at the scattering of equivalent particles we remove the case of exchange of particles as well as scattering on small angles, in other words we change u in the denominator of $|M_{fi}|^2$ in (B.7.33), (B.8.5) and (B.8.14) by the value $u \sqrt{1 + t_{\min}^2 / u^2}$.

B.11. Mass scaling for the proton-electron/positron reaction

Since proton mass is larger than electron mass-energy $M \gg m, \epsilon$ then for the CM frame

$$\mathbf{V} \approx \frac{\mathbf{p}_1 + \mathbf{p}_2}{M}, \quad \Gamma \approx 1, \quad J_1 \approx 1, \quad (\text{B.11.1})$$

$$\epsilon'_1 - \epsilon_1 \approx \mathbf{V} (\mathbf{e}'_{01} - \mathbf{e}_{01}) p_0 \propto \frac{1}{M}, \quad (\text{B.11.2})$$

and also

$$\frac{s^2}{c^4} \approx M^4 + 4mM^3 + 6m^2M^2, \quad (\text{B.11.3})$$

$$\frac{u^2}{c^4} \approx M^4 - 4mM^3 + 6m^2M^2, \quad (\text{B.11.4})$$

$$|M_{fi}|^2 \propto \frac{1}{t^2} (6m^2 - 2t) M^2, \quad (\text{B.11.5})$$

while

$$t = \frac{-2m^2\beta_{e0}^2(1 - \mathbf{e}_{e0}\mathbf{e}'_{e0})}{1 - \beta_{e0}^2} = \quad (\text{B.11.6})$$

$$= \frac{-2m^2\beta_e^2(1 - \mathbf{e}_e\mathbf{e}'_e)}{1 - \beta_e^2} \left[1 + O(M^{-1}) \right] \quad (\text{B.11.7})$$

for small angles.

This leads to the following scaling for the reaction rate

$$\eta_{ew}^{ep} - (\chi E)_{ew}^{ep} \propto \int \frac{(\epsilon'_e - \epsilon_e) |M_{fi}|^2}{\epsilon_e \epsilon_p \epsilon'_e \epsilon'_p} \propto \frac{1}{M}. \quad (\text{B.11.8})$$

We can therefore calculate $\eta_{ew}^{ep_0}$, $(\chi E)_{ew}^{ep_0}$ for a pseudo-particle with mass $M_0 \gg m, \epsilon$ instead of M and obtain

$$\eta_{ew}^{ep} \approx \frac{M_0}{M} \eta_{ew}^{ep_0}, \quad (\text{B.11.9})$$

$$(\chi E)_{ew}^{ep} \approx \frac{M_0}{M} (\chi E)_{ew}^{ep_0}. \quad (\text{B.11.10})$$

For such purpose we selected the mass of this pseudo-particle as $M_0 = 20m$.

B.12. The definition of matrix elements

Following Berestetskii et al. (1982) define the scattering matrix, being composed of real and imaginary parts

$$S_{fi} = \delta_{fi} + i (2\pi\hbar)^4 \delta^{(4)}(\mathbf{p}_f - \mathbf{p}_i) T_{fi}, \quad (\text{B.12.1})$$

where δ_{fi} is the unity matrix, $\delta^{(4)}$ stands for the four-momentum conservation and the elements of T_{fi} are scattering amplitudes.

The transition probability of a given process per unit time is then

$$w_{fi} = c (2\pi\hbar)^4 \delta^{(4)}(\mathbf{p}_f - \mathbf{p}_i) |T_{fi}|^2 V, \quad (\text{B.12.2})$$

where V is the normalization volume.

For a process involving a outgoing particles and b incoming particles the

differential probability per unit time is defined as

$$dw = c(2\pi\hbar)^4 \delta^{(4)}(\mathbf{p}_f - \mathbf{p}_i) |M_{fi}|^2 V \times \\ \times \left[\prod_b \frac{\hbar c}{2\epsilon_b V} \right] \left[\prod_a \frac{d\mathbf{p}'_a}{(2\pi\hbar)^3} \frac{\hbar c}{2\epsilon'_a} \right], \quad (\text{B.12.3})$$

where \mathbf{p}'_a and ϵ'_a are respectively momenta and energies of outgoing particles, ϵ_b are energies of particles before interaction, M_{fi} are the corresponding matrix elements, $\delta^{(4)}$ stands for energy-momentum conservation, V is the normalization volume. The matrix elements are related to the scattering amplitudes by

$$M_{fi} = \left[\prod_b \frac{\hbar c}{2\epsilon_b V} \right] \left[\prod_a \frac{\hbar c}{2\epsilon'_a V} \right] T_{fi}. \quad (\text{B.12.4})$$

For a binary process with 2 incoming and 2 outgoing particles it is convenient to introduce the differential cross-section. In fact, the differential probability for incoming particles with four momenta \mathbf{p}_1 and \mathbf{p}_2 , energies ϵ_1 and ϵ_2 and masses m_1 and m_2 respectively, is just the product of the differential cross-section and the flux density

$$dw = j d\sigma, \quad (\text{B.12.5})$$

where

$$j = \frac{cI}{\epsilon_1 \epsilon_2 V}, \quad (\text{B.12.6})$$

$$I = c \sqrt{\mathbf{p}_1 \cdot \mathbf{p}_2 - m_1 m_2 c^2}. \quad (\text{B.12.7})$$

In the CM reference frame the relation between the cross section and $|M_{fi}|^2$ acquires simplest form if cross-section is independent on the azimuth of \mathbf{p}'_1 relative to \mathbf{p}_1 then

$$d\sigma = \frac{\hbar^2 c^4}{64\pi} |M_{fi}|^2 \frac{dt}{I}, \quad (\text{B.12.8})$$

$$t = (\mathbf{p}_1 - \mathbf{p}_2)^2, \quad (\text{B.12.9})$$

$$dt = 2 |\mathbf{p}_1| |\mathbf{p}'_1| d \cos \vartheta, \quad (\text{B.12.10})$$

where ϑ is the angle between \mathbf{p}_1 and \mathbf{p}'_1 .

B.13. The discretization procedure and the computational scheme

In order to solve equations (B.3.3) we use a finite difference method by introducing a computational grid in the phase space to represent the distribution functions and to compute collisional integrals following Aksenov et al. (2004). Our goal is to construct the scheme implementing energy, baryon number and electric charge conservation laws. For this reason we prefer to use in the code, instead of distribution functions f_i , the spectral energy densities

$$E_i(\epsilon_i) = \frac{4\pi\epsilon_i^3\beta_i f_i}{c^3}, \quad (\text{B.13.1})$$

where $\beta_i = \sqrt{1 - (m_i c^2 / \epsilon_i)^2}$, in the phase space ϵ_i . Then

$$\epsilon_i f_i(\mathbf{p}, t) d\mathbf{r} d\mathbf{p} = \frac{4\pi\epsilon_i^3\beta_i f_i}{c^3} d\mathbf{r} d\epsilon_i = E_i d\mathbf{r} d\epsilon_i \quad (\text{B.13.2})$$

is the energy in the volume of the phase space $d\mathbf{r} d\mathbf{p}$. The number density of particles of type "i" is given by

$$n_i = \int f_i d\mathbf{p} = \int \frac{E_i}{\epsilon_i} d\epsilon_i, \quad dn_i = f_i d\mathbf{p}, \quad (\text{B.13.3})$$

while the corresponding energy density is

$$\rho_i = \int \epsilon_i f_i d\mathbf{p} = \int E_i d\epsilon_i.$$

We can rewrite Boltzmann equations (B.3.3) in the form

$$\frac{1}{c} \frac{\partial E_i}{\partial t} = \sum_q (\tilde{\eta}_i^q - \chi_i^q E_i), \quad (\text{B.13.4})$$

where $\tilde{\eta}_i^q = (4\pi\epsilon_i^3\beta_i/c^3)\eta_i^q$.

We introduced the computational grid for phase space $\{\epsilon_i, \mu, \phi\}$, where $\mu = \cos \vartheta$, ϑ and ϕ are angles between radius vector \mathbf{r} and the particle momentum \mathbf{p} . The zone boundaries are $\epsilon_{i,\omega \mp 1/2}$, $\mu_{k \mp 1/2}$, $\phi_{l \mp 1/2}$ for $1 \leq \omega \leq \omega_{\max}$, $1 \leq k \leq k_{\max}$, $1 \leq l \leq l_{\max}$. The length of the i -th interval is $\Delta\epsilon_{i,\omega} \equiv \epsilon_{i,\omega+1/2} - \epsilon_{i,\omega-1/2}$. On the finite grid the functions (B.13.1) become

$$E_{i,\omega} \equiv \frac{1}{\Delta\epsilon_{i,\omega}} \int_{\Delta\epsilon_{i,\omega}} d\epsilon E_i(\epsilon). \quad (\text{B.13.5})$$

Now we can replace the collisional integrals in (B.13.4) by the correspond-

ing sums.

After this procedure we get the set of ordinary differential equations (ODE's), instead of the system of partial differential equations for the quantities $E_{i,\omega}$ to be solved. There are several characteristic times for different processes in the problem, and therefore our system of differential equations is stiff. Under these conditions eigenvalues of Jacobi matrix differs significantly, and the real parts of eigenvalues are negative. We use Gear's method Hall and Watt (1976) to integrate ODE's numerically. This high-order implicit method was developed for the solution of stiff ODE's.

In our method exact energy conservation law is satisfied. For binary interactions the particles number conservation law is satisfied as we adopt interpolation of grid functions $E_{i,\omega}$ inside the energy intervals.

B.14. Numerical results

In what follows we consider in details three specific cases. In the first two cases our grid consists of 60 energy intervals and 16×32 intervals for two angles ϑ and ϕ characterizing the direction of the particle momentum. In the third case we have 40 energy intervals.

B.14.1. Case I

We take the following initial conditions: flat initial spectral densities $E_i(\epsilon_i) = \text{const}$, total energy density $\rho = 10^{24} \text{ erg/cm}^3$. Plasma is dominated by photons with small amount of electron-positron pairs, the ratio between energy densities in photons and in electron-positron pairs $\zeta = \rho_\pm / \rho_\gamma = 10^{-5}$. Baryonic loading parameter $\mathbf{B} = 10^{-3}$, corresponding to $\rho_p = 2.7 \times 10^{18} \text{ erg/cm}^3$.

The energy density in each component of plasma changes, as can be seen from fig. B.1, keeping constant the total energy density shown by dotted line in fig. B.1, as the energy conservation requires. As early as at 10^{-23} sec the energy starts to redistribute between electrons and positrons from the one hand and photons from the other hand essentially by the pair-creation process. This leads to equipartition of energies between these particles at 3×10^{-15} sec. Concentrations of pairs and photons equalize at 10^{-14} sec, as can be seen from fig. B.2. From this moment temperatures and chemical potentials of electrons, positrons and photons tend to be equal, see fig. B.3 and fig. B.4 respectively, and it corresponds to the approach to kinetic equilibrium.

This is quasi-equilibrium state since total number of particles is still approximately conserved, as can be seen from fig. B.2, and triple interactions are not yet efficient. At the moment $t_1 = 4 \times 10^{-14}$ sec, shown by the vertical line on the left in fig. B.3 and fig. B.4, the temperature of photons and pairs is $\theta_k \simeq 1.5$, while the chemical potentials of these particles are $\nu_k \simeq -7$.

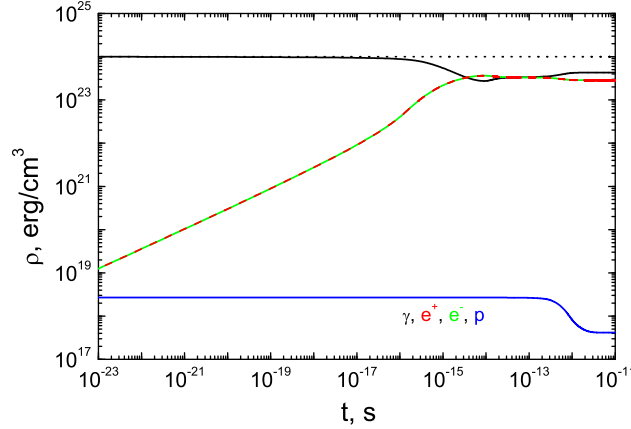


Figure B.1.: Dependence on time of energy densities of electrons (green), positrons (red), photons (black) and protons (blue) for initial conditions I. Total energy density is shown by dotted black line. Interaction between pairs and photons operates on very short timescales up to 10^{-23} sec. Quasi-equilibrium state is established at $t_k \simeq 10^{-14}$ sec which corresponds to kinetic equilibrium for pairs and photons. Protons start to interact with them as late as at $t_{th} \simeq 10^{-13}$ sec.

Concentration of protons is so small that their energy density is not affected by the presence of other components; also proton-proton collisions are inefficient. In other words, protons do not interact yet and their spectra are not yet of equilibrium form, see fig. B.5. The temperature of protons start to change only at 10^{-13} sec, when proton-electron Coulomb scattering becomes efficient.

As can be seen from fig. B.4, the chemical potentials of electrons, positrons and photons evolved by that time due to triple interactions. Since chemical potentials of electrons, positrons and photons were negative, the particles were in deficit with respect to the thermal state. This caused the total number of these particles to increase and consequently the temperature to decrease. The chemical potential of photons reaches zero at $t_2 = 10^{-12}$ sec, shown by the vertical line on the right in fig. B.3 and fig. B.4, which means that electrons, positrons and photons are now in thermal equilibrium. However, protons are not yet in equilibrium with other particle since their spectra are not thermal, as shown in the lower part of fig. B.5.

Finally, the proton component thermalize with other particles at 4×10^{-12} sec, and from that moment plasma is characterized by unique temperature, $\theta_{th} \simeq 0.48$ as fig. B.3 clearly shows. Protons have final chemical potential $\nu_p \simeq -12.8$.

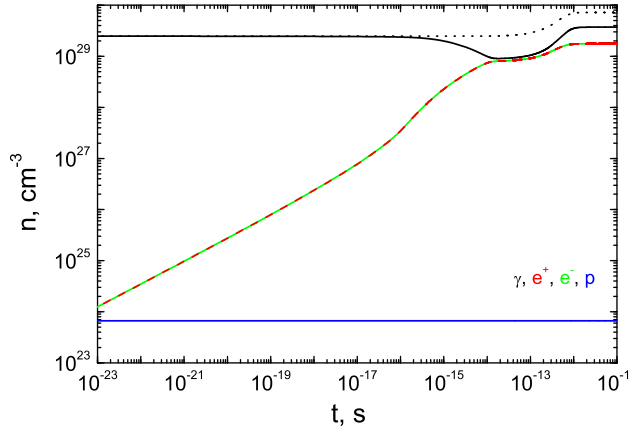


Figure B.2.: Dependence on time of concentrations of electrons (green), positrons (red), photons (black) and protons (blue) for initial conditions I. Total number density is shown by dotted black line. In this case kinetic equilibrium between electrons, positrons and photons is reached at $t_k \simeq 10^{-14}$ sec. Protons join thermal equilibrium with other particles at $t_{th} \simeq 4 \times 10^{-12}$ sec.

This state is characterized by thermal distribution of all particles as can be seen from fig. B.6. There initial flat as well as final spectral densities are shown together with fits of particles spectra with the values of the common temperature and the corresponding chemical potentials in thermal equilibrium.

B.14.2. Case II

We take the following initial conditions: power law spectral densities $E_i(\epsilon_i)$ for protons, electrons and positrons with initial energy densities $\rho_p = 2.8 \times 10^{22} \text{ erg/cm}^3$, $\rho_- = 1.5 \times 10^{24} \text{ erg/cm}^3$, $\rho_+ = 1.5 \times 10^{21} \text{ erg/cm}^3$, respectively. We chosen flat spectral density for photons with $\rho_\gamma = 2.8 \times 10^{24} \text{ erg/cm}^3$. Initial baryonic loading parameter is set to $\mathbf{B} = 608$, corresponding to a matter-dominated plasma, unlike the previous case. As in the case I, the most rapid reaction is electron-positron pair creation which starts to change the energy density of positrons at 10^{-20} sec, see fig. B.7. Initially most energy is in photons, followed by electrons and protons. In the course of the evolution the energy gets redistributed in such a way that in the final state most energy is transferred first to the electrons, then follow the protons, the photons and finally the positrons. In fig. B.8 one can see that number densities of electrons and protons are almost equal with chosen heavy proton loading. Concentrations of particles almost do not change during evolution towards

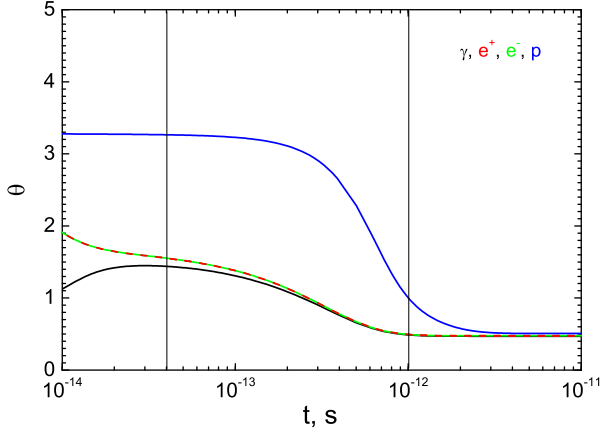


Figure B.3.: Dependence on time of dimensionless temperature of electrons (green), positrons (red), photons (black) and protons (blue) for initial conditions I. The temperature for pairs and photons acquires physical meaning only in kinetic equilibrium at $t_k \simeq 10^{-14}$ sec. Protons are cooled by the pair-photon plasma and acquire common temperature with it as late as at $t_{th} \simeq 4 \times 10^{-12}$ sec.

thermal equilibrium.

Temperatures and chemical potentials of particles are shown in fig. B.9 and B.10 respectively. Kinetic equilibrium is established at around 8×10^{-15} sec, marked by the vertical line. The temperature of pairs and photons at that moment is $\theta_k \simeq 0.53$, while the chemical potentials of these particles are $\nu_- \simeq 1, \nu_+ \simeq -0.9, \nu_\gamma \simeq 0.1$. Notice that chemical potentials of electrons and positrons are almost equal in magnitude and opposite in kinetic equilibrium, see fig. B.10. At this moment protons are not yet in equilibrium with the rest of plasma but already established kinetic equilibrium with themselves with the temperature $\theta_p \simeq 0.18$ and the chemical potential $\nu_p \simeq -2$. The common temperature is reached at the moment 10^{-13} sec, which corresponds to thermal equilibrium. Final values of temperature is $\theta_{th} \simeq 0.47$, while chemical potentials are $\nu_\pm \simeq \mp 1, \nu_p \simeq -4.7$.

The share of the proton energy density in the total energy density increased in course of time, see fig. B.7, causing an increase in the baryonic loading parameter which reached in thermal equilibrium the value $\mathbf{B} = 780$.

Since concentration of protons is chosen to be large, proton-proton collisions become more important than proton-electron/positron collisions, in contrast to the case I. In fact, protons reached equilibrium temperature already at 10^{-16} sec, while they start to interact with electrons and positrons only at 10^{-15} sec.

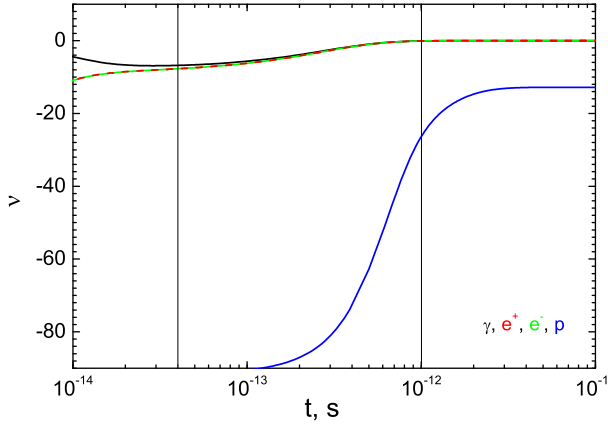


Figure B.4.: Dependence on time of dimensionless chemical potential of electrons (green), positrons (red), photons (black) and protons (blue) for initial conditions I. The chemical potential for pairs and photons acquires physical meaning only in kinetic equilibrium at $t_k \simeq 10^{-14}$ sec, while for protons this happens at $t_{\text{th}} \simeq 4 \times 10^{-12}$ sec. At this time chemical potential of photons has evolved to zero and thermal equilibrium has been already reached.

B.14.3. Case III

We take the following initial conditions: the initial ratio between concentrations of electrons and protons is $\zeta = n_p/n_- = 10^{-3}$. The total energy density is chosen in such a way that the final temperature in thermal equilibrium be $\theta_{\text{th}} = 2$. We set up flat initial spectrum for photons $E_\gamma(\epsilon_i) = \text{const}$, and power law spectra for the pairs $E_\pm(\epsilon_\pm) \propto [\epsilon_\pm - mc^2]^{-2}$ and protons $E_p(\epsilon_p) \propto [\epsilon_p - Mc^2]^{-4}$. Finally, the ratio of initial and final concentrations of positrons is chosen to be $n_+ = 10^{-1}n_+^{\text{th}}$. Given these initial conditions the baryon loading parameter is $\mathbf{B} = 0.2$. The initial conditions are chosen in a way to get larger temperature in thermal equilibrium, than in previous cases. Unlike the case II, the spectrum of protons is chosen steeper than the spectrum of pairs in order to make them colder in kinetic equilibrium.

Equipartition of energies between pairs and photons occurs earlier than in the case I, at around 10^{-17} sec, see fig. B.12, since now concentrations of particles are higher. Concentrations of pairs and photons equalize at 3×10^{-17} sec, see fig. B.13. As in the case I, from this moment temperatures and chemical potentials of electrons, positrons and photons tend to be equal, see fig. B.14 and fig. B.15 respectively, leading to kinetic equilibrium at around $t_k \simeq 10^{-16}$ sec.

At the moment t_k , shown by the vertical line on the left in fig. B.14 and fig. B.15, the temperature of photons and pairs is $\theta_k \simeq 2.2$, the chemical

potentials of these particles are $\nu_k \simeq -1.1$, while the temperature of protons, having well established spectrum by this time, is just $\theta_p \simeq 0.09$.

Thermal equilibrium is reached in the electron-positron-photon plasma at around $t_{\text{th}} \simeq 4 \times 10^{-15}$ sec, shown by the vertical line on the right of fig. B.14 and fig. B.15. Only at 4×10^{-14} sec the temperature becomes common also with protons which are heated up during this time. The temperature at this final stage is $\theta_{\text{th}} \simeq 2$ while the chemical potential of protons is $\nu_p \simeq -33$. Initial as well as final spectra are shown in fig. B.16.

B.15. Discussion and conclusions

Results presented above clearly show the existence of two types of equilibrium: the kinetic and the thermal ones. Kinetic equilibrium in pair-photon plasma occurs when Ehlers Ehlers (1973) balance conditions (B.6.6),(B.6.9) and (B.6.12) are satisfied so that pair-creation, Compton and Bhabha/Møller scattering processes all come in detailed balance. The electron-positron-photon plasma then is described by common temperature and nonzero chemical potentials which are given by (B.6.23),(B.6.24) and (B.6.25),(B.6.26). Protons at this stage may or may not have yet established equilibrium with the spectrum (B.3.16), depending on the value of the baryon loading parameter \mathbf{B} . When \mathbf{B} is small, as in the case I, proton-proton collision are inefficient since the rate (B.8.15) is much smaller than (B.8.11), and the proton spectrum is shaped up by the proton-electron/positron collisions, reaching equilibrium form at a timescale given by (B.8.11), when other particles are already in thermal equilibrium. When \mathbf{B} is large, as in the case II, protons have established their equilibrium temperature at a timescale given by (B.8.15), prior to the moment when kinetic equilibrium in the pair-photon plasma is established.

As we have seen, the final spectra are completely insensitive to the initial spectra, chosen to be flat as in the case I, power-law as in the case II, or thermal ones.

The meaning of non-zero chemical potentials in kinetic equilibrium can be understood as follows. The existence of a non-null chemical potential for photons indicates the departure of the distribution function from the one corresponding to the thermal equilibrium. Negative value of the chemical potential generates an increase of the number of particles in order to approach the one corresponding to the thermal equilibrium state. Positive value of the chemical potential leads to the opposite effect, decreasing the number of particles. Then, since the total number of particles increases (or decreases), the energy is shared between larger (or smaller) number of particles and the temperature decreases (or increases). Clearly, as thermal equilibrium is approached, the chemical potential of photons tends to zero, while the chemical potentials of electrons and positrons are given by (B.6.27), to guarantee an overall charge neutrality.

One of the basic assumptions in this work is that triple interactions are slower than binary ones, allowing to use reaction rates for triple interactions in kinetic equilibrium, explicitly depending solely on temperature, chemical potentials and concentrations of particles. For pure electron-positron plasma in the range of energies of interest (B.2.1) there is a hierarchy of relevant timescales: binary interactions are clearly faster than triple ones. However, when protons are also present, the proton-proton timescale may be shorter or longer than the corresponding binary interactions timescales for the pure pair plasma. This violates our assumption and therefore leads to loss of quantitative accuracy, although still keeping qualitative results valid. In order to overcome this difficulty and produce quantitatively precise results exact QED matrix elements must be used for calculation of emission and absorption coefficients.

Notice that there is some discrepancy between our final spectra and their thermal fits for high energy. This is due to poor energy resolution with adopted grid. The result converges with higher resolutions, but it is limited by the available computer memory. In addition, the code is quite time-consuming and processor time increases with number of operation as third power of the number of energy intervals.

In order to resolve proton-electron/positron scattering the number of energy intervals should be increased as M/m comparing to the case of pure pair plasma. Even using inhomogeneous energy grid with uniform energy step up to the peak of the spectrum $d\rho/d\varepsilon$ and decreasing energy step as ε^{-1} for higher energies, we have obtained acceptable results with about 10^3 intervals for this reaction. Using such fine grid is impossible in practice. On the other hand, a small parameter m/M expansion can be adopted. In this way we have introduced the mass scaling, which gives quite good accuracy for about 10^2 intervals in energy with inhomogeneous grid, described above. Finally, it is important to stress that our code allows solution of the Boltzmann equations for long time intervals and timescales, which may differ up to 10 orders of magnitude, from electron-positron creation and annihilation process up to proton-electron/positron scattering, see fig. B.2, unlike approaches based on Monte-Carlo technique Pilla and Shaham (1997). This gives us the possibility to follow thermalization process up to reaching steady solution, i.e. thermal equilibrium.

The assumption of the constancy of the energy density is only valid if the following three conditions are satisfied:

- plasma is optically thick for photons. This leads to the constraint on the spatial dimensions $R_0 \gg (n_{\text{th}}\sigma_T)^{-1} \sim 10^{-5}$ cm.
- neutrinos are not produced. This gives the constraint on the temperature from (B.3.15) as $\theta \ll 7 \times 10^2$.

- plasma does not expand. Given $t_{\text{dyn}} = \left(\frac{1}{R} \frac{dR}{dt}\right)^{-1} \gg t_{\text{th}}$, this leads to $R_0 \gg 10^{-2}$ cm.

To summarize, we have considered the evolution of an initially nonequilibrium optically thick electron-positron-photon plasma with proton loading up to reaching thermal equilibrium on a timescale $t_{\text{th}} \lesssim 10^{-11}$ sec. Starting from arbitrary initial conditions we obtain kinetic equilibrium, on a timescale $t_k \lesssim 10^{-14}$ sec, from first principles, solving numerically the relativistic Boltzmann equation with collisional integrals computed from exact QED matrix elements. Our results can be applied in the theories of the early universe, in high energy plasma physics, are crucial for the theoretical models of GRBs Ruffini et al. (2000) and can in principle be tested in laboratory experiments aiming the generation of electron-positron pairs.

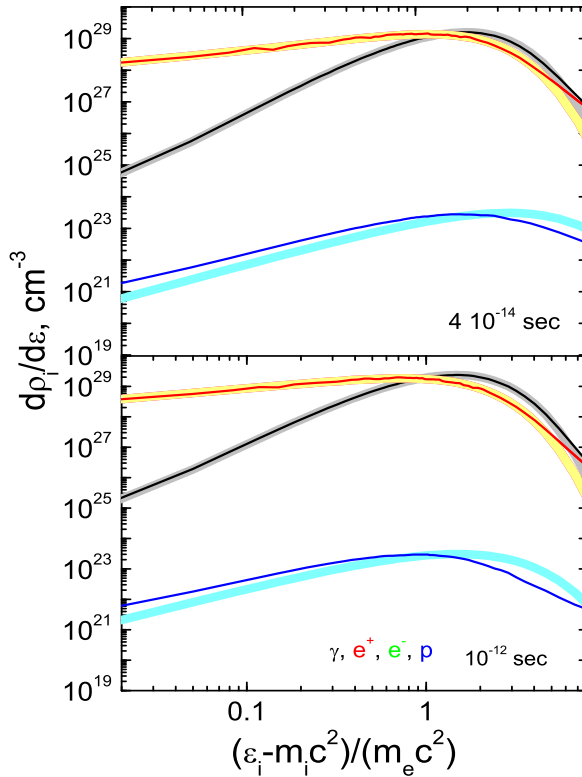


Figure B.5: Spectral density as function of particle energy for electrons (green), positrons (red), photons (black) and protons (blue) for initial conditions I at intermediate time moments $t_1 = 4 \times 10^{-14}$ sec (upper figure) and $t_2 = 10^{-12}$ sec (lower figure). Fits of the spectra with chemical potentials and temperatures corresponding to thermal equilibrium state are also shown by yellow (electrons and positrons), grey (photons) and light blue (protons) thick lines. The upper figure shows the spectra when kinetic equilibrium is established for the first time between electrons, positrons and photons while the lower figure shows the spectra at thermal equilibrium between these particles. On both figures protons are not yet in equilibrium neither with themselves nor with other particles.

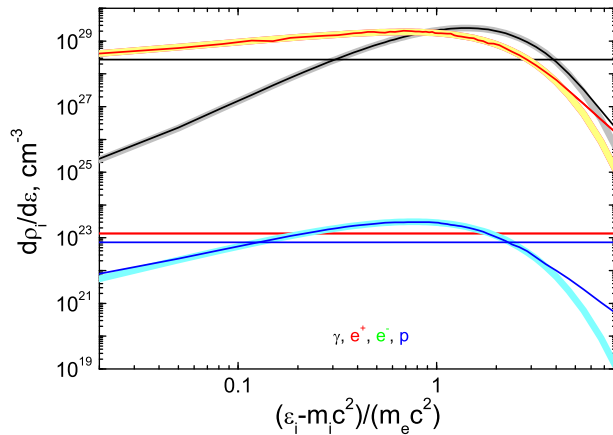


Figure B.6.: Spectral density as function of particle energy are shown as before at initial and final moments of the computations. The final photon spectrum is black body one.

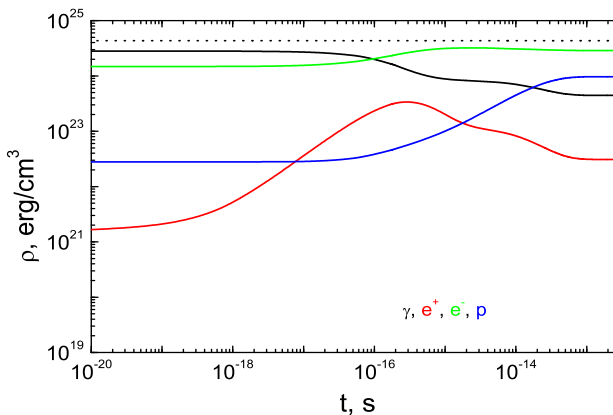


Figure B.7.: Dependence on time of energy densities for initial conditions II. Colors are as in the case I. Protons start to interact with other particles as late as at $t \simeq 10^{-16}$ sec.

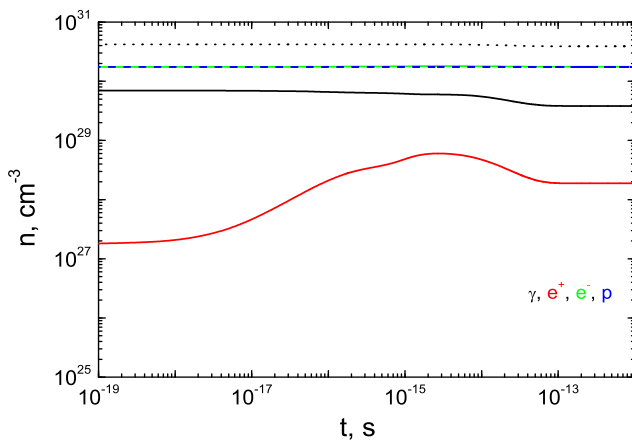


Figure B.8.: Dependence on time of concentrations for initial conditions II. Colors are as in the case I.

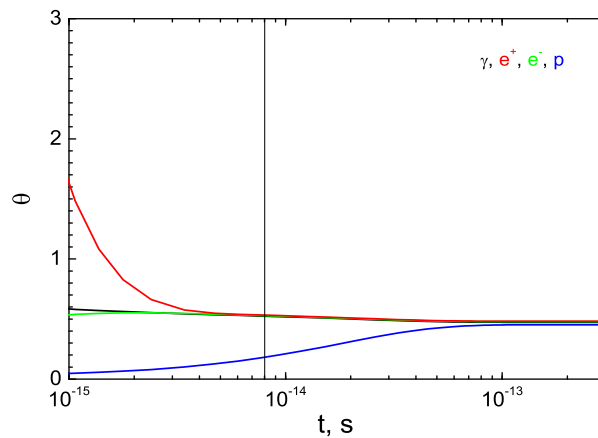


Figure B.9.: Dependence on time of dimensionless temperature for initial conditions II. Colors are as in the case I. The pair-photon plasma is heating protons. Protons join thermal equilibrium at $t_{\text{th}} \simeq 10^{-13}$ sec.

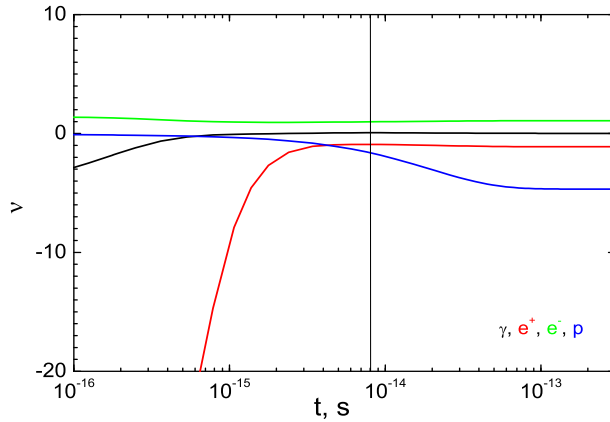


Figure B.10.: Dependence on time of dimensionless chemical potential for initial conditions II. Colors are as in the case I. The chemical potential of photons is almost zero in kinetic equilibrium. The chemical potentials of electrons and positrons are almost equal and opposite in kinetic equilibrium, to maintain electric neutrality.

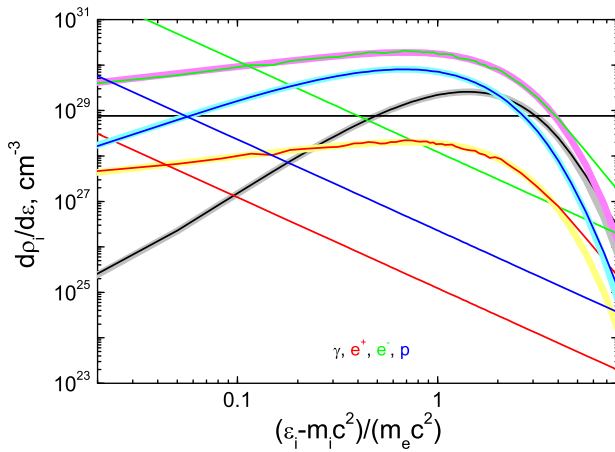


Figure B.11.: Initial and final spectral density as function of particle energy for initial conditions II. Fits of the final spectra with chemical potentials and temperatures are also shown.

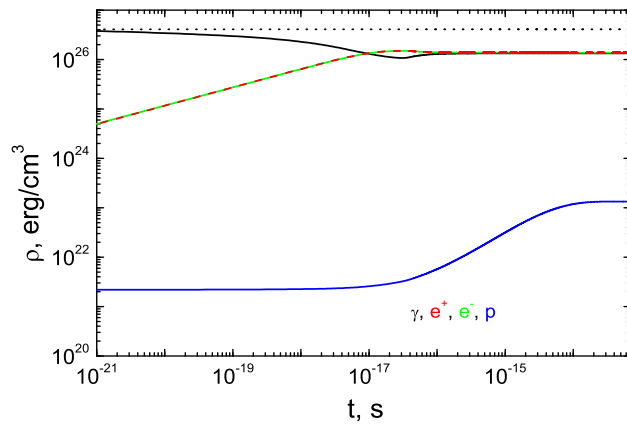


Figure B.12.: Dependence on time of energy densities for initial conditions III. Colors are as in the case I. Protons start to interact with other particles at about 10^{-17} sec.

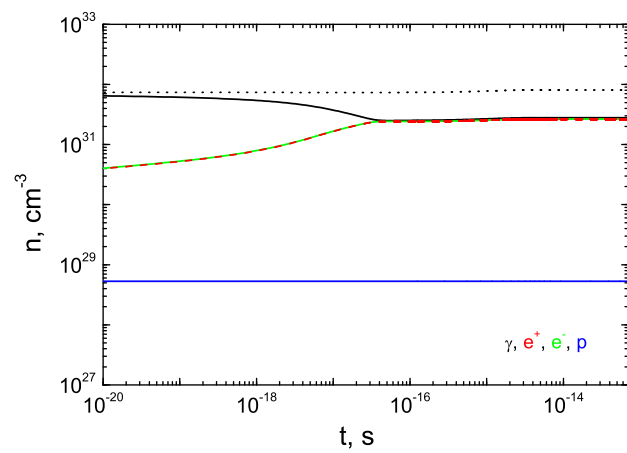


Figure B.13.: Dependence on time of concentrations for initial conditions III. Colors are as in the case I.

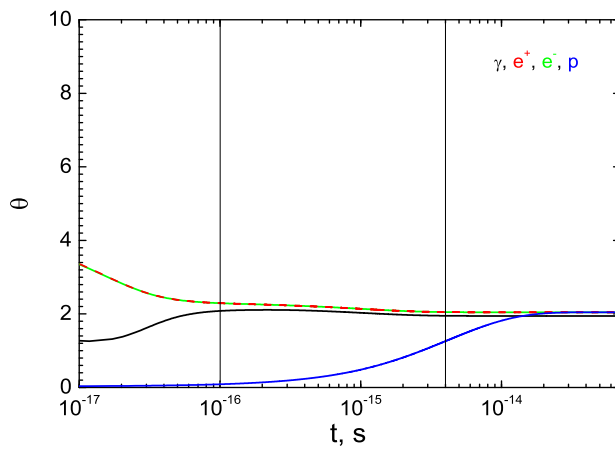


Figure B.14.: Dependence on time of dimensionless temperature for initial conditions III. Colors are as in the case I. Pairs and photons acquire the temperature at $t_k \simeq 10^{-16}$ sec.

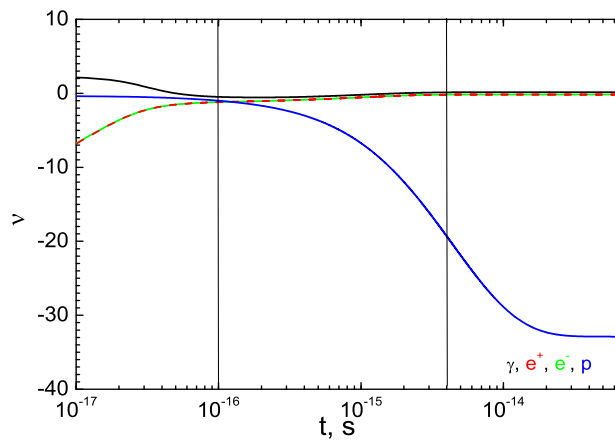


Figure B.15.: Dependence on time of dimensionless chemical potential for initial conditions III. Colors are as in the case I. The chemical potentials equalize at $t_k \simeq 10^{-16}$ sec.

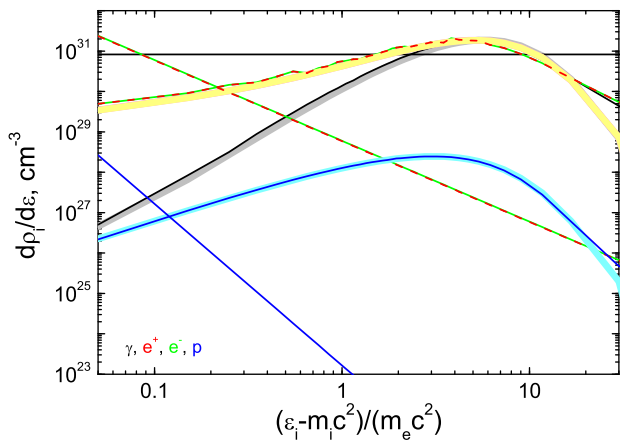


Figure B.16.: Initial and final spectral density as function of particle energy for initial conditions III. The spectrum of protons is chosen to be steeper than the one of electrons and positrons. Fits of the final spectra with chemical potentials and temperatures are also shown.

C. Hydrodynamics of the pair plasma

We give systematic derivation of the main equations, present a critical review of existing models for isotropic relativistic fireballs, compare and contrast these models, following Bianco et al. (2006). In the next section we derive basic equations and describe approximations involved. Then we present the model Ruffini et al. (1999), Ruffini et al. (2000) which differs from other models in the literature as it describes the dynamics of the fireshell taking into account the *rate equations* for electron-positron pairs. Then we compare and contrast above mentioned models.

C.1. Local, global and average conservation laws

C.1.1. Particle number

The first relevant equation represents continuity of relativistic flux and reads¹

$$(nU^\mu)_{;\mu} = \frac{1}{\sqrt{-g}} \frac{\partial (\sqrt{-g} nU^\mu)}{\partial x^\mu} = 0, \quad (\text{C.1.1})$$

where n is the number density of relativistic fluid, U^μ is its velocity field. Defining particle number as

$$N = \int_V \sqrt{-g} nU^0 dV. \quad (\text{C.1.2})$$

we see that

$$\frac{dN}{dt} = - \int_V \sqrt{-g} nU^i dV = - \oint_\Sigma \sqrt{-g} nU^i dS_i, \quad (\text{C.1.3})$$

where we have used the Ostrogradsky-Gauss theorem. Thus, if particles do not cross the surface Σ bounding considered volume V , the total number of particles is constant during system evolution.

¹Greek indices denote four-dimensional components and run from 0 to 3 while Latin indices run from 1 to 3. The general relativistic effects are neglected, which is a good approximation, but we left the general definition of the energy-momentum conservation to take into account the most general coordinate system.

Now assume spherical symmetry², which is usually done for fireballs description. With spherical spatial coordinates $x^i = \{r, \vartheta, \varphi\}$ the interval is

$$ds^2 = -dt^2 + dr^2 + r^2 d\vartheta^2 + r^2 \sin^2 \vartheta d\varphi^2. \quad (\text{C.1.4})$$

Assuming absence of fluxes through the boundary Σ we rewrite (C.1.1)

$$\frac{\partial(n\gamma)}{\partial t} + \frac{1}{r^2} \frac{\partial}{\partial r} \left(r^2 n \sqrt{\gamma^2 - 1} \right) = 0, \quad (\text{C.1.5})$$

Integrating this equation over the volume from certain $r_i(t)$ to $r_e(t)$ which we assume to be comoving with the fluid

$$\frac{dr_i(t)}{dt} = \beta(r_i, t), \quad \frac{dr_e(t)}{dt} = \beta(r_e, t), \quad (\text{C.1.6})$$

and ignoring a factor 4π we have

$$\begin{aligned} & \int_{r_i}^{r_e} \frac{\partial(n\gamma)}{\partial t} r^2 dr + \int_{r_i}^{r_e} \frac{\partial}{\partial r} \left(r^2 n \sqrt{\gamma^2 - 1} \right) dr = \\ & \frac{\partial}{\partial t} \int_{r_i}^{r_e} (n\gamma) r^2 dr - \frac{dr_e}{dt} n(r_e, t) \gamma(r_e, t) r_e^2 + \frac{dr_i}{dt} n(r_i, t) \gamma(r_i, t) r_i^2 + \\ & + r_e^2 n(r_e, t) \sqrt{\gamma^2(r_e, t) - 1} - r_i^2 n(r_i, t) \sqrt{\gamma^2(r_i, t) - 1} = \\ & = \frac{d}{dt} \int_{r_i}^{r_e} (n\gamma) r^2 dr = 0, \end{aligned} \quad (\text{C.1.7})$$

Since we deal with arbitrary comoving boundaries, this means that the number of particles in each shell between the boundaries conserves, as well as the total number of particles integrated over all shells, in other words,

$$N = 4\pi \int_0^{R(t)} n\gamma r^2 dr = \text{const}, \quad (\text{C.1.8})$$

where $R(t)$ is the external radius of the fireshell.

Following Piran et al. (1993) one can transform (C.1.5) from the variables

²The only nonvanishing components of the energy-momentum tensor are $T^{00}, T^{01}, T^{10}, T^{11}, T^{22}, T^{33}$. The factor $\sqrt{-g} = r^2 \sin \vartheta$ in all expressions above becomes simply a volume measure and the differentials are $dV = dr d\vartheta d\varphi$, $dS = d\vartheta d\varphi$, so the differential laboratory volume can be written as $dV \equiv \sqrt{-g} dV = r^2 \sin \vartheta dr d\vartheta d\varphi$.

(t, r) to the new variables $(s = t - r, r)$ and then show that

$$\frac{1}{r^2} \frac{\partial}{\partial r} \left(r^2 n \sqrt{\gamma^2 - 1} \right) = - \frac{\partial}{\partial s} \left(\frac{n}{\gamma + \sqrt{\gamma^2 - 1}} \right). \quad (\text{C.1.9})$$

Now assume the expansion velocity is ultrarelativistic,

$$\gamma \gg 1. \quad (\text{C.1.10})$$

In this approximation, therefore,

$$dN = 4\pi n \gamma r^2 dr \approx \text{const.} \quad (\text{C.1.11})$$

Relations (C.1.11) and (C.1.8) then imply

$$4\pi \int_{r_i}^{r_e} (n\gamma r^2) dr = 4\pi \left[n(r, t) \gamma(r, t) r^2 \right] \int_{r_i}^{r_e} dr = 4\pi (n\gamma r^2) \Delta \approx \text{const}, \quad (\text{C.1.12})$$

where the first argument of functions $n(r, t)$ and $\gamma(r, t)$ is restricted to the interval $r_i < r < r_e$ and

$$\Delta \equiv r_e - r_i \approx \text{const.} \quad (\text{C.1.13})$$

This means, that the fluid shell does not broaden, but rather has a constant thickness. This fact proves the constant thickness approximation, adopted in Ruffini et al. (1999), Ruffini et al. (2000).

The volume element measured by the observer outside the fireshell (to be referred to as the lab frame in what follows), for which it appears moving with velocity β is just

$$dV = 4\pi r^2 dr, \quad (\text{C.1.14})$$

while the volume element comoving with the fireshell, for which the fluid is at rest, is

$$dV = 4\pi \gamma r^2 dr, \quad (\text{C.1.15})$$

with the conversion of the volumes

$$dV = \gamma dV. \quad (\text{C.1.16})$$

Then the average value of the Lorentz factor is defined as follows

$$\langle \gamma \rangle \equiv \frac{4\pi \int \gamma r^2 dr}{4\pi \int r^2 dr} = \frac{V}{\mathcal{V}}. \quad (\text{C.1.17})$$

Now we can formulate the conservation law for the average value of the

number density in the lab frame

$$\langle n \rangle_{\text{lab}} \equiv \frac{N}{V} = \frac{\frac{4\pi}{r_i} \int_{r_i}^{r_e} n \gamma r^2 dr}{\frac{4\pi}{r_i} \int_{r_i}^{r_e} r^2 dr}, \quad (\text{C.1.18})$$

Assuming $r \gg \Delta$ we then obtain

$$\langle n \rangle_{\text{lab}} \simeq \frac{4\pi n \gamma r^2 \Delta}{4\pi r^2 \Delta} = n(r, t) \gamma(r, t) \propto r^{-2}. \quad (\text{C.1.19})$$

Therefore, the average number density in the lab frame scales as r^{-2} .

At the same time, recalling the expression for the divergence of the four-velocity

$$U^\mu_{;\mu} = \frac{1}{V} \frac{dV}{d\tau}, \quad (\text{C.1.20})$$

where τ is the proper time, and remembering that $U^\mu \frac{\partial}{\partial x^\mu} = \frac{d}{d\tau}$, from (C.1.1) we get

$$(nU^\mu)_{;\mu} = U^\mu n_{;\mu} + nU^\mu_{;\mu} = \frac{dn}{d\tau} + \frac{n}{V} \frac{dV}{d\tau} = 0, \\ d \ln n + d \ln V = 0. \quad (\text{C.1.21})$$

This means, that the number of particles is conserved along the flow lines of the fluid. The solution of this equation provides the definition for the comoving average number density

$$\langle n \rangle_{\text{com}} \equiv \frac{N}{V} = \frac{\frac{4\pi}{r_i} \int_{r_i}^{r_e} n \gamma r^2 dr}{\frac{4\pi}{r_i} \int_{r_i}^{r_e} \gamma r^2 dr} = \frac{\langle n \rangle_{\text{lab}}}{\langle \gamma \rangle}. \quad (\text{C.1.22})$$

Clearly, the condition (C.1.13) gives a link between the description of the fireshell evolution in terms of local functions, entering (C.1.5) on the one side, and global quantities (C.1.17) and (C.1.19), on the other side. The presence of the global conservation (C.1.8) in both these cases ensures equivalence of the local (C.1.5) and the average (C.1.18) descriptions for the fireshell, unless its detailed structure is considered.

C.1.2. Energy-momentum conservation

The basis of description for relativistic fireshell is the energy-momentum principle. It allows to obtain relativistic hydrodynamic equations, or equations of motion for the fireshell, energy and momentum conservation equations which are used extensively to describe interaction of relativistic baryons of the fireshell with the interstellar matter, and boundary conditions which are used to understand shock waves propagation in the decelerating baryons and in the outer medium. Consider energy-momentum conservation in the most general form:

$$(T_{\mu}^{\nu})_{;\nu} = \frac{\partial(\sqrt{-g} T_{\mu}^{\nu})}{\partial x^{\nu}} + \sqrt{-g} \Gamma_{\nu\lambda}^{\mu} T^{\nu\lambda} = 0, \quad (\text{C.1.23})$$

where $\Gamma_{\nu\lambda}^{\mu}$ are Cristoffel symbols and g is determinant of the metric tensor. Integrating over the whole three-dimensional volume we obtain

$$\int_V T_{\mu}^{\nu}{}_{;\nu} dV = 0. \quad (\text{C.1.24})$$

Integrating over the whole four-dimensional volume and applying divergence theorem we get Taub (1948)

$$\int_t \int_V T_{\mu}^{\nu}{}_{;\nu} dV dt = \oint_V T_{\mu}^{\nu} \lambda_{\nu} dV = 0, \quad (\text{C.1.25})$$

where λ_{α} are covariant components of the outward drawn normal to the three-dimensional hypersurface (volume V).

Now suppose that there is a discontinuity on the fluid flow. Taking the volume to be a spherical shell and choosing the coordinate system where the discontinuity is at rest so that in (C.1.25) for normal vectors to the discontinuity hypersurface λ_{α} , we have

$$\lambda_{\alpha} \lambda^{\alpha} = 1, \quad \lambda_0 = 0. \quad (\text{C.1.26})$$

Let the radius of the shell R_s be very large and shell thickness Δ be very small. With $R_s \rightarrow \infty$ and $\Delta \rightarrow 0$ from (C.1.25) we arrive to

$$[T^{\alpha i}] = 0, \quad (\text{C.1.27})$$

where the brackets mean that the quantity inside is the same on both sides of the discontinuity surface. This equation together with continuity condition for particle density flux $[nU^i] = 0$ was used by Taub (1948) to obtain relativistic Rankine-Hugoniot equations. These equations govern shock waves dynamics which are supposed to appear during collision of the baryonic material left from the fireshell with the interstellar medium Blandford and Mc-

Kee (1976). The origin of the afterglow could be connected to the conversion of kinetic energy into radiative energy in these shocks Piran (1999), Rees and Meszaros (1992), Narayan et al. (1992), Katz (1994).

Consider now the energy-momentum tensor of the perfect fluid in the lab frame (where the fluid was initially at rest)

$$T^{\mu\nu} = p g^{\mu\nu} + \omega U^\mu U^\nu, \quad (\text{C.1.28})$$

where $\omega = \rho + p$ is proper enthalpy, p is proper pressure and ρ is proper internal energy density.

Rewrite (C.1.23) in spherically symmetric case

$$\frac{\partial T_0}{\partial t}^0 + \frac{1}{r^2} \frac{\partial}{\partial r} \left(r^2 T_0^1 \right) = 0, \quad (\text{C.1.29})$$

$$\frac{\partial T_1}{\partial t}^0 + \frac{1}{r^2} \frac{\partial}{\partial r} \left(r^2 T_1^1 \right) - \frac{1}{r} \left(T_2^2 + T_3^3 \right) = 0, \quad (\text{C.1.30})$$

arriving to equations of motion for relativistic fireshell Piran et al. (1993), Ruffini et al. (1999), Blandford and McKee (1976), Bisnovatyi-Kogan and Murzina (1995):

$$\frac{\partial(\gamma^2\omega)}{\partial t} - \frac{\partial p}{\partial t} + \frac{1}{r^2} \frac{\partial}{\partial r} \left(r^2 \gamma^2 \beta \omega \right) = 0, \quad (\text{C.1.31})$$

$$\frac{\partial(\gamma^2\beta\omega)}{\partial t} + \frac{1}{r^2} \frac{\partial}{\partial r} \left[r^2 (\gamma^2 - 1) \omega \right] + \frac{\partial p}{\partial r} = 0, \quad (\text{C.1.32})$$

where the four-velocity and the relativistic Lorentz factor are defined as follows³

$$U^\mu = (\gamma, \gamma\beta, 0, 0), \quad \gamma \equiv (1 - \beta^2)^{-1/2}, \quad (\text{C.1.33})$$

the radial velocity β .

The total momentum of spherically symmetric expanding shell vanishes. However, from local conservation equations (C.1.31) one can find out that the radial component of the four momentum vector does not vanish. In analogy with the continuity equation (C.1.5) we integrate the first equation in (C.1.31) over volume starting from some internal radius $r_i(t)$ up to some external radius $r_e(t)$ and ignoring a factor 4π we obtain

$$\begin{aligned} & \int_{r_i}^{r_e} \frac{\partial(\gamma^2\omega)}{\partial t} r^2 dr - \int_{r_i}^{r_e} \frac{\partial p}{\partial t} r^2 dr + \int_{r_i}^{r_e} \frac{1}{r^2} \frac{\partial}{\partial r} (r^2 \gamma^2 \beta \omega) r^2 dr = \\ & \frac{\partial}{\partial t} \int_{r_i}^{r_e} \gamma^2 \omega r^2 dr + r_i^2 \gamma^2(r_i) \omega(r_i) \beta(r_i) - r_e^2 \gamma^2(r_e) \omega(r_e) \beta(r_e) - \\ & \frac{\partial}{\partial t} \int_{r_i}^{r_e} p r^2 dr + r_i^2 p(r_i) - r_e^2 p(r_e) + r_e^2 \gamma^2(r_e) \omega(r_e) \beta(r_e) - r_i^2 \gamma^2(r_i) \omega(r_i) \beta(r_i) = 0. \end{aligned} \quad (\text{C.1.34})$$

³Throughout this chapter we put the speed of light equal to 1.

If the boundaries $r_i(t)$ and $r_e(t)$ are comoving with the fluid we have

$$\frac{d}{dt} \int_{r_i}^{r_e} (\gamma^2 \omega - p) r^2 dr = r_e^2 p(r_e) - r_i^2 p(r_i). \quad (\text{C.1.35})$$

Further, if one assumes (C.1.10), one gets the following result

$$E = 4\pi \int_0^{R(t)} \gamma^2 \omega r^2 dr = \text{const.} \quad (\text{C.1.36})$$

The differential conservation law follows from the same arguments which lead to (C.1.11), so we also have

$$dE = 4\pi \gamma^2 \omega r^2 dr \approx \text{const.} \quad (\text{C.1.37})$$

Analogously to (C.1.18) we introduce the average energy density in the lab frame

$$\langle \rho \rangle_{\text{lab}} \equiv \frac{E}{\mathcal{V}} = \frac{4\pi \int_{r_i}^{r_e} (\gamma^2 \omega) r^2 dr}{4\pi \int_{r_i}^{r_e} r^2 dr}, \quad (\text{C.1.38})$$

Taking the polytropic equation of state with the thermal index

$$\Gamma \equiv 1 + \frac{p}{\rho}, \quad (\text{C.1.39})$$

and requiring also $r \gg \Delta$ and (C.1.10) we find from (C.1.38)

$$\langle \rho \rangle_{\text{lab}} \simeq \rho(r) \gamma^2(r) \propto r^{-2}. \quad (\text{C.1.40})$$

The radial momentum equation follows from (C.1.32) as

$$\begin{aligned} & \int_{r_i}^{r_e} \frac{\partial(\gamma^2 \beta \omega)}{\partial t} r^2 dr + \int_{r_i}^{r_e} \frac{1}{r^2} \frac{\partial}{\partial r} [r^2 (\gamma^2 - 1) \omega] r^2 dr + \int_{r_i}^{r_e} \frac{\partial p}{\partial r} r^2 dr = \\ & \frac{\partial}{\partial t} \int_{r_i}^{r_e} \gamma^2 \beta \omega r^2 dr + r_i^2 \gamma^2(r_i) \omega(r_i) \beta^2(r_i) - r_e^2 \gamma^2(r_e) \omega(r_e) \beta^2(r_e) + \quad (\text{C.1.41}) \\ & + r_e^2 (\gamma^2(r_e) - 1) \omega(r_e) - r_i^2 (\gamma^2(r_i) - 1) \omega(r_i) + \int_{r_i}^{r_e} \frac{\partial p}{\partial r} r^2 dr = \\ & \frac{\partial}{\partial t} \int_{r_i}^{r_e} (\gamma^2 \beta \omega) r^2 dr + \int_{r_i}^{r_e} \frac{\partial p}{\partial r} r^2 dr = 0. \end{aligned}$$

This leads to

$$\frac{d}{dt} \int_{r_i}^{r_e} (\gamma^2 \beta \omega) r^2 dr = 2 \int_{r_i}^{r_e} pr dr + r_i^2 p(r_i) - r_e^2 p(r_e). \quad (\text{C.1.42})$$

For the radial momentum we have

$$\frac{d\mathbf{P}_{tot}}{dt} = \frac{d}{dt} \int_0^{R(t)} 4\pi (\gamma^2 \beta \omega) r^2 dr = 8\pi \int_0^{R(t)} pr dr. \quad (\text{C.1.43})$$

The left hand side of this equation is the time derivative of the radial momentum, i.e. the radial "force". The right hand side is the integral of pressure over all shells, so it is clear that unless the pressure in the fireshell is zero, it experiences self-acceleration due to internal pressure.

C.1.3. Entropy conservation

Yet another relevant equation is entropy conservation which may be obtained from (C.1.23) by projection on the flow line

$$\begin{aligned} U^\mu (T_\mu{}^\nu)_{;\nu} &= (U^\mu T_\mu{}^\nu)_{;\nu} - T_\mu{}^\nu (U^\mu)_{;\nu} = \\ &= -(\rho U^\mu)_{;\mu} - \omega U^\nu (U_\mu U^\mu{}_{;\nu}) - p U^\mu{}_{;\mu} = 0. \end{aligned} \quad (\text{C.1.44})$$

The second term on the last line vanishes since $U_\mu U^\mu = -1$, so we have another conservation equation

$$-U^\mu (T_\mu{}^\nu)_{;\nu} = (\rho U^\mu)_{;\mu} + p U^\mu{}_{;\mu} = 0. \quad (\text{C.1.45})$$

This conservation law corresponds to another conserved quantity, the entropy. In fact, equation (C.1.45) can be rewritten as

$$(\rho U^\mu)_{;\mu} + p U^\mu{}_{;\mu} = (\omega U^\mu)_{;\mu} - U^\mu p_{;\mu} = 0. \quad (\text{C.1.46})$$

Now using continuity equation (C.1.1) and the identity $\omega U^\mu = n U^\mu (\frac{\omega}{n})$ we find

$$(\omega U^\mu)_{;\mu} - U^\mu p_{;\mu} = n U^\mu \left[\left(\frac{\omega}{n} \right)_{;\mu} - \frac{1}{n} p_{;\mu} \right] = 0. \quad (\text{C.1.47})$$

But inside the brackets there are scalar functions, and therefore covariant derivatives can be replaced by usual derivatives. Then we recall the second law of thermodynamics Landau and Lifshits (1987)

$$d \left(\frac{\omega}{n} \right) = T d \left(\frac{\sigma}{n} \right) + \frac{1}{n} dp, \quad (\text{C.1.48})$$

and finally obtain

$$nTU^\mu \left(\frac{\sigma}{n} \right)_{;\mu} = 0, \quad (\text{C.1.49})$$

which can be rewritten using (C.1.1) as

$$(\sigma U^\mu)_{;\mu} = 0. \quad (\text{C.1.50})$$

This is continuity equation for the entropy. Since it has exactly the same form as (C.1.1), all conservation equations such as (C.1.11) and (C.1.8) hold for the entropy as well,

$$d\sigma = 4\pi (\sigma\gamma) r^2 dr \approx \text{const}, \quad (\text{C.1.51})$$

$$\mathbf{S} = \int_0^{R(t)} d\sigma = \text{const}. \quad (\text{C.1.52})$$

Assuming (C.1.39) we find from (C.1.45) and (C.1.20) the following result

$$\begin{aligned} U^\mu \rho_{;\mu} + \Gamma \rho U^\mu_{;\mu} &= \\ d \ln \rho + \Gamma d \ln V &= 0, \\ \langle \rho \rangle_{\text{com}} V^\Gamma &= \text{const}. \end{aligned} \quad (\text{C.1.53})$$

Finally, due to similarity of equations (C.1.11) and (C.1.51), the average entropy can be defined in the same manner as (C.1.18).

C.1.4. Analogy with a Friedmann Universe

It is easy to show that conservation equations (C.1.11),(C.1.37) and (C.1.51) imply an analogy between the fireball and the Friedmann Universe, noticed first by Shemi and Piran Shemi and Piran (1990),Piran et al. (1993). In fact, this analogy is valid for polytropic equation of state (C.1.39) and ultrarelativistic expansion condition (C.1.10). First, using (C.1.39) and the integral form of (C.1.48) we obtain

$$\sigma = \frac{\omega}{T},$$

which leads to

$$\rho \propto \sigma^\Gamma, \quad (\text{C.1.54})$$

we rewrite the above mentioned conservation equations using (C.1.39)

$$\begin{aligned} n\gamma r^2 &= \text{const}, \\ \rho^{\frac{1}{\Gamma}} \gamma r^2 &= \text{const}, \\ \rho \gamma^2 r^2 &= \text{const}. \end{aligned} \quad (\text{C.1.55})$$

From these equations we then easily find

$$\begin{aligned}\gamma &\propto r^{\frac{2(\Gamma-1)}{2-\Gamma}}, \\ n &\propto r^{-\frac{2}{2-\Gamma}}, \\ \rho &\propto r^{-\frac{2\Gamma}{2-\Gamma}}.\end{aligned}\tag{C.1.56}$$

Taking ultrarelativistic equation of state with $\Gamma = 4/3$ we immediately obtain

$$\begin{aligned}\gamma &\propto r, \\ n &\propto r^{-3}, \\ \rho &\propto r^{-4},\end{aligned}\tag{C.1.57}$$

as opposed to the nonrelativistic equation of state with $\Gamma = 1$ with different scalings

$$\begin{aligned}\gamma &= \text{const}, \\ n &\propto r^{-2}, \\ \rho &\propto r^{-2}.\end{aligned}\tag{C.1.58}$$

Actually, scaling laws (C.1.57) for number and energy densities take place for the homogeneous isotropic radiation-dominated Universe Shemi and Piran (1990), Piran et al. (1993). This fact allowed the authors of Piran et al. (1993) to speak about the frozen-pulse profile for $\gamma \gg 1$ where number, energy and entropy density is conserved within each differential shell with thickness dr , although radial distribution of matter and energy can be inhomogeneous.

Although for observer *inside* the radiation-dominated fireshell it looks indistinguishable from a portion of radiation-dominated Universe, for the observer *outside* it looks drastically different. In fact, validity of differential conservation laws (C.1.11), (C.1.37) and (C.1.51) together with integral ones (C.1.8), (C.1.36) and (C.1.52) implies constant thickness approximation assumed in Ruffini et al. (1999), Ruffini et al. (2000).

Clearly, if the condition (C.1.10) is satisfied, also

$$\Delta \ll R(t)\tag{C.1.59}$$

is valid. Given the scalings (C.1.57) we then find

$$V = 4\pi \int_{R(t)-\Delta}^{R(t)} \gamma r^2 dr \simeq 4\pi \int_{R(t)-\Delta}^{R(t)} \delta r^3 dr \simeq 4\pi R^3,\tag{C.1.60}$$

where we put $\gamma = \delta r$, δ is a constant. At the same time,

$$\mathcal{V} = 4\pi \int_0^{R(t)} r^2 dr = \frac{4\pi}{3} R^3. \quad (\text{C.1.61})$$

Equality of (C.1.60) and (C.1.61) up to a numerical factor suggests that the initially homogeneous energy and particle number distribution looks highly compressed in the lab frame expanding with ultrarelativistic velocity, with the compression factor γ .

C.2. Self acceleration of the fireshell

For a fireshell which is initially optically thick the total energy conserves. Assume, that the fireshell consists of relativistic electrons, positrons and photons, and also some admixture of a plasma in the form of photons and electrons is present, such that the total charge is zero. While electrons are relativistic, protons are not. Equation of state for pairs and electrons in such a case is given by that of ultrarelativistic fluid with a good approximation: $p_{e^\pm, \gamma} = \rho_{e^\pm, \gamma}/3$. At the same time for protons we have $p_p \simeq 0$. Therefore positrons and electrons together with photons can be considered as one fluid with $p_r = \rho_r/3$ as they are strongly coupled since the medium is optically thick. Instead protons have small pressure and internal energy comparing to their rest mass energy.

According to (C.1.36) we find

$$\int_0^{R(t)} (\gamma^2 \omega - p) r^2 dr = \int_0^{R(t)} \gamma^2 \rho_p r^2 dr + \frac{4}{3} \int_0^{R(t)} \gamma^2 \rho_r r^2 dr. \quad (\text{C.2.1})$$

These two terms are the rest mass energy of protons M_B and energy of the ultrarelativistic fluid E correspondingly, so we arrive to a simple result, expressing the total energy of expanding relativistic shell in the lab frame:

$$\gamma(E + M) = \text{const}, \quad (\text{C.2.2})$$

which reads simply as $E + M = \text{const}$ in the comoving frame taking into account the conversion of volumes (C.1.16).

For homogeneous distributions of matter, energy density and pressure the integrals (C.1.7), (C.1.35) and (C.1.42) reduce to

$$\begin{aligned} n\gamma\mathcal{V} &= \text{const}, \\ \left[\gamma^2 (\rho + p) \right] \mathcal{V} &= \text{const}, \end{aligned} \quad (\text{C.2.3})$$

while in the comoving frame instead we would have

$$nV = \text{const}, \quad (\text{C.2.4})$$

$$\rho V = \text{const}, \quad (\text{C.2.5})$$

which means energy and number of particles do not change.

From the above we have

$$nU_{com}^0 V = nV = \text{const} = nU_{lab}^0 \mathcal{V} = n\gamma \mathcal{V}, \quad (\text{C.2.6})$$

$$T_{com}^{00} V = \rho V = \text{const} = T_{lab}^{00} \mathcal{V} = [\gamma^2 (\rho + p)] \mathcal{V}, \quad (\text{C.2.7})$$

remembering that all quantities n, ρ, p are always defined as comoving ones.

Energy conservation (C.2.1) for (C.1.10) implies

$$\gamma = \gamma_0 \sqrt{\frac{\rho_p^0 + \Gamma \rho_0 \mathcal{V}_0}{\rho_p + \Gamma \rho \mathcal{V}}}. \quad (\text{C.2.8})$$

Clearly all the equations given above can be written for the average values of the number and energy densities.

D. Cosmological structure formation

D.1. The Cosmological Principle

Modern Cosmology is based upon a fundamental principle, the so called *cosmological principle*, that can be stated in the following way:

All positions in the Universe are equivalent.

As long as we look at our ‘neighbour’ Universe, this statement is certainly false, because the distribution of matter is far from homogeneous: there are planets, stars, and, going to larger scales, galaxies and clusters of galaxies, separated by almost empty regions. However, when we average this distribution over a volume large enough to contain thousands of clusters, it appears to be very close to homogeneous (see fig D.1).

Homogeneous and isotropic solution of Einstein equations of general relativity was first obtained by Friedmann in 1922. A remarkable property of this solution is that it describes a non-static Universe. At that time, there were no observational evidences for the temporal evolution of the whole Universe; then, many decades passed before the Big Bang model, which is based on Friedmann solution, became the standard paradigm in cosmology, following the discovery of cosmic microwave background radiation by Penzias & Wilson in 1969.

In effect, one of the strongest predictions of Big Bang model is the presence of a background microwave radiation, relic of the early Universe. This radiation is highly isotropic, reflecting, through the coupling with matter, the high isotropy and homogeneity of the primeval plasma. This tells us that the cosmological principle, and then Friedmann picture, safely applies to the early Universe; but what about the present one?

Hubble was the first trying to study the spatial distribution of objects as large as the galaxies, at that time thought to be the largest self-gravitating systems to exist. His results, namely Hubble law, imply, that the galaxy distribution is close to homogenous on the large-scale average. Homogeneity on very large scales is confirmed by present day observations of, in particular:

- X-ray background

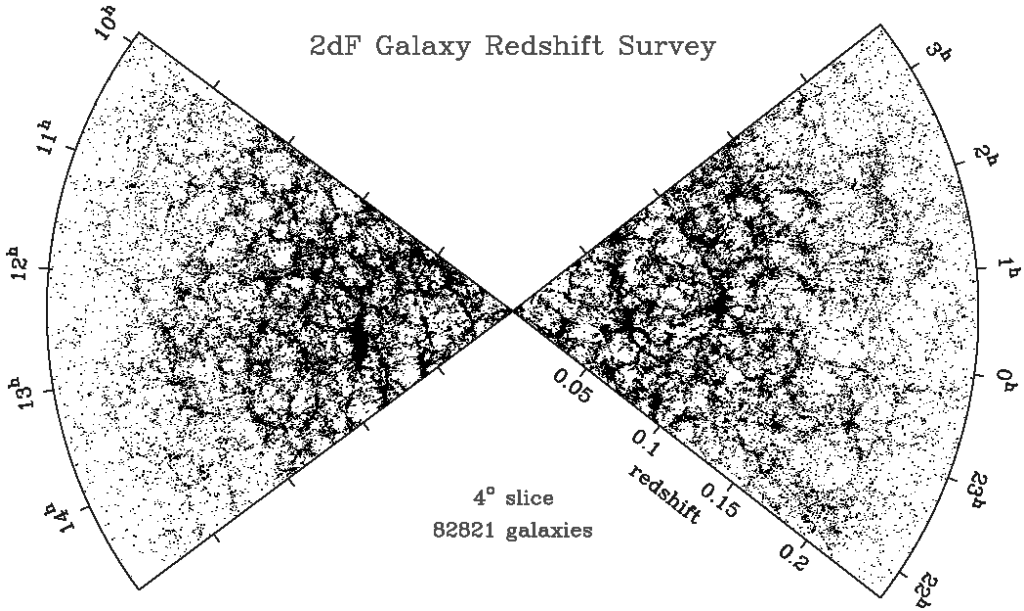


Figure D.1.: The distribution of galaxies in the 2dFGRS (from Peacock (2002)).

- radio sources
- gamma ray bursts
- galaxies and clusters of galaxies

On the other hand, on smaller scales, distribution of matter is far from homogeneous: galaxies tend to cluster, forming structures separated by large voids. These clusters of galaxies are themselves members of even larger structures, so called superclusters of galaxies. To study such a complicated distribution of matter, it is necessary to use a statistical approach. In the next section we will introduce the mathematical tools usually used to study large scale structure (LSS).

D.2. Two-point Correlation Function

The statistical description of clustering is based upon the concept of correlation, namely, in a more rigorous way, the probability of finding an object in the vicinity of another one. The standard way to quantify this probability is to define the two-point correlation function $\xi(\vec{x})$ Peebles (1993).

Let's consider a distribution of objects in space, described by the number density function $n(\vec{x})$. The probability that an object is found in an infinites-

imal volume δV centered around the point \vec{x} is proportional to the volume itself:

$$\delta P \propto \delta V. \quad (\text{D.2.1})$$

In the absence of structure, the joint probability of finding two objects in two different infinitesimal volumes δV_1 and δV_2 , centered respectively around \vec{x}_1 and \vec{x}_2 is given by the product of the two probabilities:

$$\delta P = \delta P_1 \delta P_2 \propto \delta V_1 \delta V_2 \quad (\text{D.2.2})$$

On the other hand, if objects have a tendency to cluster, we will find an excess probability:

$$\delta P \propto \delta V_1 \delta V_2 \cdot (1 + \xi(\vec{x}_1, \vec{x}_2)) \quad (\text{D.2.3})$$

According to the cosmological principle, we don't expect the correlation function to depend on the position neither on the direction, but only on separation between volumes: $\xi(\vec{x}_1, \vec{x}_2) = \xi(r_{12})$, where $r_{12} \equiv |\vec{x}_1 - \vec{x}_2|$.

An equivalent definition of the two-point correlation function is the following:

$$\xi(r_{12}) = < \delta(\vec{x}_1) \delta(\vec{x}_2) >, \quad (\text{D.2.4})$$

where $< \dots >$ denotes averaging over all pairs of points in space separated by a distance r_{12} , and $\delta(\vec{x}) \equiv (n(\vec{x}) - \bar{n})/\bar{n}$.

D.2.1. Observed Galaxy Distribution

Observational data coming from galactic surveys are usually expressed in the form of correlation function in redshift space, $\xi(\pi, \sigma)$, where π is a separation along the line of sight and σ is a angular separation on the plane of the sky between two galaxies. It is then possible to obtain the real-space correlation function $\xi(r)$; this step is never a trivial one, but we are not going into details since it is beyond the purpose of this review.

Peebles Peebles (1993) have shown that distribution of galaxies can be described by a two point correlation function with a simple power law form:

$$\xi_g(r) = \left(\frac{r}{r_g} \right)^{-1.77}, \quad r < 10h^{-1}\text{Mpc}, \quad (\text{D.2.5})$$

where h is a Hubble parameter today measured in $100 \frac{\text{km}}{\text{s Mpc}}$. The correlation length r_g determines the typical distance between objects. For galaxies, it was estimated to be $\simeq 5h^{-1}\text{Mpc}$.

For clusters of galaxies the same power law was found first by Bahcall and Soneira Bahcall and Soneira (1983) and Klypin and Kopylov Klypin and

Kopylov (1983)

$$\xi_c(r) = \left(\frac{r}{r_c}\right)^{-1.8}, \quad 5h^{-1} < r < 150h^{-1}\text{Mpc}. \quad (\text{D.2.6})$$

with different correlation length, namely $r_c \simeq 25h^{-1}\text{Mpc}$. Further, Bahcall and Burgett Bahcall and Burgett (1986) have found correlation function for superclusters of galaxies with the same power law.

Recent observations support these conclusions. Results from the Sloan Digital Sky Survey (SDSS) on galaxy clustering Zehavi et al. (2005) for about 200,000 galaxies give a real-space correlation function as

$$\xi_g(r) = \left(\frac{r}{r_0}\right)^{-1.8}, \quad 0.1h^{-1} < r < 10h^{-1}\text{Mpc}, \quad (\text{D.2.7})$$

where $r_0 \simeq 5.0h^{-1}\text{Mpc}$, although the brightest subsample of galaxies has a significantly steeper $\xi(r)$. The geometry of samples in SDSS is quite close to Las Campanas Redshift Survey Shectman et al. (1996) and the results are very similar, but with much better resolution.

The 2dF Galaxy Redshift Survey Peacock et al. (2001) (see fig.D.1) consists of approximately 250,000 galaxies redshifts. Their result is Hawkins et al. (2003):

$$\xi_g = \left(\frac{r}{r_0}\right)^{-1.67}, \quad 0.1h^{-1} < r < 12h^{-1}\text{Mpc}, \quad (\text{D.2.8})$$

with $r_0 = 5.05h^{-1}\text{Mpc}$

Their measurements are in agreement with previous surveys. However, having much smaller statistical errors they were able to find a slight difference of the power law exponent as well as the correlation length on distances or redshifts, colors and types of galaxies. For a summary of measurements of $\xi(r)$ by different surveys other than the ones cited here, see Table 2 of Ref. Hawkins et al. (2003).

D.2.2. Power Law Clustering and Fractals

It is clear that, once a correlation function is given, the density of objects around any randomly chosen member of the system is:

$$n(r) \propto 1 + \xi(r) \quad (\text{D.2.9})$$

If the correlation function has a power law behaviour with exponent γ :

$$\xi(r) \propto r^{-\gamma} \quad (\text{D.2.10})$$

as for galaxies and clusters of galaxies, where $\gamma \simeq 1.8$, then the number of objects in a given volume scales in a similar way:

$$N(r) \propto r^{3-\gamma} \quad (\text{D.2.11})$$

So, for non integer γ , the number of objects scales with a fractional power of the radius of the volume under consideration. This behaviour is typical of fractal sets.

A fractal is a set in which ‘mass’ and ‘radius’ are linked by a fractional power law Mandelbrot (1983):

$$M(r) \propto r^{D_F} \quad (\text{D.2.12})$$

where D_F is the fractional or Hausdorff dimension of the set. So galaxies seem to show, at least up to scales of about 100 Mpc, a fractal distribution with $D_F \simeq 1.2$.

A crucial characteristic of a fractal distribution is the presence of fluctuations at all length scales and, consequently, impossibility of defining an average value for the density. It can be stressed that a fractal structure in a cosmological model, although not spatially homogeneous, is not in conflict with weaker form of the cosmological principle Mandelbrot (1983): in a homogeneous fractal set each observer at a matter point belonging to the set observes the same matter distribution as any other observer belonging to the set.

The question about fractality in galaxy distribution is still under debate Coleman and Pietronero (1992), de Bernardis et al. (2002), Kolb and Turner (1990), Luo and Schramm (1992), de Gouveia dal Pino et al. (1995), Durrer and Labini (1998), Gaite et al. (1999), Joyce et al. (2005). There are two main problems that are to be faced with:

1. Most of the matter in the Universe is in the form of dark matter, while observations are about luminous matter. It is still unclear how (and even if) light traces mass: this is in particular related to the problem of matching the clustering of galaxies, that tells us about distribution of luminous (baryonic) matter, with the CMB anisotropies, that tell us about distribution of gravitating matter.
2. On the other hand, still little is known about fluctuations on intermediate scales between those of local galaxy surveys ($\sim 100h^{-1}$ Mpc) and those probed by the observation of CMB anisotropies ($\sim 1000h^{-1}$ Mpc). However, this gap is greatly reduced in recent times de Bernardis et al. (2002), Peacock et al. (2001).

Assuming that the fractal framework is, at least up to some large scale, a good description of the real matter distribution, a consistent model of structure formation has been proposed by Ruffini in the eighties (see Ruffini et al.

(1988) and references therein). In this model fractality arises from successive fragmentations of primordial structures, so called ‘elementary cells’, formed via gravitational instability in the neutrino component of the matter in the Universe. In the following chapter we shall analyse in detail this model. First we are going to discuss the general idea of gravitational instability.

D.3. Gravitational instability

The gravitational instability is usually considered as the basic mechanism of structure formation in the Universe (see for example Kolb and Turner (1990)). It is believed, that small inhomogeneities are already present at some initial time in the early Universe. Such small perturbations will grow due to gravitational attraction, because overdense regions will accrete matter from the neighbouring regions, raising a density contrast.

One of the simplest examples, showing the process of gravitational instability is a perfect fluid model. If density distribution in selfgravitating fluid is slightly nonuniform, i.e. small density perturbations exist, they will tend to grow. When the density contrast is small, linear approximation can be used. The main advantage of linear theory is that perturbations on different scales evolve independently.

It is the main result of this theory, that the growth of perturbations are damped by the Hubble expansion. It leads to a power law for the time dependence of density perturbations. For instance, in the Einstein-de Sitter model, that is thought to describe our Universe after recombination perturbations amplitude grow as $(1 + z)^{-1}$. Only during the nonlinear stage with large density contrast, the evolution becomes faster. At nonlinear stage, however, perturbations grow much faster, leading to formation of gravitationally bound objects.

The theory of linear density perturbations in a homogeneous medium was first developed by Jeans Jeans (1902), Jeans (1929). His study was motivated by intention to explain the mechanism of star formation. We describe this theory below. First, however, the validity range i.e. the evolution of cosmological horizon is discussed.

The linear perturbations in the expanding homogeneous and isotropic Friedman Universe were studied by Lifshitz Lishitz (1946) using completely relativistic treatment. Relativistic theory, however, is necessary only when the scale of perturbations lays outside the horizon, or when perturbations in ultrarelativistic matter are studied. In the most interesting cases, such as perturbations in dark matter well inside the horizon after equivalence epoch (when energy densities of radiation and other components are equal) it is sufficient to consider nonrelativistic theory, based on Newtonian gravity. Bonnor Bonnor (1957) (see also Heath (1991)) was the first, who studied evolution of spherically symmetric perturbations in Newtonian cosmology.

The theory of linear density perturbations in Newtonian treatment is developed in details in some textbooks, see e.g. Weinberg (1972), Peacock (1999), Padmanabhan (1993), Zeldovich and Novikov (1975).

D.3.1. Horizon scale and mass evolution

The Newtonian treatment is only applicable on scales smaller than horizon scale $\lambda_H = cH^{-1}$. Associated mass scale, defined as the mass contained within the sphere of a radius $\lambda_H/2$, where H is the Hubble parameter, is given by

$$M_H = \frac{4}{3}\pi\rho \left(\frac{\lambda_H}{2}\right)^3. \quad (\text{D.3.1})$$

Beyond this scale events are causally disconnected and thus any correlation breaks outside horizon. Thus structures cannot form on scales larger than λ_H . It monotonically increases with time, because the distance that light travels increases with time. There are different regimes, separated by the moment of equivalence in energy densities of radiation and nonrelativistic matter:

$$M_H \propto \begin{cases} a^3 & z > z_{eq} \\ a^{3/2} & z < z_{eq}. \end{cases} \quad (\text{D.3.2})$$

Today the horizon scale is approximately 3000Mpc, that corresponds to a mass scale $M \sim 10^{22}M_\odot$ for $\Omega = 1$ Universe. At recombination the total mass inside the horizon, thus, was approximately $(1/z_{rec})^{-3/2} \simeq 10^{17}M_\odot$, where $M_\odot = 2 \cdot 10^{30}$ kg is the mass of the sun.

D.3.2. Selfgravitating ideal fluid: linear theory

Fluid equations and background solutions

We consider a perfect fluid with density ρ and pressure p , in the Newtonian space with Cartesian ("physical") coordinate system r_i ¹. We assume that the fluid has a velocity field v_i . A gravitational potential Φ is induced in the fluid by its own mass density ρ distribution. All these quantities are related through the continuity, Euler and Poisson equations respectively:

$$\frac{\partial \rho}{\partial t} + \partial_i(\rho v_i) = 0, \quad (\text{D.3.3})$$

$$\frac{\partial v_i}{\partial t} + v_j \partial_j v_i + \frac{1}{\rho} \partial_i p + \partial_i \Phi = 0, \quad (\text{D.3.4})$$

¹Greek indices denote comoving coordinates, latin indices denote physical coordinates, both take values 1,2,3; Einstein summation rule is adopted.

$$\partial^2 \Phi - 4\pi G\rho = 0, \quad (\text{D.3.5})$$

where $\partial^2 = \partial_i \partial_i$. The cosmologically relevant solution of the above equations (D.3.3-D.3.5) is

$$v_i^0 = H(t)r_i, \quad (\text{D.3.6})$$

$$\frac{d\rho_0}{dt} + 3H\rho_0 = 0, \quad (\text{D.3.7})$$

$$p_0(t) = 0, \quad (\text{D.3.8})$$

$$\Phi_0 = \frac{2}{3}\pi G\rho_0 r^2, \quad (\text{D.3.9})$$

$$\frac{dH}{dt} + H^2 = -\frac{4}{3}\pi G\rho_0, \quad (\text{D.3.10})$$

where $r^2 = r_i r_i$, and density depends on time only: $\rho_0 = \rho_0(t)$.

It is interesting to note, that both the Hubble law (D.3.6) and the continuity equation in expanding space (D.3.7) could be obtained by transition to a new coordinate system, namely the so called comoving system x_α defined by

$$r_\alpha = a(t)x_\alpha, \quad (\text{D.3.11})$$

where $a(t)$ is a scale factor. This transformation implies the relation between coordinate differences Δr_i and Δx_α in these two systems

$$\frac{d\Delta r_\alpha}{dt} = a \frac{d\Delta x_\alpha}{dt} + \frac{da}{dt} \Delta x_\alpha = a \frac{d\Delta x_\alpha}{dt} + H(t)\Delta r_\alpha, \quad (\text{D.3.12})$$

where

$$H(t) = \frac{1}{a} \frac{da}{dt}. \quad (\text{D.3.13})$$

The same relation holds for velocity fields

$$v_\alpha(r_\beta, t) = u_\alpha(x_\beta, t) + Hr_\alpha = u_\alpha(x_\beta, t) + v_\alpha^0. \quad (\text{D.3.14})$$

Thus the solution (D.3.6-D.3.10) means uniform distribution of the fluid with zero peculiar velocity $u_\alpha^0 = 0$ and zero pressure $p_0 = 0$.

Usually, pressure and density are linked through equation of state $p = p(\rho)$. The five equations (D.3.3-D.3.5) together with the equation of state form a complete set, allowing to study the temporal evolution of the density and velocity distributions as well as pressure and gravitational potential.

Perturbed quantities

As well known, solutions (D.3.6-D.3.10) represent isotropic and homogeneous distribution of matter. In order to study density perturbations in linear ap-

proximation suppose, that

$$\rho(r_i, t) = \rho_0(t) [1 + \delta(r_i, t)], \quad (\text{D.3.15})$$

$$v_i(r_j, t) = v_i^0(r_j, t) + \delta v_i(r_j, t), \quad (\text{D.3.16})$$

$$\Phi(r_i, t) = \Phi_0(r_i, t) + \delta\Phi(r_i, t), \quad (\text{D.3.17})$$

$$p(r_i, t) = \delta p(r_i, t), \quad (\text{D.3.18})$$

where $\delta \equiv \frac{\rho - \rho_0}{\rho_0}$. Here all perturbed quantities δ , δv_i , δp and $\delta\Phi$ are assumed to be much smaller than the background quantities. All zero order values are given by (D.3.6-D.3.10). It is also assumed that the spatial and temporal derivatives of perturbed quantities are of the same order of magnitude as the quantities themselves.

Note that the condition of perturbed quantities smallness is not necessary to hold in the whole space. In particular, it could be the region in space where relation $|\delta v_i| > |v_i^0|$ takes place Meszaros (1974). In this case the standard linearization procedure leads to different perturbations equations and, consequently, to different solutions representing density contrast $\delta(r_i, t)$ time dependence.

Linearized perturbations equations

We rewrite (D.3.3-D.3.5) in comoving coordinates:

$$\frac{\partial \rho}{\partial t} + 3H\rho + \frac{1}{a}\rho\partial_\alpha u_\alpha + \frac{1}{a}u_\alpha\partial_\alpha\rho = 0, \quad (\text{D.3.19})$$

$$\frac{d^2a}{dt^2}x_\alpha + \frac{\partial u_\alpha}{\partial t} + Hu_\alpha + \frac{1}{a}u_\beta\partial_\beta u_\alpha + \frac{1}{a\rho}\partial_\alpha p + \frac{1}{a}\partial_\alpha\Phi = 0, \quad (\text{D.3.20})$$

$$\partial^2\Phi - 4\pi Ga^2\rho = 0. \quad (\text{D.3.21})$$

Here all quantities, except for H^2 , depend on comoving coordinates x_α and time t . Equations (D.3.19-D.3.21) can be found for example in Meszaros (1993) written in physical coordinates. One arrives at the above from (D.3.3-D.3.5) on using the transformation laws $(\partial/\partial t)_{phys} = (\partial/\partial t)_{com} - Hx_\alpha\partial_\alpha$ and $(\partial_\alpha)_{phys} = (1/a)(\partial_\alpha)_{com}$.

With the goal to obtain equations for density contrast δ in linear approximation we substitute (D.3.15-D.3.18) into equations (D.3.19-D.3.21). Taking into account that the spatial as well as temporal derivatives of perturbed quantities have the same order of magnitude as the perturbed quantities

²If one suppose in addition that Hubble parameter also can be disturbed (can have spatial dependence) then the system of equations becomes overdefined. There is another approach Ellis and Bruni (1989), Ellis (1990), however, where $\partial_\alpha\delta$ and $\partial_\alpha H$ are taken as independent variables in order to study density perturbations.

themselves, and using (D.3.6-D.3.10), the perturbations equations read

$$\frac{\partial \delta}{\partial t} + \frac{1}{a} \partial_\alpha \delta u_\alpha = 0, \quad (\text{D.3.22})$$

$$\frac{\partial \delta u_\alpha}{\partial t} + H \delta u_\alpha + \frac{1}{a} \partial_\alpha \delta p + \frac{1}{a} \partial_\alpha \delta \Phi = 0, \quad (\text{D.3.23})$$

$$\partial^2 \delta \Phi - 4\pi G a^2 \rho_0 \delta = 0, \quad (\text{D.3.24})$$

where $\delta u_\alpha(x_\beta, t)$ is a first order quantity, because its unperturbed value is $u_\alpha^0(x_\beta, t) = 0$.

The simplest way to find the equation governing density perturbations is to take the time derivative of equation (D.3.22) and use the divergence of equation (D.3.23) together with equation (D.3.24). After some calculations one finds the final expression:

$$\frac{\partial^2 \delta}{\partial t^2} + 2H \frac{\partial \delta}{\partial t} - \frac{v_s^2}{a^2} \partial^2 \delta - 4\pi G \rho_0 \delta = 0, \quad (\text{D.3.25})$$

where v_s denotes the sound speed in the fluid:

$$v_s^2 = \frac{dp}{d\rho} \quad (\text{D.3.26})$$

The Jeans criterion

Equation (D.3.25) governs dynamics of density perturbations. It is a wave-like second order partial differential equation. Thus, it is natural to perform Fourier transformation

$$\delta = \sum_k h(t) e^{ik_\alpha x_\alpha} \quad (\text{D.3.27})$$

in order to split perturbations on different scales.

The equation (D.3.25) can be rewritten in k -space, taking into account that $\partial_\alpha \delta \rightarrow ik_\alpha h$:

$$\frac{d^2 h}{dt^2} = -2H \frac{dh}{dt} + (4\pi G \rho_0 - \frac{v_s^2 k^2}{a^2}) h, \quad (\text{D.3.28})$$

where k_α is a comoving wavevector and $k = \sqrt{k_\alpha k_\alpha}$ is a corresponding wavenumber. The comoving wavelength of the perturbative mode is given by $l = 2\pi/k$, while the proper (physical) wavelength is simply $\lambda = al$.

Jeans criterion takes place for (D.3.28)

$$\lambda_J = v_s \sqrt{\frac{\pi}{G \rho_0}}, \quad (\text{D.3.29})$$

where λ_J separates gravitationally stable scales from unstable ones. Fluctu-

ations on scales well beyond λ_J grow via gravitational instability, while on scales smaller than λ_J pressure overwhelms gravity and perturbations do not grow.

The first term on the right-hand side of (D.3.28) comes from the general expansion. In the static world, initially considered by Jeans, such term is absent, leading to exponential growth of perturbations. In expanding space perturbations grow with time according to a power law.

A very important quantity is usually associated with the Jeans length (D.3.29), namely the Jeans mass

$$M_J = \frac{4}{3}\pi\rho \left(\frac{\lambda_J}{2}\right)^3, \quad (\text{D.3.30})$$

defined as the mass contained within a sphere of radius $\lambda_J/2$, where ρ is density of the perturbed component.

Multi-component system

Perturbations for a given mode in a single component evolve according to (D.3.28). When several components such as Cold Dark Matter (CDM), Hot Dark Matter (HDM), baryons and radiation are present simultaneously, it is possible to generalize (D.3.25). Assuming gravitational interaction between components only, we arrive at

$$\frac{d^2 h_i}{dt^2} = -2H\frac{dh_i}{dt} + (4\pi G\rho_0 \sum_j \epsilon_j h_j - \frac{(v_s^2)_i k^2}{a^2} h_i), \quad (\text{D.3.31})$$

where index i refers to the component under consideration, the sum is over all components and $\epsilon_i = \rho_i / \sum_j \rho_j$. Notice, that any smoothly distributed component (like cosmological constant) does not contribute to the right-hand side of (D.3.31).

D.3.3. Applications

Some important cases of matter content of the Universe will be considered below. First we discuss perturbations dynamics in the dominant nonrelativistic component (baryonic or not). Second example is a dark matter perturbations in the presence of dominant radiation component.

Einstein-de Sitter Universe

First of all, consider the dust dominated $\Omega = 1$ Universe. This condition (Ω is a density parameter) means flat-type cosmological model. In other words, curvature parameter $k = 0$ in Friedman solution of Einstein General Relativity equations. This model is thought to provide a good description of

our Universe after recombination. To zero order $a \sim t^{2/3}$, $H = 2/3t$ and $\rho_0 = 1/6\pi G t^2$. For perturbations well inside horizon we have

$$t^2 \frac{d^2 h}{dt^2} + \frac{4}{3} t \frac{dh}{dt} - \frac{2}{3} \left[1 - \left(\frac{\lambda_J}{\lambda} \right)^2 \right] h = 0. \quad (\text{D.3.32})$$

For modes well inside the horizon and still larger than the Jeans length the solution is

$$h(k, t) = h_1(k) \left(\frac{t}{t_0} \right)^{2/3} + h_2(k) \left(\frac{t}{t_0} \right)^{-1}. \quad (\text{D.3.33})$$

As expected there are two solutions, one growing and one decaying. At late time, however, only growing mode is important. Perturbations evolve proportionally to the scale factor or as $(1+z)^{-1}$, where z is the redshift defined by:

$$1+z = \frac{a_0}{a(t)}, \quad (\text{D.3.34})$$

and a_0 denotes the value of a scale factor today.

Perturbations on scales smaller than the Jeans length cease to grow and oscillate with time.

Mixture of radiation and dark matter

Consider the radiation dominated Universe when $a \sim t^{1/2}$ and $H = 1/2t$. The second component to be considered is a collisionless dark matter with $v_{DM} = 0$. We still can use Newtonian treatment on scales much smaller than the horizon size.

Since the small scale photon distribution is smooth and the energy density is dominated by the radiation, the equation governing dark matter instability reduces to

$$t \frac{d^2 h_{DM}}{dt^2} + \frac{dh_{DM}}{dt} = 0. \quad (\text{D.3.35})$$

It possesses the solution

$$h_{DM}(k, t) = h_1(k) \log \left(\frac{t}{t_0} \right) + h_2(k). \quad (\text{D.3.36})$$

Perturbations in dark matter component inside the horizon experience a slow logarithmic growth. This is known as Meszaros effect Meszaros (1974).

D.3.4. Initial spectrum of perturbations

In the first example we have shown, that perturbations on scales between horizon size and Jeans length $\lambda_J \ll \lambda \ll \lambda_H$ grow as $\delta \propto (1+z)^{-1}$. In order

to study perturbations dynamics one have to know, in addition, initial values of perturbations at some moment in early Universe.

One great possibility provide cosmic microwave background radiation anisotropy measurements, because density inhomogeneities when photons were coupled to baryons can be extracted from temperature fluctuations observed in cosmic microwave background radiation. Since $\frac{\delta T}{T} \simeq 10^{-5}$ it is usually assumed that at the moment of recombination $\delta \simeq 10^{-4}$ Kolb and Turner (1990).

Perturbations amplitudes on different scales are usually represented by a power spectrum $P(k)$, that is a Fourier transform of a previously introduced correlation function Peacock (1999)

$$\xi(r) = \frac{V}{(2\pi)^3} \int P(k) \frac{\sin kr}{kr} 4\pi k^2 dk. \quad (\text{D.3.37})$$

There is no evidence, that initial spectrum contained some preferred scales, thus it should be a featureless power law

$$P(k) \propto k^n, \quad (\text{D.3.38})$$

where index n governs the balance between perturbation amplitudes on large and small scales. The value $n = 0$ corresponds to a white noise, that have the same amplitude forevery mass scale. The value $n = 1$ corresponds to a so-called Harrison-Zel'dovich scale invariant spectrum. Term ‘scale invariance’ means that perturbations had the same amplitude at the moment of horizon crossing.

D.3.5. Damping of Perturbations

In addition to the Jeans scale some other cosmologically important scales appear in the theory of structure formation. They are related to physical processes, that cannot be described within perfect fluid approximation. However, fortunately, such processes take place on limited scale intervals and outside such intervals fluid description is still possible. We are going to discuss some dissipative effects, such as collisional damping of baryonic perturbations and free streaming of collisionless light particles.

Silk damping

Close to recombination the coupling between photons and baryons makes possible for the former to erase perturbations on the latter. This is because at that time the free mean path of photons becomes larger, so they can travel from overdense into underdense regions dragging baryons with them, thus smoothing inhomogeneities in primeval plasma. This effect was discovered by Silk (1967). The physical scale, associated with it is Kolb and Turner

(1990)

$$l_S \simeq 3.5(\Omega h^2)^{-3/4} \text{Mpc}, \quad (\text{D.3.39})$$

that gives a mass scale

$$M_S \simeq 6.2 \cdot 10^{12}(\Omega h^2)^{-5/4} \text{M}_\odot. \quad (\text{D.3.40})$$

This scale is close the mass of a typical galaxy $10^{11} M_\odot$. However, Silk damping affects baryonic perturbations only. Moreover, it is important only around recombination when the coupling is still sufficiently strong to make photons drag baryons with them.

Free streaming

Another damping process is Landau damping or free streaming, that originates from free motion of collisionless particles on small scales. They can travel far if velocity dispersion is large. This is important after particles decouple from plasma and until they become nonrelativistic.

Free streaming discovery became a dramatic moment for structure formation scenarios based upon Hot Dark Matter (HDM) models Bond and Szalay (1983). Name Hot Dark Matter means that particles, that constitutes such matter were ultrarelativistic at equivalence. Thus their velocity dispersion was near the light speed c . The maximum scale travelled by collisionless particles from decoupling can be estimated as Padmanabhan (1993)

$$l_{FS} \simeq 0.5 \left(\frac{m_{DM}}{1 \text{keV}} \right)^{-4/3} (\Omega_{DM} h^2)^{1/3} \text{Mpc}, \quad (\text{D.3.41})$$

and a corresponding mass scale has an order of supercluster of galaxies or even larger if the particle mass is $m_{DM} < 30 \text{ eV}$.

Cold thermal relics, that constitutes Cold Dark Matter (CDM) content, are slow enough to allow to neglect the free streaming on cosmologically important scales. Therefore, Landau damping affects only light particles such as neutrinos with $m_\nu \sim 10 \text{ eV}$, and in the Universe dominated by HDM erase all perturbations on scales smaller than superclusters of galaxies. At the same time, after particles become nonrelativistic at z_{nr} , their velocity dispersion becomes small enough, making free streaming negligible.

D.3.6. Structure formation on late times

Nonlinear clustering

In previous sections we dealt with linear evolution of cosmological perturbations. During a long period of time from recombination and even earlier, until almost recent times such treatment allows to describe the growth of inhomogeneity in the Universe, because condition $\delta \ll 1$ were satisfied. On recent

times, say, at $z \sim 10$, nonlinear behaviour of perturbations becomes important. During nonlinear stage gravitationally bound objects, such as galaxies, form. Nonlinear evolution is a rapid process, where not only gravitational effects are important, in particular during formation of galaxy different dissipation and relaxation processes take place Peacock (1999).

We are not going into details of galaxy formation here. The LSS formation is the subject of this section. Here the main interaction remains gravity. However, theoretical description, based on linear equations for ideal fluid becomes inadequate.

Usually N-body simulations are implemented in order to study nonlinear clustering Peacock (1999). However, some useful simplified models are still possible even on nonlinear stage, because numerical simulations provide limited physical insight into the physics of gravitational clustering. Among nonlinear approximations, the most famous are Zel'dovich approximation Zel'dovich (1970) and spherical collapse model (see for example Peebles (1993)).

The key point in Zel'dovich model is that during collapse in almost spherically symmetric overdense region gravitational interaction amplifies asymmetry. Therefore, final structure acquires a preferred direction and finally collapsed body will look like a 'pancake'.

In the spherical collapse model, on the contrary, it is assumed, that spherical symmetry preserves during the whole period of collapse. It allows to split the spherical overdensity region into concentric shells and study evolution of each shell separately, that sufficiently simplifies a problem. This model will be described in detail in the next chapter.

Structure formation scenarios

Historically two different pictures of structure formation were considered, namely HDM (see Primack and Mardon (2002)) and CDM models (see Primack (2003)). We will discuss them briefly below.

HDM models

The neutrino dominated Universe with $m_\nu \sim 10$ eV is a typical HDM model. The HDM model is associated with so-called "top-down" scenario, where structures form on large scales first. This is so, because the Jeans mass for HDM is of the order of supercluster mass or even higher. At the same time, free streaming erase perturbations on smaller scales. Thus, only when perturbations reach nonlinear regime on large scales they can induce fragmentation on smaller scales.

Usually it is assumed, that large scale perturbations become non-spherical according to the Zel'dovich model and thus LSS look like a "net" of density condensations separated by huge voids. Simulations agree with such picture.

The HDM model is in a good agreement with observational data on scales larger than 10 Mpc. On smaller scales, however, HDM simulations can agree with observed correlation function of galaxies only if the epoch of pancaking takes place at $z \simeq 1$ or less, which is too late, because we can see galaxies and quasars with much greater z .

The crucial cosmological property of HDM with neutrinos, as was mentioned above, is the damping of perturbations on small scales due to free streaming. Neutrino dominated models ($\Omega_\nu \sim 1$) alone could not describe the real Universe because on scales smaller than ~ 100 Mpc no structure appears at all.

One important prediction of HDM models with neutrinos is existence of large smooth halos around galaxies. At the end of collapse, during formation of the galaxy, baryonic component can dissipate its energy via collisions, but the neutrino component cannot. Thus, neutrinos remain less condensed than baryons, forming a large galactic halos.

CDM models

CDM models do not have troubles with free streaming, because its particles have negligible velocities at decoupling. Moreover, the Jeans mass for typical CDM model lays well below $10^6 M_\odot$. Thus, perturbations start to develop on small scales simultaneously with perturbations on large scales.

In the CDM models the important feature is the weak growth experienced by perturbations between horizon crossing and equivalence (see §D.3.3). It means, that the density contrast increases when we move to smaller scales, or that the perturbations spectrum has more small-scale power.

After collapse first structures in CDM models virialize through violent relaxation Lynden-Bell (1967), Shu (1978) into gravitationally bound objects that form galactic halos. Structures form in self-similar manner from small to large scales, in other words according to a ‘bottom-up’ scenario.

A pure CDM models, however, fail to predict the observed correlation function for galaxies on large scales. If one wants to retain the CDM hypothesis, the simplest way is to reduce the matter density. This shifts matter-radiation equivalence to a later epoch, resulting in redistribution of power in the spectrum of perturbations in favour of larger scales.

Today Λ CDM model with $\Omega_{tot} = 1$ and $\Omega_\Lambda = 0.7$ is considered as the best fit to the full set of observational data.

E. Massive degenerate neutrinos in Cosmology

In Appendix D we have described the evolution of perturbations, and we saw that the nature of dark matter particles is crucial in determining the way structure formation goes. In spite of the fact that a lot of candidates for CDM particles are being considered (see Ref. Bertone et al. (2005) for a review, there are no experimental detections of such particles at present. From the other hand, neutrinos are the only candidates for DM known to exist.

'Light' neutrinos ($m_\nu \ll 1$ MeV) Dolgov (2002), namely neutrinos that decouple while still in their ultrarelativistic regime (see below), may provide a significant contribution to the energy density of the Universe ($\Omega_\nu \sim 1$). Models with light neutrinos were extensively studied in the eighties; a large literature exists on this subject Bisnovatyi-Kogan and Novikov (1980), Zeldovich and Syunyaev (1980), Doroshkevich and Khlopov (1981), Peebles (1982).

The key prediction of the cosmological model with neutrinos is a cellular structure on large scales (see Fig.3.1). The qualitative drawing of cellular structure of the Universe is represented at Fig.D.1.

Ruffini and collaborators have studied such models with particular attention to the problem of clustering on large scales and its relation to the fractal distribution of matter. In the following, we are going to describe their works in detail.

E.1. Neutrino decoupling

The cosmological evolution of a gas of particles can be split in two very different regimes. At early times, the particles are in thermal equilibrium with the cosmological plasma; this corresponds to the situation in which the rate $\Gamma = <\sigma v n>$ of the reactions supposed to maintain the equilibrium (such as $\nu_e + \bar{\nu}_e \leftrightarrow e^+ + e^- \leftrightarrow 2\gamma$ in the case of electronic neutrinos) is much greater than the expansion rate, given by the Hubble parameter. The gas evolves then through a sequence of thermodynamic equilibrium states, described by the usual Fermi-Dirac statistics:

$$f(p) = \frac{1}{\exp [(E(p) - \mu)/k_B T] + 1}, \quad (\text{E.1.1})$$

where p , μ and T are the momentum, chemical potential and temperature of neutrinos respectively, and k_B is a Boltzmann constant.

However, as the Universe expands and cools, the collision rate Γ becomes lower than the expansion rate; this means that the mean free path is greater than the Hubble radius, thus we can consider the gas as expanding without collisions. It is customary to describe the transition between the two regimes by saying that the gas has decoupled from the cosmological plasma.

E.2. The redshifted statistics

Since in a spatially homogeneous and isotropic Universe, described by the Robertson-Walker metric, the product of the three-momentum $p(t)$ of a free particle times the scale factor $a(t)$ is a constant of the motion:

$$p(t) \cdot a(t) = \text{const}, \quad (\text{E.2.1})$$

each particle in the gas changes its momentum according to this relation. This fact, together with Liouville's theorem, implies that the distribution function after the decoupling time t_d (defined as the time at which $\Gamma = H$) is given by Ruffini et al. (1983):

$$f(p, t > t_d) = f\left(\frac{a(t)}{a_d} p, t_d\right) = \frac{1}{\exp\left[\left(E\left(\frac{a(t)}{a_d}\right)p - \mu_d\right)/k_B T_d\right] + 1} \quad (\text{E.2.2})$$

where the subscript d denotes quantities evaluated at the decoupling time.

Now let's turn our attention to the special case of neutrinos with $m_\nu \lesssim 10 \text{ eV}$. The ratio Γ/H , as a function of the cosmological temperature, can be evaluated using quantum field theory Kolb and Turner (1990)

$$\frac{\Gamma}{H} \simeq \left(\frac{T}{1 \text{ MeV}}\right)^3 \quad (\text{E.2.3})$$

as long as $T \gg m$.

Therefore, neutrinos decouple from the cosmological plasma, when $T = T_d \simeq 1 \text{ MeV}$. Since $kT_d \gg mc^2$, many of the particles obey $pc \gg mc^2$ and then, when performing integration over the distribution function (E.2.2), we can safely approximate:

$$f(p, t > t_d) = f\left(\frac{a(t)}{a_d} p, t_d\right) \simeq \frac{1}{\exp\left[\left(\frac{a(t)}{a_d} pc - \mu_d\right)/k_B T_d\right] + 1}, \quad (\text{E.2.4})$$

since the tail of the distribution function for which $mc^2 \gg pc$ gives little contribution.

In the following, we will need to compute the mean value of physical quantities over this distribution. It will be useful to consider two limiting regimes, namely the nonrelativistic one and the ultrarelativistic one. They correspond to two approximations for the single particle energy Ruffini et al. (1983):

$$\begin{array}{lll} E \simeq mc^2 & kT \ll mc^2 & \text{NR} \\ E \simeq pc & kT \gg mc^2 & \text{UR} \end{array}$$

We stress the fact that this substitution has to be performed only in the function to be integrated, and not on the distribution function. The approximation (E.2.4) depends only on the fact that the particles are ultrarelativistic at the time of decoupling, and then it is valid even when $kT \ll mc^2$.

Then, with a suitable substitution of variables, all the relevant integrals can be recast in a very simple, dimensionless form:

$$I_n(\xi) \equiv \int_0^\infty \frac{y^n dy}{\exp[(y - \xi)] + 1}, \quad (\text{E.2.5})$$

where $\xi \equiv \mu_d/kT_d$ is the dimensionless chemical potential, or degeneracy parameter. These integrals can be expressed using Riemann zeta and related functions.

E.3. Energy density of neutrinos

The present density parameter of neutrinos can be easily evaluated using the method outlined in the previous section. The energy density is given by:

$$\rho_{\nu+\bar{\nu}}(t_0) = \frac{g}{h_P^3} \int_0^\infty E(p) f(p, t_0) d^3 p \quad (\text{E.3.1})$$

where g is the number of helicity states and h_P is the Planck constant. By normalization with respect to the critical density $\rho_c = 1.054 h^2 \cdot 10^4 \frac{\text{eV}}{\text{cm}^3}$, we obtain Ruffini and Song (1986), Ruffini et al. (1988):

$$\Omega_{\nu+\bar{\nu}} h^2 \simeq 1.10 \cdot 10^{-1} g \frac{m}{10 \text{ eV}} A(\xi), \quad (\text{E.3.2})$$

where $A(\xi)$ is defined as follows

$$A(\xi) \equiv \frac{I_2(\xi) + I_2(-\xi)}{2I_2(0)} = \frac{1}{4\eta(3)} \left[\frac{1}{3} |\xi|^3 + 4\eta(2)|\xi| + 4 \sum_{k=1}^{\infty} (-1)^{k+1} \frac{e^{-k|\xi|}}{k^3} \right], \quad (\text{E.3.3})$$

and $\eta(n)$ is the Riemann eta function of index n .

The term $I_2(-\xi)$ appears because we have to take into consideration the

presence of antiparticles, for which the relation $\xi_{\bar{\nu}} = -\xi_{\nu}$ holds. This result follows from the fact that, if we consider a reaction such as

$$\nu + \bar{\nu} \longleftrightarrow \dots \longleftrightarrow \gamma + \gamma \quad (\text{E.3.4})$$

we get that, since the chemical potentials of the initial and final states have to be equal, and the chemical potential of the latter is equal to zero, it follows, that $\xi_{\bar{\nu}} = -\xi_{\nu}$.

E.3.1. Neutrino mass

We now know from neutrino oscillation experiments that neutrino do have mass (see Ref. Maltoni et al. (2004) for a review). It is a remarkable fact that neutrino flavour and mass eigenstates do not coincide, but are instead related by a rotation in flavour space:

$$|\nu_{\alpha}\rangle = \sum_{i=1}^3 U_{\alpha i} |\nu_i\rangle \quad (\text{E.3.5})$$

where $\alpha = e, \mu, \tau$ labels flavour eigenstates, while $i = 1, 2, 3$ labels mass eigenstates. The “rotation” matrix $U_{\alpha i}$ is called the neutrino mixing matrix. A great deal of effort is presently being put now in measuring the elements of the mixing matrix and the mass differences, which are the parameters actually probed in oscillation experiments. On the other hand, this kind of experiments do not give any information on the absolute scale of the neutrino mass. In this regard, useful information can be obtained by 1. tritium beta decay experiments, 2. neutrinoless beta decay experiments, 3. cosmological observations.

The tritium β decay experiments are sensitive to the “electron neutrino mass” (this is actually a misnomer since the electron neutrino is not a mass eigenstate and thus does not possess a well definite mass) m_e :

$$m_e = \left(\sum_{i=1}^3 |U_{ei}|^2 m_i^2 \right)^{1/2}. \quad (\text{E.3.6})$$

The present 95% CL bounds are:

$$\begin{aligned} m_e < 2.05 \text{ eV} & \quad \text{Troitsk experiment } \textit{Lobashev} \text{ (2003)} \\ m_e < 2.3 \text{ eV} & \quad \text{Mainz experiment } \textit{Kraus et al.} \text{ (2005)} \end{aligned} \quad (\text{E.3.7})$$

The upcoming KATRIN experiment KATRIN collaboration (2001) is expected to improve this bounds by nearly an order of magnitude, reaching a discovery potential for 0.3-0.35 eV masses.

At the same time, no direct measurements or constraints on muonic and

tauonic neutrino masses exist, although we know from oscillation experiments that the difference between masses should in the sub-eV range. Moreover, it is still unknown, whether neutrinos are Majorana or Dirac particles.

Experiments on neutrinoless double β decay (Aalseth et al. (1999),Klapdor-Kleingrothaus et al. (2001),Arnaboldi et al. (2005)) are instead sensitive to the “Majorana mass” $m_{\beta\beta}$:

$$m_{\beta\beta} = \left| \sum_{i=1}^3 U_{ei}^2 m_i \right| \quad (\text{E.3.8})$$

A recent paper Strumia and Vissani (2005) gives the following upper bound at 99% CL:

$$|m_{\beta\beta}| \lesssim 0.6 \text{eV}. \quad (\text{E.3.9})$$

Cosmology is mainly sensitive, at least to leading order, to the sum of neutrino masses M_ν :

$$M_\nu = \sum_{i=1}^3 m_i \quad (\text{E.3.10})$$

We should stress that there is no single limit that can be obtained on M_ν by means of cosmological observables, since the exact result depends of several factor, like the datasets considered, and the theoretical assumptions that are made (“priors”). However, we can summarize the present status as follows:

$$M_\nu \lesssim 0.2 - 2.3 \text{eV} \quad (\text{E.3.11})$$

where of course the largest value should be taken as the most conservative one, i.e., the one that is obtained by using only the more robust pieces of data (basically the CMB spectrum) and without making any assumption other than the standard FRW cosmological model. It is worth noting that these bounds are competitive with the ones coming from particle physics experiments. They are also expected to improve by an order of magnitude with the next generation of cosmological observations. For a review on the current limits on neutrino mass from cosmology, and how these will be improved in the future, we refer the reader to the work of Lesgourgues and Pastor Lesgourgues and Pastor (2006).

E.3.2. Chemical potential

First constraints on neutrino degeneracy parameter from BBN were obtained in Doroshkevich et al. (1971),Beaudet and Goret (1976). It was shown later Bianconi et al. (1991) that a small value of ξ_e and large values of $|\xi_{\mu,\tau}|$ simultaneously, can lead to BBN abundances which are consistent with observations. It is found in particular that

$$0 \leq \xi_e \lesssim 1.5, \quad (\text{E.3.12})$$

with the additional constraint $F(\xi_\mu) + F(\xi_\tau) \approx F(10\xi_e)$, where $F(\xi) \equiv \xi^2 + \xi^4/2\pi^2$. This, in particular, implies $|\xi_{\mu,\tau}| \lesssim 10\xi_e$.

Recent data both from BBN and CMBR Orito et al. (2001),Kneller et al. (2001),Hansen et al. (2002),Orito et al. (2002),Hansen et al. (2002) strongly constrain neutrino degeneracy parameters. In the paper Orito et al. (2001) these constraints are surprisingly wide, $\xi_e < 1.4$ and $|\xi_{\mu,\tau}| < 40$. Other papers give essentially stronger constraints using additional assumptions,

$$\begin{aligned} \xi_e &< 0.3 \\ |\xi_{\mu,\tau}| &< 2.6. \end{aligned} \quad (\text{E.3.13})$$

Recently, a very robust albeit less stringent limit has been obtained by the analysis of CMB data Lattanzi et al. (2005):

$$|\xi| \leq 1.1 \quad (\text{E.3.14})$$

where the same limit holds for every flavour.

E.3.3. Neutrino oscillations

When one consider different chemical potentials for all neutrino flavors at the epoch prior to BBN, neutrino oscillations equalize chemical potentials Savage et al. (1991), if there is enough time to relaxation process Abazajian et al. (2002). On the basis of large mixing angle solution of the solar neutrino problem,which is favored by recent data Ahmad et al. (2001), the BBN consideration constrains degeneracy parameters of all neutrino flavors Dolgov et al. (2002):

$$|\xi| \leq 0.07. \quad (\text{E.3.15})$$

However the situation when flavor equilibrium is not achieved before BBN is also possible. Thus in the following we consider quite high values of the degeneracy parameter and assume it is positive without loss of generality.

The main result that comes from oscillations consideration is that masses of different neutrino species are nearly equal: $m_{\nu_e} \simeq m_{\nu_\mu} \simeq m_{\nu_\tau}$.

E.4. The Jeans mass of neutrinos

In neutrino dominated Universe the first possible structure occurs when these particles become nonrelativistic, since at earlier times free streaming erases all perturbations. At this epoch the cosmological redshift has the value Ruffini et al. (1988)

$$1 + z_{nr} = 1.698 \cdot 10^4 \left(\frac{m_\nu}{10eV} \right) A(\xi)^{\frac{1}{2}} B(\xi)^{-\frac{1}{2}}, \quad (\text{E.4.1})$$

where

$$B(\xi) \equiv \frac{I_3(\xi) + I_3(-\xi)}{I_3(0)} = \\ = \frac{1}{48\eta_R(5)} \left[\frac{1}{5}\xi^5 + 8\eta_R(2)\xi^3 + 48\eta_R(4)\xi + 48 \sum_{n=1}^{\infty} (-1)^{n+1} \frac{e^{-n\xi}}{n^5} \right]. \quad (\text{E.4.2})$$

The basic mechanism of fragmentation of the initial inhomogeneities in an expanding Universe is the Jeans instability described in the previous section.

However, in the calculation of Jeans' length of nonrelativistic collisionless neutrinos, we cannot use the velocity of sound obtained by the classical formula (D.3.26). In fact, since particles are collisionless, their effective pressure is zero and this would lead to a vanishing Jeans length, meaning that even the smallest perturbation would be unstable. This is not the case, since, in the absence of pressure, another mechanism works against gravitational collapse, namely the free streaming of particles (see §D.3.5). The characteristic velocity associated with this process is simply the dispersion velocity $\sqrt{\langle v^2 \rangle / 3}$, where the factor 3 comes from averaging over spatial directions. Thus, we have to make the substitution $v_s^2 \rightarrow \langle v^2 \rangle / 3$ Ruffini and Song (1986). The correct expression for $\langle v^2 \rangle$ can be obtained using the method described above:

$$\langle v^2 \rangle = \begin{cases} c^2 & z > z_{nr} \\ 12 \frac{\eta_R(5)}{\eta_R(3)} \left(\frac{kT_{\nu 0}}{m_{\nu}} \right)^2 \frac{B(\xi)}{A(\xi)} & z < z_{nr}, \end{cases} \quad (\text{E.4.3})$$

where $T_{\nu 0} = 1.97 \text{ K}$ is the present temperature of neutrinos.

As a result, the Jeans mass grows in UR regime and decreases in NR regime Bond et al. (1980). The evolution of Jeans mass of neutrinos for $m_{\nu} = 2.5 \text{ eV}$ and $\xi = 2.5$ with redshift z is represented at fig.E.1. It is clear, that for such values of neutrino mass the peak of Jeans mass lay above $10^{17} M_{\odot}$ and the corresponding comoving Jeans length is $\lambda_0 > 100 \text{ Mpc}$. From the other hand, Jeans mass today is still larger, than the mass of massive galaxy $10^{12} M_{\odot}$.

Finally, the maximum value of Jeans mass at the moment (E.4.1) is Ruffini and Song (1986)

$$M_J(z_{nr}) = 1.475 \cdot 10^{17} M_{\odot} g_{\nu}^{-\frac{1}{2}} N_{\nu}^{-\frac{1}{2}} \left(\frac{m_{\nu}}{10 \text{ eV}} \right)^{-2} A(\xi)^{-\frac{5}{4}} B(\xi)^{\frac{3}{4}}. \quad (\text{E.4.4})$$

The peak of Jeans mass depending on degeneracy parameter for different fixed values of energy density as well as with constant mass $m_{\nu} = 2.5 \text{ eV}$ is shown at Fig.E.2.

By comparing different curves with fixed value of ξ one can find the well

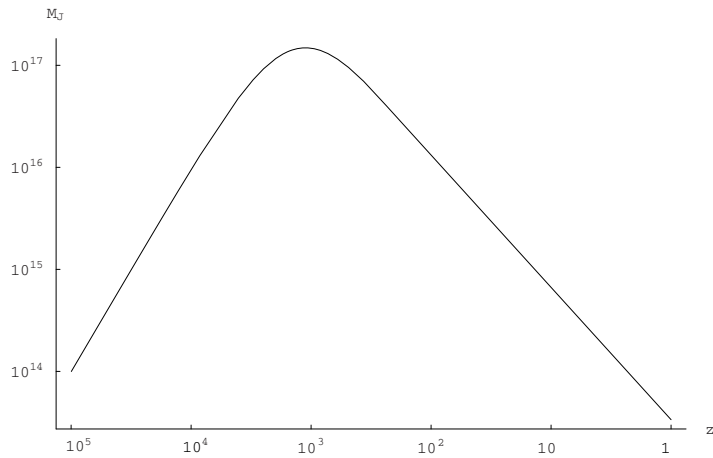


Figure E.1.: The Jeans mass dependence on redshift for neutrinos with mass $m_\nu = 2.5\text{eV}$ and degeneracy parameter $\xi = 2.5$.

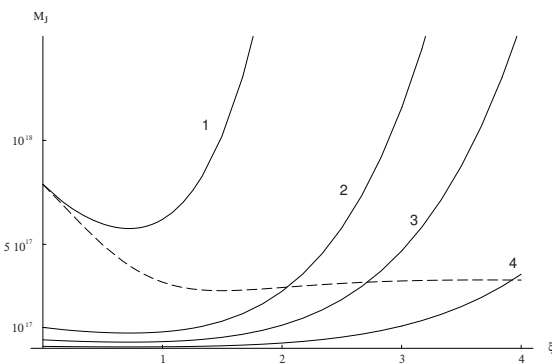


Figure E.2.: The Jeans mass dependence on degeneracy parameter with fixed value of energy density, curves (1-4). Curve (1) corresponds to energy density $\Omega_\nu = 0.11$. Curve (2) corresponds to $\Omega_\nu = 0.3$. Curve (3) represents neutrino energy density $\Omega_\nu = 0.5$ and, finally, curve (4) gives Jeans mass for $\Omega_\nu = 1$. The dashed line represents Jeans mass dependence on degeneracy parameter with fixed neutrino mass $m_\nu = 2.5\text{ eV}$.

known result, that the Jeans mass increases with decreasing of neutrino mass. With growth of degeneracy parameter, however, neutrino mass decreases in the beginning, and its different values correspond to different points at the same curve.

The space above the dashed line at Fig.E.2 represents the region in which the neutrino mass is less than 2.5 eV. It is interesting to note, that this value of m_ν is still sufficient to obtain $\Omega_\nu = 1$ with $\xi \approx 4$.

Bibliography

- AALSETH, C.E., AVIGNONE, F.T., BRODZINSKI, R.L., COLLAR, J.I., GARCIA, E., GONZÁLEZ, D., HASENBALG, F., HENSLEY, W.K., KIRPICHNIKOV, I.V., KLIMENKO, A.A. ET AL.
Neutrinoless double- β decay of ^{76}Ge : First results from the International Germanium Experiment (IGEX) with six isotopically enriched detectors.
Phys. Rev. C, **59**, pp. 2108–2113 (1999).
doi:10.1103/PhysRevC.59.2108.
- ABAZAJIAN, K.N., BEACOM, J.F. AND BELL, N.F.
Stringent constraints on cosmological neutrino-antineutrino asymmetries from synchronized flavor transformation.
Phys. Rev. D, **66**(1), pp. 013008–+ (2002).
- AHMAD, Q.R., ALLEN, R.C., ANDERSEN, T.C., ANGLIN, J.D., BÜHLER, G., BARTON, J.C., BEIER, E.W., BERCOVITCH, M., BIGU, J., BILLER, S. ET AL.
Measurement of the Rate of $\nu_e + d \rightarrow p + p + e^-$ Interactions Produced by ^8B Solar Neutrinos at the Sudbury Neutrino Observatory.
Phys. Rev. Lett. , **87**(7), pp. 071301–+ (2001).
- AKHIEZER, A. AND BERESTETSKII, V.
Quantum Electrodynamics (Moscow, Nauka, 1981).
- AKSENOV, A.G., MILGROM, M. AND USOV, V.V.
Structure of Pair Winds from Compact Objects with Application to Emission from Hot Bare Strange Stars.
ApJ , **609**, pp. 363–377 (2004).
doi:10.1086/421006.
- AKSENOV, A.G., RUFFINI, R. AND VERESHCHAGIN, G.V.
Thermalization of Nonequilibrium Electron-Positron-Photon Plasmas.
Phys. Rev. Lett. , **99**(12), pp. 125003–+ (2007).
doi:10.1103/PhysRevLett.99.125003.
- AKSENOV, A.G., RUFFINI, R. AND VERESHCHAGIN, G.V.
Thermalization of Electron-Positron-Photon Plasmas with an application to GRB.
In *American Institute of Physics Conference Series*, volume 966 of *American Institute of Physics Conference Series*, pp. 191–196 (2008).
doi:10.1063/1.2836994.

Bibliography

- AKSENOV, A., RUFFINI, R. AND VERESHCHAGIN, G.
Thermalization of mildly relativistic plasma with proton loading.
submitted to PRD, **2008** (????).
- ARBOLINO, M.V. AND RUFFINI, R.
The ratio between the mass of the halo and visible matter in spiral galaxies and limits on the neutrino mass.
A&A , **192**, pp. 107–116 (1988).
- ARNABOLDI, C., ARTUSA, D.R., AVIGNONE, F.T., BALATA, M., BANDAC, I., BARUCCI, M., BEEMAN, J.W., BROFFERIO, C., BUCCI, C., CAPELLI, S. ET AL.
New Limit on the Neutrinoless $\beta\beta$ Decay of ^{130}Te .
Phys. Rev. Lett. , **95(14)**, pp. 142501–+ (2005).
doi:10.1103/PhysRevLett.95.142501.
- BAHCALL, N.A. AND BURGETT, W.S.
Are superclusters correlated on a very large scale?
ApJ , **300**, pp. L35–L39 (1986).
doi:10.1086/184598.
- BAHCALL, N.A. AND SONEIRA, R.M.
The spatial correlation function of rich clusters of galaxies.
ApJ , **270**, pp. 20–38 (1983).
doi:10.1086/161094.
- BEAUDET, G. AND GORET, P.
Leptonic numbers and the neutron to proton ratio in the hot big bang model.
A&A , **49**, pp. 415–419 (1976).
- BEAUDET, G., PETROSIAN, V. AND SALPETER, E.E.
Energy Losses due to Neutrino Processes.
ApJ , **150**, pp. 979–+ (1967).
- BEGELMAN, M.C., REES, M.J. AND SIKORA, M.
Energetic and radiative constraints on highly relativistic jets.
ApJ , **429**, pp. L57–L60 (1994).
doi:10.1086/187412.
- BELYAEV, S. AND BUDKER, G.
Relativistic Kinetic Equation.
DAN SSSR, **107**, pp. 807–810 (1956).
- BERESTETSKII, V.B., LIFSHITZ, E.M. AND PITAEVSKII, V.B.
Quantum Electrodynamics (Elsevier, 1982).

- BERTONE, G., HOOPER, D. AND SILK, J.
Particle dark matter: evidence, candidates and constraints.
Phys. Rep. , **405**, pp. 279–390 (2005).
doi:10.1016/j.physrep.2004.08.031.
- BIANCO, C.L., RUFFINI, R., VERESHCHAGIN, G. AND XUE, S.S.
Equations of motion, initial and boundary conditions for GRB.
J.Korean Phys.Soc., **49**, pp. 722–731 (2006).
- BIANCONI, A., LEE, H.W. AND RUFFINI, R.
Limits from cosmological nucleosynthesis on the leptonic numbers of the universe.
A&A , **241**, pp. 343–357 (1991).
- BIRDSALL, C.K. AND LANGDON, A.B.
Plasma Physics via Computer simulation (McGraw-Hill Book Company, 1985).
- BISNOVATYI-KOGAN, G.S. AND MURZINA, M.V.A.
Early stages of relativistic fireball expansion.
Phys. Rev. D, **52**, pp. 4380–4392 (1995).
- BISNOVATYI-KOGAN, G.S. AND NOVIKOV, I.D.
Cosmology with a Nonzero Neutrino Rest Mass.
Soviet Astronomy, **24**, pp. 516–+ (1980).
- BISNOVATYI-KOGAN, G.S., ZEL'DOVICH, Y.B. AND SYUNYAEV, R.A.
Physical Processes in a Low-Density Relativistic Plasma.
Soviet Ast. , **15**, pp. 17–+ (1971).
- BLANDFORD, R. AND EICHLER, D.
Particle Acceleration at Astrophysical Shocks - a Theory of Cosmic-Ray Origin.
Phys. Rep. , **154**, pp. 1–+ (1987).
- BLANDFORD, R.D. AND MCKEE, C.F.
Fluid dynamics of relativistic blast waves.
Phys. of Fluids, **19**, pp. 1130–1138 (1976).
- BLASCHKE, D.B., PROZORKEVICH, A.V., ROBERTS, C.D., SCHMIDT, S.M.
AND SMOLYANSKY, S.A.
Pair Production and Optical Lasers.
Phys. Rev. Lett. , **96(14)**, pp. 140402–+ (2006).
doi:10.1103/PhysRevLett.96.140402.
- BOND, J.R., EFSTATHIOU, G. AND SILK, J.
Massive neutrinos and the large-scale structure of the universe.
Phys. Rev. Lett. , **45**, pp. 1980–1984 (1980).

Bibliography

BOND, J.R. AND SZALAY, A.S.

The collisionless damping of density fluctuations in an expanding universe.

ApJ , **274**, pp. 443–468 (1983).

doi:10.1086/161460.

BONNOR, W.B.

Jeans' formula for gravitational instability.

MNRAS , **117**, pp. 104–+ (1957).

CALZETTI, D., GIAVALISCO, M. AND RUFFINI, R.

The normalization of the correlation functions for extragalactic structures.

A&A , **198**, pp. 1–2 (1988).

CALZETTI, D., GIAVALISCO, M., RUFFINI, R., EINASTO, J. AND SAAR, E.

The correlation function of galaxies in the direction of the Coma cluster.

Ap&SS, **137**, pp. 101–106 (1987).

CAVALLO, G. AND REES, M.J.

A qualitative study of cosmic fireballs and gamma-ray bursts.

MNRAS , **183**, pp. 359–365 (1978).

CHANG, P., SPITKOVSKY, A. AND ARONS, J.

Long-Term Evolution of Magnetic Turbulence in Relativistic Collisionless Shocks: Electron-Positron Plasmas.

ApJ , **674**, pp. 378–387 (2008).

doi:10.1086/524764.

CHECHETKIN, V.M., DYACHENKO, V.F., GINZBURG, S.L., FIMIN, N.N., RUFFINI, R. AND VERESHCHAGIN, G.V.

Kinetic instabilities in collisionless ultra-relativistically streaming cold electron-ion plasma.

to be published (2008).

CHURAZOV, E., SUNYAEV, R., SAZONOV, S., REVNIVTSEV, M. AND VARSHALOVICH, D.

Positron annihilation spectrum from the Galactic Centre region observed by SPI/INTEGRAL.

MNRAS , **357**, pp. 1377–1386 (2005).

doi:10.1111/j.1365-2966.2005.08757.x.

COLEMAN, P.H. AND PIETRONERO, L.

The fractal structure of the universe.

Phys. Rep. , **213**, pp. 311–389 (1992).

COPPI, P.S. AND BLANDFORD, R.D.

Reaction rates and energy distributions for elementary processes in relativistic pair plasmas.

- MNRAS , **245**, pp. 453–507 (1990).
- DE BERNARDIS, P., ADE, P.A.R., BOCK, J.J., BOND, J.R., BORRILL, J., BOSCALERI, A., COBLE, K., CONTALDI, C.R., CRILL, B.P., DE TROIA, G. ET AL.
Multiple Peaks in the Angular Power Spectrum of the Cosmic Microwave Background: Significance and Consequences for Cosmology.
ApJ , **564**, pp. 559–566 (2002).
doi:10.1086/324298.
- DE GOUVEIA DAL PINO, E.M., HETEM, A., HORVATH, J.E., DE SOUZA, C.A.W., VILLELA, T. AND DE ARAUJO, J.C.N.
Evidence for a very large scale fractal structure in the universe from COBE measurements.
ApJ , **442**, pp. L45–L48 (1995).
doi:10.1086/187812.
- DIACHENKO, V.F.
Analysis of collisionless plasma problems.
Zhurnal Vychislitelnoi Matematiki i Matematicheskoi Fiziki, **25**, pp. 622–627 (1985).
- DICUS, D.A.
Stellar energy-loss rates in a convergent theory of weak and electromagnetic interactions.
Phys. Rev. D, **6**, pp. 941–949 (1972).
- DOLGOV, A.D.
Neutrinos in cosmology.
Phys. Rep. , **370**, pp. 333–535 (2002).
- DOLGOV, A.D., HANSEN, S.H., PASTOR, S., PETCOV, S.T., RAFFELT, G.G. AND SEMIKOZ, D.V.
Cosmological bounds on neutrino degeneracy improved by flavor oscillations.
Nuclear Physics B, **632**, pp. 363–382 (2002).
- DOROSHKEVICH, A.G. AND KHLOPOV, M.Y.
The formation of structure in the neutrino universe.
AZh, **58**, pp. 913–924 (1981).
- DOROSHKEVICH, A.G., NOVIKOV, I.D., SUNYAEV, R.A. AND ZELODOVICH, Y.B.
Helium Production in the Different Cosmological Models.
Highlights of Astronomy, **2**, pp. 318–+ (1971).
- DURRER, R. AND LABINI, F.S.
A fractal galaxy distribution in a homogeneous universe?

Bibliography

- A&A , **339**, pp. L85–L88 (1998).
- EHLERS, J.
Survey of general relativity theory.
In *Relativity, Astrophysics and Cosmology*, pp. 1–125 (1973).
- ELLIS, G.F.R.
The evolution of inhomogeneities in expanding Newtonian cosmologies.
MNRAS , **243**, pp. 509–516 (1990).
- ELLIS, G.F.R. AND BRUNI, M.
Covariant and gauge-invariant approach to cosmological density fluctuations.
Phys. Rev. D, **40**, pp. 1804–1818 (1989).
- FREDERIKSEN, J.T., HEDEDAL, C.B., HAUGBØLLE, T. AND NORDLUND, Å.
Magnetic Field Generation in Collisionless Shocks: Pattern Growth and Transport.
ApJ , **608**, pp. L13–L16 (2004).
doi:10.1086/421262.
- GAITE, J., DOMÍNGUEZ, A. AND PÉREZ-MERCADER, J.
The Fractal Distribution of Galaxies and the Transition to Homogeneity.
ApJ , **522**, pp. L5–L8 (1999).
doi:10.1086/312204.
- GAO, J.G. AND RUFFINI, R.
Relativistic limits on the masses of self-gravitating systems of degenerate neutrinos.
Physics Letters B, **97**, pp. 388–390 (1980).
- GIAVALISCO, M.
Ph.D. thesis, University of Rome "La Sapienza" (1992).
- GINZBURG, S.L., DIACHENKO, V.F., PALEYCHIK, V.V., SUDARIKOV, A.L.
AND CHECHETKIN, V.M.
Plasma Instability in Relativistic Jets.
Astronomy Letters, **30**, pp. 376–381 (2004).
doi:10.1134/1.1764883.
- GOODMAN, J.
Are gamma-ray bursts optically thick?
ApJ , **308**, pp. L47–L50 (1986).
doi:10.1086/184741.
- GOULD, R.J.
Thermal bremsstrahlung from high-temperature plasmas.
ApJ , **238**, pp. 1026–1033 (1980).
doi:10.1086/158068.

GOULD, R.J.

Kinetic theory of relativistic plasmas.

Physics of Fluids, **24**, pp. 102–107 (1981).

GOULD, R.J.

Processes in relativistic plasmas.

ApJ, **254**, pp. 755–766 (1982).

doi:10.1086/159787.

GOULD, R.J.

The cross section for double Compton scattering.

ApJ, **285**, pp. 275–278 (1984).

doi:10.1086/162503.

GREINER, W. AND REINHARDT, J.

Quantum Electrodynamics (Berlin, Springer, 2003).

GRUZINOV, A. AND WAXMAN, E.

Gamma-Ray Burst Afterglow: Polarization and Analytic Light Curves.

ApJ, **511**, pp. 852–861 (1999).

doi:10.1086/306720.

GUILBERT, P.W. AND STEPNEY, S.

Pair production, Comptonization and dynamics in astrophysical plasmas.

MNRAS, **212**, pp. 523–544 (1985).

HALL, G. AND WATT, J.M.

Modern Numerical Methods for Ordinary Differential Equations (New York, Oxford University Press, 1976).

HANSEN, S.H., MANGANO, G., MELCHIORRI, A., MIELE, G. AND PISANTI, O.

Constraining neutrino physics with big bang nucleosynthesis and cosmic microwave background radiation.

Phys. Rev. D, **65(2)**, pp. 023511–+ (2002).

HAUG, E.

Electron-positron bremsstrahlung in mildly relativistic thermal plasmas.

A&A, **148**, pp. 386–390 (1985).

HAUG, E.

Energy loss and mean free path of electrons in a hot thermal plasma.

A&A, **191**, pp. 181–185 (1988).

HAWKINS, E., MADDOX, S., COLE, S., LAHAV, O., MADGWICK, D.S., NORBERG, P., PEACOCK, J.A., BALDRY, I.K., BAUGH, C.M., BLAND-HAWTHORN, J. ET AL.

Bibliography

The 2dF Galaxy Redshift Survey: correlation functions, peculiar velocities and the matter density of the Universe.
MNRAS , **346**, pp. 78–96 (2003).
doi:10.1046/j.1365-2966.2003.07063.x.

HEATH, D.J.
Gravitational instability.
Ap&SS, **175**, pp. 35–50 (1991).

HEDEDAL, C.
Gamma-Ray Bursts, Collisionless Shocks and Synthetic Spectra.
Ph.D. thesis, Niels Bohr Institute (2005).

HEDEDAL, C.B., HAUGBØLLE, T., FREDERIKSEN, J.T. AND NORDLUND, Å.
Non-Fermi Power-Law Acceleration in Astrophysical Plasma Shocks.
ApJ , **617**, pp. L107–L110 (2004).
doi:10.1086/427387.

HU, W.T.
Wandering in the Background: a Cosmic Microwave Background Explorer.
Ph.D. thesis, AA(UNIVERSITY OF CALIFORNIA, BERKELEY.) (1995).

IWAMOTO, S. AND TAKAHARA, F.
Wien Fireball Model of Relativistic Outflows in Active Galactic Nuclei.
ApJ , **601**, pp. 78–89 (2004).
doi:10.1086/380300.

JEANS, J.H.
The universe around us (New York, The Macmillan company; Cambridge, Eng., The University press [c1929], 1929).

JEANS, J.
The Stability of a Spherical Nebula.
Philosophical Transactions A, **199**, pp. 1–53 (1902).

JOYCE, M., SYLOS LABINI, F., GABRIELLI, A., MONTUORI, M. AND PIETRONERO, L.
Basic properties of galaxy clustering in the light of recent results from the Sloan Digital Sky Survey.
A&A , **443**, pp. 11–16 (2005).
doi:10.1051/0004-6361:20053658.

KATRIN COLLABORATION.
KATRIN: A next generation tritium beta decay experiment with sub-eV sensitivity for the electron neutrino mass.
ArXiv High Energy Physics - Experiment e-prints (2001).

KATZ, J.I.

Two populations and models of gamma-ray bursts.
ApJ , **422**, pp. 248–259 (1994).

KLAPDOR-KLEINGROTHAUS, H.V., DIETZ, A., BAUDIS, L., HEUSSER, G., KRIVOSHEINA, I.V., MAJOROVITS, B., PAES, H., STRECKER, H., ALEXEEV, V., BALYSH, A. ET AL.

Latest results from the HEIDELBERG-MOSCOW double beta decay experiment.
European Physical Journal A, **12**, pp. 147–154 (2001).

KLIMONTOVICH, Y.L.

Physics of collisionless plasma.
Uspekhi Fizicheskikh Nauk, **40**, pp. 21–51 (1997).

KLYPIN, A.A. AND KOPYLOV, A.I.

The Spatial Covariance Function for Rich Clusters of Galaxies.
Soviet Astronomy Letters, **9**, pp. 41–+ (1983).

KNELLER, J.P., SCHERRER, R.J., STEIGMAN, G. AND WALKER, T.P.

How does the cosmic microwave background plus big bang nucleosynthesis constrain new physics?
Phys. Rev. D, **64(12)**, pp. 123506–+ (2001).

KOERS, H.B.J. AND WIJERS, R.A.M.J.

The effect of neutrinos on the initial fireballs in gamma-ray bursts.
MNRAS , **364**, pp. 934–942 (2005).
doi:10.1111/j.1365-2966.2005.09622.x.

KOLB, E.W. AND TURNER, M.S.

The Early Universe (Frontiers in Physics, Reading, MA: Addison-Wesley, 1990).

KRAUS, C., BORNSCHEIN, B., BORNSCHEIN, L., BONN, J., FLATT, B., KOVALIK, A., OSTRICK, B., OTTEN, E.W., SCHALL, J.P., THÜMMLER, T. ET AL.

Final results from phase II of the Mainz neutrino mass searchin tritium β decay.
European Physical Journal C, **40**, pp. 447–468 (2005).
doi:10.1140/epjc/s2005-02139-7.

KUZNETSOVA, I., HABS, D. AND RAFELSKI, J.

Pion and muon production in $e^{[sup -]}$, $e^{[sup +]}$, gamma plasma.
Physical Review D (Particles and Fields), **78(1)**, 014027 (2008).
doi:10.1103/PhysRevD.78.014027.

LANDAU, L.D. AND LIFSHITS, E.M.

Fluid Mechanics (Course of Theoretical Physics) (Pergamon, New York, 1987).

Bibliography

LANDAU, L.D. AND LIFSHITZ, E.M.

Physical Kinetics (Elsevier, 1981).

LATTANZI, M., RUFFINI, R. AND VERESHCHAGIN, G.

On the possible role of massive neutrinos in cosmological structure formation.

In M. Novello and S.E. Perez Bergliaffa (eds.), *Cosmology and Gravitation*, volume 668 of *American Institute of Physics Conference Series*, pp. 263–287 (2003).

LATTANZI, M., RUFFINI, R. AND VERESHCHAGIN, G.V.

Joint constraints on the lepton asymmetry of the Universe and neutrino mass from the Wilkinson Microwave Anisotropy Probe.

Phys. Rev. D, **72**(6), pp. 063003–+ (2005).

doi:10.1103/PhysRevD.72.063003.

LATTANZI, M., RUFFINI, R. AND VERESHCHAGIN, G.V.

Do WMAP data constraint the lepton asymmetry of the Universe to be zero?

In *Albert Einstein Century International Conference*, volume 861 of *American Institute of Physics Conference Series*, pp. 912–919 (2006).

doi:10.1063/1.2399677.

LEE, B.W. AND WEINBERG, S.

Cosmological lower bound on heavy-neutrino masses.

Phys. Rev. Lett. , **39**, pp. 165–168 (1977).

LEMOINE, D.

Fluctuations in the relativistic plasma and primordial magnetic fields.

Phys. Rev. D, **51**(6), pp. 2677–2686 (1995).

doi:10.1103/PhysRevD.51.2677.

LESGOURGUES, J. AND PASTOR, S.

Massive neutrinos and cosmology.

Phys. Rep. , **429**, pp. 307–379 (2006).

doi:10.1016/j.physrep.2006.04.001.

LIGHTMAN, A.P.

Double Compton emission in radiation dominated thermal plasmas.

ApJ , **244**, pp. 392–405 (1981).

doi:10.1086/158716.

LIGHTMAN, A.P.

Relativistic thermal plasmas - Pair processes and equilibria.

ApJ , **253**, pp. 842–858 (1982).

doi:10.1086/159686.

LIGHTMAN, A.P. AND BAND, D.L.

Relativistic thermal plasmas - Radiation mechanisms.

ApJ , **251**, pp. 713–726 (1981).
doi:10.1086/159516.

LISHITZ, E.

Journal of Physics, (USSR), **10**, pp. 116–? (1946).

LOBASHEV, V.M.

The search for the neutrino mass by direct method in the tritium beta-decay and perspectives of study it in the project KATRIN.

Nuclear Physics A, **719**, pp. 153–+ (2003).
doi:10.1016/S0375-9474(03)00985-0.

LUO, X. AND SCHRAMM, D.N.

Fractals and cosmological large-scale structure.
Science, **256**, pp. 513–515 (1992).

LYNDEN-BELL, D.

Statistical mechanics of violent relaxation in stellar systems.
MNRAS , **136**, pp. 101–+ (1967).

MALTONI, M., SCHWETZ, T., TÓRTOLA, M. AND VALLE, J.W.F.

Status of global fits to neutrino oscillations.
New Journal of Physics, **6**, pp. 122–+ (2004).
doi:10.1088/1367-2630/6/1/122.

MANDELBROT, B.B.

The fractal geometry of nature /Revised and enlarged edition/ (New York, W.H. Freeman and Co., 1983, 495 p., 1983).

MARASCHI, L.

Jets at different scales.

In S. Collin, F. Combes and I. Shlosman (eds.), *Active Galactic Nuclei: From Central Engine to Host Galaxy*, volume 290 of *Astronomical Society of the Pacific Conference Series*, pp. 275–+ (2003).

MEDVEDEV, M.V.

Theory of “Jitter” Radiation from Small-Scale Random Magnetic Fields and Prompt Emission from Gamma-Ray Burst Shocks.
ApJ , **540**, pp. 704–714 (2000).
doi:10.1086/309374.

MEDVEDEV, M.V. AND LOEB, A.

Generation of Magnetic Fields in the Relativistic Shock of Gamma-Ray Burst Sources.
ApJ , **526**, pp. 697–706 (1999).
doi:10.1086/308038.

Bibliography

- MEDVEDEV, M.V. AND SPITKOVSKY, A.
Radiative cooling in relativistic collisionless shocks. Can simulations and experiments probe relevant GRB physics?
ArXiv e-prints (2008).
- MESZAROS, A.
A possible fast growth of adiabatic cosmological perturbations.
A&A, **278**, pp. 1–5 (1993).
- MESZAROS, P.
The behaviour of point masses in an expanding cosmological substratum.
A&A, **37**, pp. 225–228 (1974).
- MIHALAS, D. AND MIHALAS, B.W.
Foundations of Radiation Hydrodynamics (New York, Oxford University Press, 1984).
- MILLER-JONES, J.C.A., FENDER, R.P. AND NAKAR, E.
Opening angles, Lorentz factors and confinement of X-ray binary jets.
MNRAS, **367**, pp. 1432–1440 (2006).
doi:10.1111/j.1365-2966.2006.10092.x.
- MISIASZEK, M., ODRZYWOŁEK, A. AND KUTSCHERA, M.
Neutrino spectrum from the pair-annihilation process in the hot stellar plasma.
Phys. Rev. D, **74(4)**, pp. 043006–+ (2006).
doi:10.1103/PhysRevD.74.043006.
- NARAYAN, R., PACZYNSKI, B. AND PIRAN, T.
Gamma-ray bursts as the death throes of massive binary stars.
ApJ, **395**, pp. L83–L86 (1992).
- NISHIKAWA, K.I., HARDEE, P.E., HEDEDAL, C.B. AND FISHMAN, G.J.
Acceleration Mechanics in Relativistic Shocks by the Weibel Instability.
ApJ, **642**, pp. 1267–1274 (2006).
doi:10.1086/501426.
- OCHELKOV, I.P., PRILUTSKII, O.F., ROZENTAL, I.L. AND USOV, V.V.
Relativistic kinetics and hydrodynamics (Moscow, Atomizdat, 1979).
- ORITO, M., KAJINO, T., MATHEWS, G.J. AND BOYD, R.N.
Primordial nucleosynthesis and neutrinos with mass and degeneracy.
Nuclear Physics A, **688**, pp. 17–20 (2001).
- ORITO, M., KAJINO, T., MATHEWS, G.J. AND WANG, Y.
Constraints on neutrino degeneracy from the cosmic microwave background and primordial nucleosynthesis.
Phys. Rev. D, **65(12)**, pp. 123504–+ (2002).

PADMANABHAN, T.

Structure Formation in the Universe (Structure Formation in the Universe, by T. Padmanabhan, pp. 499. ISBN 0521424860. Cambridge, UK: Cambridge University Press, June 1993., 1993).

PEACOCK, J.A.

Cosmological Physics (Cosmological Physics, by John A. Peacock, pp. 704. ISBN 052141072X. Cambridge, UK: Cambridge University Press, January 1999., 1999).

PEACOCK, J.A.

Studying Large-scale Structure with the 2dF Galaxy Redshift Survey.

In N. Metcalfe and T. Shanks (eds.), *A New Era in Cosmology*, volume 283 of *Astronomical Society of the Pacific Conference Series*, pp. 19–+ (2002).

PEACOCK, J.A., COLE, S., NORBERG, P., BAUGH, C.M., BLAND-HAWTHORN, J., BRIDGES, T., CANNON, R.D., COLLESS, M., COLLINS, C., COUCH, W. ET AL.

A measurement of the cosmological mass density from clustering in the 2dF Galaxy Redshift Survey.

Nature , **410**, pp. 169–173 (2001).

PEEBLES, P.J.E.

Primeval adiabatic perturbations - Effect of massive neutrinos.

ApJ , **258**, pp. 415–424 (1982).

doi:10.1086/160094.

PEEBLES, P.J.E.

Principles of physical cosmology (Princeton Series in Physics, Princeton, NJ: Princeton University Press, —c1993, 1993).

PILLA, R.P. AND SHAHAM, J.

Kinetics of Electron-Positron Pair Plasmas Using an Adaptive Monte Carlo Method.

ApJ , **486**, pp. 903–+ (1997).

doi:10.1086/304534.

PIRAN, T.

Gamma-ray bursts and the fireball model.

Phys. Rep. , **314**, pp. 575–667 (1999).

PIRAN, T.

The physics of gamma-ray bursts.

Reviews of Modern Physics, **76**, pp. 1143–1210 (2005).

doi:10.1103/RevModPhys.76.1143.

Bibliography

PIRAN, T., SHEMI, A. AND NARAYAN, R.

Hydrodynamics of Relativistic Fireballs.

MNRAS , **263**, pp. 861–867 (1993).

PRIMACK, J. AND MURDIN, P.

Hot Dark Matter.

Encyclopedia of Astronomy and Astrophysics (2002).

doi:10.1888/0333750888/5474.

PRIMACK, J.R.

Status of cold dark matter cosmology.

Nuclear Physics B Proceedings Supplements, **124**, pp. 3–12 (2003).

doi:10.1016/S0920-5632(03)02071-1.

RAMIREZ-RUIZ, E., NISHIKAWA, K.I. AND HEDEDAL, C.B.

$e^{+/-}$ Pair Loading and the Origin of the Upstream Magnetic Field in GRB Shocks.

ApJ , **671**, pp. 1877–1885 (2007).

doi:10.1086/522072.

REES, M.J. AND MESZAROS, P.

Relativistic fireballs - Energy conversion and time-scales.

MNRAS , **258**, pp. 41P–43P (1992).

RUFFINI, R.

On the de Vaucouleurs density-radius relation and the cellular intermediate large-scale structure of the universe.

In H.G. Corwin Jr. and L. Bottinelli (eds.), *World of Galaxies (Le Monde des Galaxies)*, pp. 461–472 (1989).

RUFFINI, R., BERNARDINI, M.G., BIANCO, C.L., CAITO, L., CHARDONNET, P., DAINOTTI, M.G., FRASCHETTI, F., GUIDA, R., ROTONDO, M., VERESHCHAGIN, G. ET AL.

The Blackholic energy and the canonical Gamma-Ray Burst.

In *American Institute of Physics Conference Series*, volume 910 of *American Institute of Physics Conference Series*, pp. 55–217 (2007).

doi:10.1063/1.2752480.

RUFFINI, R., SALMONSON, J.D., WILSON, J.R. AND XUE, S.S.

On the pair electromagnetic pulse of a black hole with electromagnetic structure.

A&A , **350**, pp. 334–343 (1999).

RUFFINI, R., SALMONSON, J.D., WILSON, J.R. AND XUE, S.S.

On the pair-electromagnetic pulse from an electromagnetic black hole surrounded by a baryonic remnant.

A&A , **359**, pp. 855–864 (2000).

RUFFINI, R. AND SONG, D.J.

On the Jeans mass of weakly interacting, neutral, massive leptons.

In F. Melchiorri and R. Ruffini (eds.), *Gamow cosmology*, p. 370 - 385, pp. 370–385 (1986).

RUFFINI, R., SONG, D.J. AND STELLA, L.

On the statistical distribution off massive fermions and bosons in a Friedmann universe.

A&A , **125**, pp. 265–270 (1983).

RUFFINI, R., SONG, D.J. AND TARAGLIO, S.

The 'ino' mass and the cellular large-scale structure of the universe.

A&A , **190**, pp. 1–2 (1988).

SAVAGE, M.J., MALANEY, R.A. AND FULLER, G.M.

Neutrino oscillations and the leptonic charge of the universe.

ApJ , **368**, pp. 1–11 (1991).

doi:10.1086/169665.

SHECTMAN, S.A., LANDY, S.D., OEMPLER, A., TUCKER, D.L., LIN, H., KIRSHNER, R.P. AND SCHECHTER, P.L.

The Las Campanas Redshift Survey.

ApJ , **470**, pp. 172–+ (1996).

doi:10.1086/177858.

SHEMI, A. AND PIRAN, T.

The appearance of cosmic fireballs.

ApJ , **365**, pp. L55–L58 (1990).

SHU, F.H.

On the statistical mechanics of violent relaxation.

ApJ , **225**, pp. 83–94 (1978).

doi:10.1086/156470.

SIGOV, Y.S.

Computing Experiment: a Bridge between the Past and Future of Plasma Physics.

Selected Works (Moscow: Fizmatlit, 2001).

SILK, J.

Fluctuations in the Primordial Fireball.

Nature , **215**, pp. 1155–+ (1967).

SILVA, L.O.

Physical Problems (Microphysics) in Relativistic Plasma Flows.

In P.A. Hughes and J.N. Bregman (eds.), *Relativistic Jets: The Common Physics of AGN, Microquasars, and Gamma-Ray Bursts*, volume 856 of *American Institute of Physics Conference Series*, pp. 109–128 (2006).

Bibliography

doi:10.1063/1.2356387.

SILVA, L.O., FONSECA, R.A., TONGE, J.W., DAWSON, J.M., MORI, W.B.
AND MEDVEDEV, M.V.

*Interpenetrating Plasma Shells: Near-equipartition Magnetic Field Generation
and Nonthermal Particle Acceleration.*

ApJ , **596**, pp. L121–L124 (2003).
doi:10.1086/379156.

SPITKOVSKY, A.

Simulations of relativistic collisionless shocks: shock structure and particle acceleration.

In T. Bulik, B. Rudak and G. Madejski (eds.), *Astrophysical Sources of High Energy Particles and Radiation*, volume 801 of *American Institute of Physics Conference Series*, pp. 345–350 (2005).

doi:10.1063/1.2141897.

SPITKOVSKY, A.

On the Structure of Relativistic Collisionless Shocks in Electron-Ion Plasmas.

ApJ , **673**, pp. L39–L42 (2008a).
doi:10.1086/527374.

SPITKOVSKY, A.

Particle Acceleration in Relativistic Collisionless Shocks: Fermi Process at Last?

ApJ , **682**, pp. L5–L8 (2008b).
doi:10.1086/590248.

STEPNEY, S.

Two-body relaxation in relativistic thermal plasmas.

MNRAS , **202**, pp. 467–481 (1983).

STEPNEY, S. AND GUILBERT, P.W.

Numerical FITS to important rates in high temperature astrophysical plasmas.

MNRAS , **204**, pp. 1269–1277 (1983).

STRUMIA, A. AND VISSANI, F.

Implications of neutrino data circa 2005.

Nuclear Physics B, **726**, pp. 294–316 (2005).
doi:10.1016/j.nuclphysb.2005.07.031.

SVENSSON, R.

Electron-Positron Pair Equilibria in Relativistic Plasmas.

ApJ , **258**, pp. 335–+ (1982a).
doi:10.1086/160082.

SVENSSON, R.

The pair annihilation process in relativistic plasmas.

- ApJ , **258**, pp. 321–334 (1982b).
doi:10.1086/160081.
- SVENSSON, R.
Steady mildly relativistic thermal plasmas - Processes and properties.
MNRAS , **209**, pp. 175–208 (1984).
- TAUB, A.H.
Relativistic Rankine-Hugoniot Equations.
Phys. Rev., **74**, pp. 328–334 (1948).
- TREMAINE, S. AND GUNN, J.E.
Dynamical role of light neutral leptons in cosmology.
Phys. Rev. Lett. , **42**, pp. 407–410 (1979).
- USOV, V.V.
Bare Quark Matter Surfaces of Strange Stars and e^+e^- Emission.
Phys. Rev. Lett. , **80**, pp. 230–233 (1998).
- VERESHCHAGIN, G.V.
Pair Plasma and Gamma Ray Bursts.
Ph.D. thesis, IRAP PhD (2008).
- VERGANI, S.D.
Direct GRB fireball Lorentz factor measurements through REM early afterglow observations.
Ap&SS, **311**, pp. 197–201 (2007).
doi:10.1007/s10509-007-9544-2.
- WARDLE, J.F.C., HOMAN, D.C., OJHA, R. AND ROBERTS, D.H.
Electron-positron jets associated with the quasar 3C279.
Nature , **395**, pp. 457–461 (1998).
doi:10.1038/26675.
- WAXMAN, E.
Gamma-ray bursts and collisionless shocks.
Plasma Physics and Controlled Fusion, **48**, pp. B137–B151 (2006).
doi:10.1088/0741-3335/48/12B/S14.
- WEAVER, T.A.
Reaction rates in a relativistic plasma.
Phys. Rev. A, **13**, pp. 1563–1569 (1976).
- WEINBERG, S.
Gravitation and Cosmology: Principles and Applications of the General Theory of Relativity (Gravitation and Cosmology: Principles and Applications of the General Theory of Relativity, by Steven Weinberg, pp. 688. ISBN 0-471-92567-5. Wiley-VCH , July 1972., 1972).

Bibliography

WEINBERG, S.

Cosmology (Oxford University Press, April 2008., 2008).

ZDZIARSKI, A.A.

Spectra from pair-equilibrium plasmas.

ApJ , **283**, pp. 842–847 (1984).

doi:10.1086/162370.

ZEHAVI, I., ZHENG, Z., WEINBERG, D.H., FRIEMAN, J.A., BERLIND, A.A., BLANTON, M.R., SCOCCHIMARRO, R., SHETH, R.K., STRAUSS, M.A., KAYO, I. ET AL.

The Luminosity and Color Dependence of the Galaxy Correlation Function.

ApJ , **630**, pp. 1–27 (2005).

doi:10.1086/431891.

ZELDOVICH, I.B. AND NOVIKOV, I.D.

Structure and evolution of the universe (Moscow, Nauka, 1975).

ZELDOVICH, Y.B.

Gravitational instability: An approximate theory for large density perturbations.

A&A , **5**, pp. 84–89 (1970).

ZELDOVICH, Y.B. AND SYUNYAEV, R.A.

Astrophysical implications of the neutrino rest mass. I - The universe.

Pis ma Astronomicheskii Zhurnal, **6**, pp. 451–456 (1980).